HAL
open science

Classical Losses in Soft Magnetic Composites using Homogenization Techniques

Xiaotao Ren

To cite this version:

Xiaotao Ren. Classical Losses in Soft Magnetic Composites using Homogenization Techniques. Electromagnetism. Université Paris Saclay (COmUE), 2017. English. NNT : 2017SACLS159 . tel-01576559

HAL Id: tel-01576559

https://theses.hal.science/tel-01576559v1

Submitted on 23 Aug 2017

HAL is a multi-disciplinary open access archive for the deposit and dissemination of scientific research documents, whether they are published or not. The documents may come from teaching and research institutions in France or abroad, or from public or private research centers.

L'archive ouverte pluridisciplinaire **HAL**, est destinée au dépôt et à la diffusion de documents scientifiques de niveau recherche, publiés ou non, émanant des établissements d'enseignement et de recherche français ou étrangers, des laboratoires publics ou privés.

NNT : 2017SACLS159

Thèse de doctorat de l'Université Paris-Saclay préparée à l'Université Paris-Sud

Ecole doctorale n°575

Electrical, Optical, Bio-physics and Engineering

Spécialité de doctorat: Génie Électrique

par

M. Xiaotao REN

Modélisation semi-analytique des pertes par courants de Foucault dans les matériaux composites

Classical Losses in Soft Magnetic Composites using Homogenization Techniques

Thèse présentée et soutenue à Gif-sur-Yvette, le 3 Juillet 2017.

Composition du Jury :

M.	Stéphane CLENET	Professeur des Universités Arts et Métiers ParisTech	(Président du jury)
M.	Zhuoxiang REN	Professeur des Universités Université Pierre et Marie Curie	(Rapporteur)
M.	Didier TRICHET	Professeur des Universités Université de Nantes	(Rapporteur)
M.	Olivier DE LA BARRIERE	Chargé de recherche CNRS	(Examinateur)
M.	Laurent DANIEL	Professeur des Universités CentraleSupélec	(Directeur de thèse)
M.	Romain CORCOLLE	Maître de Conférences Université Paris-Sud	(Encadrant)

Acknowledgements

I would like to express my gratitude to Prof. Stéphane Clénet who did me the honor of presiding the jury of my thesis. I would also like to thank my jury members, Prof. Zhuoxiang Ren and Prof. Didier Trichet for having attentively reviewed my thesis report. I also thank Dr. Olivier de la Barrière, for his interesting and thought-provoking questions and remarks.

I wish also to express my thanks to Prof. Frédéric Bouillault, former director of Laboratory GeePs, for having enrolled me in Université Paris-Sud and having secured a position for me in the laboratory.

My gratitude is given to my supervisor Laurent Daniel for providing me this great opportunity to study the theory of homogenization. I have learned much from his meticulous manner of scholarship.

Sincere thanks are given to Romain Corcolle, encadrant of my thesis, for introducing and training me in this interesting and challenging research work, for taking care of the administrative jobs within and outside of Université, and for, together with his wife, Pingping Ding, helping me commence an exciting study and daily life in Paris.

The four-year life in GeePs has offered me a fantastic opportunity to meet many nice colleagues. I thank Lionel Pichon, Xavier Mininger, Yves Bernard, and Zuqi Tang for discussions and patiently answering my questions. My thanks also to Olivier Hubert and Laurent Santandrea for maintaining software and hardware environment. I am grateful to Yann Le Bihan for explaining many interesting stuff and pointing out that “18h, c’est seulement le milieu de la journée”.

I also wish to thank my Chinese friends Chao Liu, Chenjiang Yu, Qi Jiang, Xiang Liu, Mingyong Liu, Man Zhang, and Shuangfeng Zhang for their help and encouragement.

My sincerest and warmest thanks are given to my family for their great support and confidence. Many thanks to all the people who have helped and accompanied me in this wonderful journey in Paris.

Abstract

English: Composite materials have been widely used in Electrical Engineering, and they have stimulated a growing number of scientific research, especially when it comes to energy savings. Soft Magnetic Composites (SMC) incorporate the attributes of different constituents. They can be designed to exhibit high permeability and to dissipate low Eddy Current (EC) losses compared to more conventional structures such as laminated steel.

Nevertheless, electromagnetic properties of SMC are not easily determined. Numerical tools such as finite element method (FEM) are usually employed to provide a full-field description of SMC. As the microstructure has to be finely meshed, it brings significant numerical burden and instabilities. To overcome this restriction, semi-analytical homogenization methods are adapted and applied here. They consist in developing a complex permeability model.

In the complex permeability model for SMC, the static magnetic permeability and EC losses are integrated respectively as the real and imaginary part of the complex permeability. Classical estimates are applied to determine the macroscopic effective magnetic permeability. A correct determination of the effective permeability, i.e. the real part of the complex permeability, is crucial for the estimate of EC losses. EC losses formulas are derived for SMC with periodic microstructure in 2D and 3D cases. Furthermore, different approaches of field averaging are employed to obtain lower and upper bounds on the EC losses in SMC.

The complex permeability model is then applied to analyze a magnetic circuit structure. The magnetic field and EC losses distribution can be obtained on the equivalent homogenized magnetic circuit. The results are compared to the full-field calculations on the heterogeneous magnetic circuit. A good consistency is observed.

Finally, the effect of mechanical stress on the magnetic permeability and loss property of SMC is studied, which leads to a coupled formula of EC loss density as a function of macroscopic stress and magnetic field.

Français : L'emploi de matériaux composites dans le domaine du Génie Electrique est actuellement un sujet de recherche en plein essor, notamment pour des considérations d'économie d'énergie. Les composites magnétiques doux (SMC - Soft Magnetic Composites) intègrent les propriétés de leurs différents constituants. Ils sont conçus pour présenter une perméabilité élevée et avoir une faible densité de pertes par courants de Foucault (EC - Eddy Current) par comparaison aux structures plus classiques comme l'acier laminé.

Néanmoins, la détermination des propriétés électromagnétiques des SMC n'est pas aisée. Une approche classique est d'appliquer les outils numériques tels que la méthode des éléments finis (FEM - Finite Element Method) pour obtenir une description complète du SMC. Cependant, la microstructure doit être finement maillée, ce qui représente un fardeau numérique significatif et des instabilités dans l'approche par FEM. Pour surmonter cette restriction, les méthodes d'homogénéisation semi-analytiques sont appliquées.

Ce travail consiste d'abord à développer un modèle de perméabilité complexe pour SMC. La perméabilité magnétique et les pertes EC sont intégrées respectivement comme les parties réelle et imaginaire de la perméabilité complexe. La perméabilité magnétique effective macroscopique peut s'obtenir par des estimations classiques en homogénéisation. Une détermination correcte de la perméabilité effective, i.e. la partie réelle de la perméabilité complexe, est cruciale pour une estimation précise de pertes EC. Les formules de pertes EC sont dérivées pour des SMC à microstructure périodique dans les cas 2D et 3D. En outre, différentes approches s'appuyant sur différentes moyennes du champ magnétique permettent d'obtenir des limites inférieures et supérieures pour l'estimation des pertes EC dans les SMC.

La perméabilité complexe ainsi obtenue est ensuite appliquée à une structure de circuit magnétique. Le champ magnétique et la répartition des pertes EC peuvent être obtenus sur le circuit magnétique équivalent (homogénéisé). Les résultats sont comparés aux calculs en champ complet du circuit magnétique hétérogène. Un bon accord est observé.

Enfin, on étudie l'effet des contraintes mécaniques sur la perméabilité magnétique et les pertes EC des SMC, ce qui conduit à une formule couplée de la densité de pertes EC en fonction de la contrainte mécanique macroscopique et du champ magnétique.

Table of contents

List of figures xi

Résumé en Français xvii

General Introduction 1

1 Basic Equations for the Modeling of Soft Magnetic Composites 5

1.1 Maxwell's Equations . . . 7
1.2 Constitutive Relations . . . 8
1.2.1 Magnetic Behavior . . . 9
1.2.2 Mechanical Behavior . . . 11
1.2.3 Magneto-Mechanical Behavior . . . 12
1.3 Eddy Current Losses . . . 13
1.3.1 EC Loss Density Definition . . . 13
1.3.2 EC Loss Density of Homogeneous Structures . . . 14
1.4 Soft Magnetic Composites . . . 15
1.4.1 EC Loss Density of SMC . . . 17
1.5 Homogenization Techniques . . . 17
1.6 Conclusion . . . 20

2 A Complex Permeability Model for EC Losses in SMC 21

2.1 EC Loss Density of Single Inclusion . . . 23
2.1.1 Cylindrical Inclusion . . . 24
2.1.2 Spherical Inclusion . . . 25
2.2 EC Loss Density of SMC . . . 27
2.3 Effective Permeability of SMC . . . 29
2.3.1 MG Estimate . . . 29
2.3.2 Series Expansion Estimate . . . 30
2.4 Complex Permeability Definition . . . 30

2.4.1 Complex Permeability of Single Inclusion 32
2.4.2 Complex Permeability of SMC 32
2.5 Validation using FEM computations 33
2.5.1 Microstructure 33
2.5.2 Parameters 34
2.5.3 Effective Permeability Comparison 36
2.5.4 EC Loss Density Comparison 37
2.5.5 EC Loss Density by Average Field Assumption 39
2.5.6 EC Loss Density by Effective Complex Permeability Tensor 39
2.6 Discussion 44
2.6.1 Square Microstructure 45
2.6.2 Cube Microstructure 46
2.6.3 Complex Permeability 46
2.7 Conclusion 47

3 Bounds and Estimates on EC Losses in SMC 49
3.1 EC Loss Density in SMC 51
3.2 Bounds 52
3.2.1 Cylinder Microstructure 52
3.2.2 Sphere Microstructure 55
3.2.3 Extension to More Generic Microstructures 57
3.3 EC Loss Density Estimates 60
3.3.1 Cylinder Microstructure 61
3.3.2 Sphere Microstructure 65
3.4 Discussion 67
3.4.1 Numerical Calculations on EC Losses Estimates 67
3.4.2 Model Validation 69
3.5 Conclusion 71

4 Complex Permeability for SMC: Application to Magnetic Circuit 73
4.1 EC Loss Density of High Concentration SMC 75
4.1.1 Perpendicular field 76
4.1.2 In-plane field 76
4.1.3 Complex permeability for SMC 78
4.2 Magnetic Circuit Application 80
4.2.1 Magnetic Behavior 83
4.2.2 EC Loss Density 84

4.3 Conclusion 86

5 Effect of Stress on Eddy Current Losses in Soft Magnetic Composites 89

5.1 Basic Constitutive Equations 91

5.1.1 EC Loss Density in a Cube-shaped Inclusion 91

5.1.2 Stress-dependent Magnetic Permeability 91

5.1.3 EC Losses In a Cube Subjected To Stress 92

5.2 Loss Density in SMC 92

5.2.1 Homogenization Technique 94

5.3 Model Prediction and Results 98

5.3.1 Material Parameters 98

5.3.2 Stress Effect 99

5.4 Conclusion 105

Conclusion and Perspectives 107

References 111

Appendix A EC Loss Density For Basic Shapes 119

A.1 Homogeneous Plate 120

A.2 Homogeneous Circle 121

A.3 Homogeneous Square 122

A.4 Validity Range of Frequency 125

Appendix B Energy Density 129

Appendix C Spherical Symmetry 131

Appendix D Mechanical Localization Tensor 135

Publications 137

List of figures

1.1 Boundary condition at the interface between two material domains Ω_1 and Ω_2 8
1.2 Hysteresis loop (red curve) for a nonlinear irreversible magnetic material (the blue curve is the anhysteretic curve). 10
1.3 *BH* curves for linear (red line) or nonlinear (blue curve) reversible magnetic material. 11
1.4 Magnetization curves for a nonoriented Iron-Silicon alloy subjected to a uniaxial compression applied in the direction parallel to the magnetic field [84]. 12
1.5 Sketch of homogeneous structures 14
1.6 Schematic diagram of SMC and a ferromagnetic inclusion 16
1.7 Commercial ABS motor: (left) original laminated motor; (right) improved new SMC design (Courtesy of Aisin Seiki Co Ltd). The application of SMC core brings 17% in weight reduction and a more compact design (36% shorter in length) [87]. 16
1.8 Homogenization principle 17
1.9 Effective permeability estimated by Wiener bounds (W+ and W-), Hashin–Shtrikman bounds (HS+ and HS-) and Bruggeman's model (Br). Parameters: $\mu_1 = \mu_0$, $\mu_2 = 100\,\mu_0$. 19

2.1 A 2D sketch of cylindrical inclusion. 24
2.2 A cross-section Ω in the spherical inclusion. 26
2.3 Cylindrical coordinates (ρ, ϕ, z) and spherical coordinates (r, θ, ϕ). 26
2.4 (a) 2D sketch of cubic lattice of spherical inclusions or square lattice of fiber inclusions. The domain confined by dashed lines 1-4 forms an elementary cell of periodic pattern. (b) 3D view of cubic lattice of spherical inclusions (case 1). (c) 3D view of square lattice of fiber inclusions (case 2). 33
2.5 Rotating vector potential to generate a flux density in the z direction. 34
2.6 Vector potential boundary condition to generate a flux density in the y direction. 35

2.7 Effective permeability obtained from FEM (blue squares), series expansion (red dashed line) and MG estimate (black line). (a) case 1: Cubic lattice of spheres: magnetic field loading along z-direction, (b) case 2: Square lattice of fibers: in-plane loading field along y-direction. For all calculations: lattice size $L_1 = 50\,\mu$m, $\mu_2 = 4000\mu_0$, $\mu_1 = \mu_0$, $\sigma_2 = 1.12 \times 10^7$ S/m, average flux density $B_0 = 1$ T. 36

2.8 Errors of the effective permeability generated by series expansion and MG estimate by comparing with the reference values (FEM). Configuration: the same as Fig. 2.7. 37

2.9 EC loss density as a function of inclusion volume fraction evaluated by full FEM computation (squares), by approximation (2.18) using the average magnetic field obtained by FEM (circles) and by the proposed analytical formulation (line). (a) case 1: Cubic lattice of spheres: magnetic field loading along z-direction, (b) case 2: Square lattice of fibers: in-plane loading field along y-direction. For all calculations: frequency $f = 100$ Hz, lattice size $L_1 = 50\,\mu$m, $\mu_2 = 4000\,\mu_0$, $\mu_1 = \mu_0$, $\sigma_2 = 1.12 \times 10^7$ S/m, average flux density $B_0 = 1$ T. 38

2.10 Errors on EC losses of the proposed homogenization model as a function of volume fraction ξ_2 for different frequencies. (a) case 1: Cubic lattice of spheres: magnetic field loading along z-direction, (b) case 2: Square lattice of fibers: in-plane loading field along y-direction. For all calculations: lattice size $L_1 = 50\,\mu$m, $\mu_2 = 4000\mu_0$, $\mu_1 = \mu_0$, $\sigma_2 = 1.12 \times 10^7$ S/m, average flux density $B_0 = 1$ T 40

2.11 Errors on EC losses attributed to the average field assumption in equation (2.18) as a function of volume fraction ξ_2 for different frequencies. (a) case 1: Cubic lattice of spheres: magnetic field loading along z-direction, (b) case 2: Square lattice of fibers: in-plane loading field along y-direction. For all calculations: lattice size $L_1 = 50\,\mu$m, $\mu_2 = 4000\mu_0$, $\mu_1 = \mu_0$, $\sigma_2 = 1.12 \times 10^7$ S/m, average flux density $B_0 = 1$ T. 40

2.12 EC loss density U_{SE} evaluated with the proposed approach (lines) for cases 1 and 2 and corresponding FEM results U_{FEM} (dots) as a function of the permeability contrast between matrix and inclusions. For all calculations: $f = 100$Hz, lattice size $L_1 = 50\,\mu$m, $R = 24\,\mu$m, $\mu_1 = \mu_0$, $\sigma_2 = 1.12 \times 10^7$ S/m, average flux density $B_0 = 1$ T. 42

2.13 Errors on EC losses of the proposed homogenization model as a function of the permeability contrast between matrix and inclusions for cases 1 and 2. Configuration: the same as Fig. 2.12. 43

2.14 EC loss density versus different inclusion size. The filling factor is fixed for each case: 46.32 % for case 1 and 72.38% for case 2. For all calculations: $f = 100$Hz, $\mu_1 = \mu_0$, $\mu_2 = 4000\mu_0$, $\sigma_2 = 1.12 \times 10^7$ S/m, average flux density $B_0 = 1$ T. 44

2.15 Errors on EC losses of the proposed homogenization model as a function of the inclusion size for cases 1 and 2. Configuration: the same as Fig. 2.14. . 44

3.1 Sketch of SMC in a 2D problem with in-plane magnetic field loading. 53

3.2 Spherical coordinates (r, θ, ϕ). 55

3.3 A schematic plot of EC loss density bounds as a function of volume fraction of the inclusion. 58

3.4 A schematic plot of EC loss density bounds as a function of permeability contrast. 59

3.5 A schematic plot of EC loss density bounds as a function of frequency. . . . 59

3.6 EC loss density as a function of filling factor of the inclusion. For all calculations: $f = 100$ Hz, lattice size $L_1 = 50\,\mu$m, $\mu_2 = 4000\,\mu_0$, $\mu_1 = \mu_0$, $\sigma_2 = 1.12 \times 10^7$ S/m, average flux density $B_0 = 1$ T. 62

3.7 EC loss density as a function of the permeability contrast. Parameters: $f = 100$ Hz, lattice size $L_1 = 50\,\mu$m, $\xi_2 = 72.38\%$, $\mu_1 = \mu_0$, $\sigma_2 = 1.12 \times 10^7$ S/m, average flux density $B_0 = 1$ T. 64

3.8 EC loss density as a function of the filling factor of the inclusions. Parameters: $f = 100$ Hz, lattice size $L_1 = 50\,\mu$m, $\mu_2 = 4000\,\mu_0$, $\mu_1 = \mu_0$, $\sigma_2 = 1.12 \times 10^7$ S/m , average flux density $B_0 = 1$ T. 66

3.9 EC loss density as a function of the permeability contrast. For all calculations: $f = 100$ Hz, lattice size $L_1 = 50\,\mu$m, $\xi_2 = 46.32\%$, $\mu_1 = \mu_0$, $\sigma_2 = 1.12 \times 10^7$ S/m, average flux density $B_0 = 1$ T. 67

3.10 An example of SMC with random distribution of same-size cylinders. 68

3.11 EC loss density and the corresponding bounds. Disk size: $R = 18\,\mu$m, Disk count: 16. $L_1 = 200\,\mu$m, $f = 100$ Hz, $\mu_2 = 4000\mu_0$, $\mu_1 = \mu_0$, $\sigma_2 = 1.12 \times 10^7$ S/m, average flux density $B_0 = 1$ T 69

3.12 Cross-sectional microscopic view of SMCs 70

3.13 Comparison of EC loss density from different models with experimental results. (Sinusoidal polarization, peak value: 1 T). 'Experimental' results are from [91]; 'distribution' results are the prediction from [73] considering the distributions of cross sections. 70

4.1 Sketch of periodic high concentration SMC. The domain confined by dashed lines 1-4 forms an elementary cell of the periodic pattern. 75
4.2 Flux density and eddy current density norm distribution in the inclusion. Lattice size $L_1 = 50\,\mu$m, volume fraction $\xi_2 = 97.6\%$, $\mu_2 = 4000\mu_0$, $\mu_1 = \mu_0$, $\sigma_2 = 1.12 \times 10^7$ S/m, average flux density $B_0 = 1$ T, frequency $f = 100$ Hz. 77
4.3 Ratio of standard deviation of flux density to the average flux density norm in the inclusion as a function of the filling factor. Lattice size $L_1 = 50\,\mu$m, $\mu_2 = 4000\mu_0$, $\mu_1 = \mu_0$, $\sigma_2 = 1.12 \times 10^7$ S/m, average flux density $B_0 = 1$ T, frequency $f = 100$ Hz. 77
4.4 Effective permeability (real component) from MG estimate by comparing to FEM results, and the corresponding discrepancy. (2D SMC, cross-section magnetic permeability). Lattice size $L_1 = 50\,\mu$m, $\mu_2 = 4000\mu_0$, $\mu_1 = \mu_0$, magnetostatics. 79
4.5 EC loss density from complex permeability (MG) by comparing to FEM results, and the corresponding discrepancy. Lattice size $L_1 = 50\,\mu$m, $\mu_2 = 4000\mu_0$, $\mu_1 = \mu_0$, $\sigma_2 = 1.12 \times 10^7$ S/m. The applied field is along y-axis, and the average flux density $B_0 = 1$ T, frequency $f = 100$ Hz. 80
4.6 Sketch of a schematic magnetic circuit made of SMC with square inclusions. The domain confined by red dashed lines forms an elementary cell of periodic pattern. 81
4.7 Geometry of the heterogeneous magnetic circuit calculated. 81
4.8 Geometry of equivalent virtual material (EVM) calculated. The red line in the gap is the cutline to examine the magnetic field distribution. 82
4.9 Magnetic field distributions on the homogeneous magnetic circuit. Relative Permeability: $48.9 - j4.2 \times 10^{-3}$, electric conductivity: 0. Frequency: 100 Hz. 83
4.10 H_y distribution comparison for magnetic circuit made of SMC (blue dashed line) and the homogeneous one (red line) and the corresponding errors. Parameters: same as the Fig. 4.9. 84
4.11 EC loss density (mJ/m^3) distribution on the heterogeneous magnetic circuit. 84
4.12 Distribution of the errors on the EC losses over the magnetic circuit cells, obtained by comparison between homogenization results and full field FEM calculation. 85

4.13 EC loss error distribution of homogeneous magnetic circuit by comparing with the heterogeneous one. The color bar indicates the error values (%). The labels of the map are the dimensions of the magnetic circuit (in unit: μm) 86

5.1 Sketch of cubic lattice of cubic inclusions. The domain confined by its surrounding matrix (in red cube) forms an elementary cell of periodic pattern. 93
5.2 Magnetic flux density distribution in the inclusion. Lattice size: 50 μm, volume fraction $\xi = 96\%$, $\mu_i = 4000\mu_0$, $\sigma_i = 1.12 \times 10^7$ S/m, average flux density $B_0 = 1$ T, frequency $f = 100$ Hz. 93
5.3 Ratio of standard deviation of flux density to the average flux density norm in the inclusion as a function of the filling factor. Lattice size: 50 μm, $\mu_i = 4000\mu_0$, $\sigma_i = 1.12 \times 10^7$ S/m, average flux density $B_0 = 1$ T, frequency $f = 100$ Hz. 94
5.4 Flow chart for the modeling scheme 95
5.5 Average stress in the inclusion from MT estimate (5.9) by comparison to FEM results, and corresponding discrepancy. Lattice size: 50 μm. $\overline{T}_{11} = 1$ MPa The mechanical parameters are listed in Tab. 5.1. 96
5.6 Effective permeability (real component) from MG estimate by comparing to FEM results, and the corresponding discrepancy. Lattice size: 50 μm, $\mu_i = 4000\mu_0$. 97
5.7 Parallel component of the permeability of the inclusion as a function of macroscopic stress $\mathbb{T}_a$. Lattice length = 50 μm, volume fraction of inclusion $\xi = 99\%$. Material parameters as in Tab. 5.1. 100
5.8 Parallel component of the effective relative permeability as a function of macroscopic stress $\mathbb{T}_a$. Lattice length = 50 μm, volume fraction of inclusion $\xi = 99\%$. Material parameters as in Tab. 5.1. 101
5.9 Experimental secant susceptibility under mechanical loadings [95]. 102
5.10 Normalized EC loss density as a function of macroscopic stress $\mathbb{T}_a$. (Fixed flux density B_0). Parameters: the same as Fig. 5.7 102
5.11 Parallel component of the permeability of the inclusion as a function of $\mathbb{T}_a$ for certain proportional coefficients. Parameters: the same as Fig.5.7 104
5.12 Effective permeability (parallel component) as a function of $\mathbb{T}_a$ for certain proportional coefficients. Parameters: the same as Fig. 5.11 105

A.1 Sketch of homogeneous structure 120
A.2 EC loss density in a homogeneous square as a function of frequency. $\sigma = 1.12 \times 10^7$ S/m, permeability $\mu = 4000\mu_0$; Average flux density: 1 T. 123

A.3 Discrepancies between EC loss density by the linear fitting equation (A.24) and the reference values from (A.22). 124
A.4 Distribution of normalized eddy current density of a circle along a radius (red cut line in (b)). Radius: $R = 25\,\mu$m 125
A.5 Normalized eddy current density (and the corresponding errors) as a function of the ratio between skin depth and size. 126

B.1 Phase shift between **B** and **H**, forming an ellipse in a period time. The area of this ellipse is the energy density during one time-period. 129

C.1 Sketch of the cubic lattice of spherical inclusions. 131
C.2 Induced electric field. 133

Résumé en Français

Le développement d'appareils légers, solides et peu énergivores est naturellement préférable. Dans les applications du génie électrique, les moteurs et les transformateurs utilisent des noyaux magnétiques afin de canaliser spatialement et de façon optimale le flux magnétique. Les performances de telles machines dépendent grandement des propriétés du noyau magnétique utilisé. Le noyau magnétique est généralement conçu à partir de matériaux ferromagnétiques qui, malheureusement, sont aussi de bons conducteurs électriques. Lorsqu'un conducteur est placé dans un champ magnétique alternatif, des courants de Foucault (EC – Eddy Current) naissent, entraînant des pertes Joule dans le matériau. Dans la conception et l'analyse des machines électriques, la perméabilité magnétique et les pertes sont les deux caractéristiques dominantes à prendre en considération. Les matériaux composites permettent de réaliser des matériaux combinant les attributs des différents constituants pour fournir les caractéristiques souhaitées qui ne peuvent pas être facilement obtenues à partir de l'un ou l'autre des composants individuels.

Les composites magnétiques doux (SMC – Soft Magnetic Composites), généralement composés d'inclusions ferromagnétiques intégrées dans une matrice polymère diélectrique, présentent des pertes EC faibles tout en ayant une perméabilité magnétique relativement élevée. La matrice diélectrique confine les courants de Foucault dans chaque particule, réduisant ainsi considérablement les pertes EC du composite. Une autre particularité des SMC est l'isotropie magnétique et thermique [1, 2], ce qui les rend adaptés à la construction de dispositifs électriques à structure complexe, avec des flux magnétiques tridimensionnels - en comparaison avec les structures laminées classiques. Les SMC présentent ainsi un fort potentiel pour une utilisation dans l'industrie aérospatiale, maritime et automobile en remplacement des matériaux ferromagnétiques traditionnels [3–9]. La recherche continue sur les SMC a montré une large gamme d'applications dans la conception de moteurs [10], tel que les moteurs à aimants permanents à flux transversal [11–13], les moteur à aimants permanents à flux axial [14] pour les véhicules électriques hybrides ainsi que les moteurs à induction [15]. Les SMC sont normalement fabriqués à partir de techniques issues de la métallurgie des poudres [16]. Les inclusions, sous forme de poudre, doivent être revêtues

d'une matrice diélectrique pour réduire les courants de Foucault globaux et les confiner dans chaque particule. Les particules de poudre sont généralement de forme irrégulière, avec un diamètre moyen d'environ 50 à 250 μm. Les matériaux ferromagnétiques généralement sélectionnés sont du fer pur ou des alliages à base de fer, tels que les alliages Fe-Ni (haute perméabilité), les alliages Fe-Si (résistivité électrique élevée) et les alliages Fe-Co (haute saturation magnétique) [3]. Une forte concentration d'inclusions magnétiques donne une densité plus élevée, une bonne résistance mécanique et une perméabilité magnétique élevée du composite. Les matériaux de revêtement peuvent être inorganiques ou organiques. L'époxy est souvent choisi comme matériau matriciel. Une fraction de revêtement plus élevée réduira considérablement les pertes EC, mais la performance magnétique globale sera alors diminuée. L'équilibre entre ces caractéristiques (perméabilité versus pertes) doit donc être pris en compte dans la conception de SMC.

L'étude des propriétés effectives des matériaux composites fait l'objet d'un vaste effort de recherche [17–25]. L'idée principale est de remplacer la microstructure du composite par un matériau homogène équivalent, qui peut ensuite être utilisé dans des outils d'analyse structurale standard, avec une complexité numérique réduite. Différents modèles analytiques et numériques ont été proposés.

Les techniques d'homogénéisation par la Méthode des éléments finis (FEM) [26–29] ont été introduites pour aborder ce type de problèmes électromagnétiques à différentes échelles. Diverses stratégies ont été proposées [30, 31] pour réduire le temps et les ressources de calcul dans une certaine mesure tout en maintenant la précision. Néanmoins, ces méthodes numériques ont souvent l'inconvénient d'être peu flexibles, par exemple pour des études paramétriques nécessitant de multiples calculs numériques. En outre, il est difficile de considérer les problèmes avec des contrastes élevés en propriété, nécessitant souvent un maillage raffiné, à moins que des techniques numériques spécifiques ne soient utilisées [31, 32].

Ainsi, il est crucial de développer de nouveaux modèles pour les pertes EC dans les SMC. D'autres approches basées sur des formulations analytiques et semi-analytiques ont également été étudiées. Les approches en champ moyen ont par exemple été développées pour déterminer la perméabilité magnétique effective des polycristaux ferromagnétiques [33, 34]. Des stratégies d'homogénéisation analytiques ont également été utilisées pour déterminer la permittivité effective de composites pour des applications de blindage électromagnétique [35–37]. Puisque les échelles de la taille des grains et la taille typique du dispositif sont bien séparées, ces stratégies d'homogénéisation sont un choix pertinent pour les SMC. En électromagnétisme, les techniques d'homogénéisation sont utilisées pour déterminer les propriétés électriques et magnétiques effectives des matériaux. La monographie de Si-

hvola [23] donne un aperçu utile des techniques d'homogénéisation pour les comportements des matériaux en régime quasistatique.

Les propriétés effectives sont définies comme le tenseur des propriétés reliant les champs duaux macroscopiques. A partir de lois de comportements locales (propres à chaque constituant) reliant les champs duaux locaux (par exemple le champ magnétique H et l'induction magnétique B, reliés par le tenseur de perméabilité μ), et à travers des opérations de moyenne volumique, les propriétés effectives d'un matériau composite peuvent être obtenues. Une approche simplifiée des problèmes d'homogénéisation peut être utilisée avec les approches en champs moyens. Celle-ci se contente d'une quantité limitée d'informations sur la microstructure (fractions volumiques et quelques indicateurs statistiques). Dans les cas pratiques, une connaissance complète de la microstructure des composites n'est pas nécessairement disponible, et les propriétés effectives pour le matériau homogène équivelent (EHM – equivalent homogeneous medium) ne peuvent être exactement déterminées. Néanmoins, les formules d'homogénéisation permettent de fournir des estimations ou des bornes du comportement effectif à partir des informations connues sur la microstructure. Considérons par exemple un composite biphasé avec des inclusions placées dans une matrice. La perméabilité effective d'un tel matériau se situe nécessairement entre les limites inférieures et supérieures fournies par les bornes de Wiener [19]. Des limites plus étroites peuvent être obtenues si l'information d'isotropie globale du matériau est considérée, menant aux bornes de Hashin-Shtrikman [20, 38]. Fournir des bornes du comportement effectif peut être insuffisant tant l'écart entre les bornes peut parfois être large. Il est alors utile de fournir une estimation du comportement effectif. Le formalisme de Maxwell-Garnett (MG) a été présenté en 1904 pour estimer la permittivité effective d'un EHM diélectrique isotrope pour un matériau composite fabriqué à partir d'une dispersion de particules sphériques dans un matériau hôte [18]. Ce modèle est particulièrement valide pour les composites à faible fraction volumique d'inclusions (matériaux dilués). C'est l'une des méthodes les plus utilisées pour calculer les propriétés macroscopiques des matériaux non homogènes [39–44]. L'estimation de MG est identique à la limite inférieure de Hashin-Shtrikman. Un autre modèle, celui de Bruggeman [45] permet de fournir une estimation plus pertinente pour les matériaux non dilués. Les matériaux constitutifs du matériau composite sont alors considérés comme jouant des rôles similaires (plus de distinction matrice/inclusion). En réalité, dans le modèle de Bruggeman, on suppose que les phases constitutives sont dispersées dans l'EHM lui-même. Les estimations des propriétés effectives dépendent alors seulement des propriétés des matériaux constitutifs et de leurs fractions volumiques. Le principal avantage de ces modèles réside dans leur simplicité relative (modèles analytiques ou quasi-analytiques).

Dans le cas de microstructures périodiques, la technique d'expansion asymptotique [26–29, 46] peut être utilisée. Parmi les méthodes alternatives, des expériences sur des SMC commerciaux ou des prototypes ont été menées pour étudier les propriétés magnétiques et les caractéristiques des pertes [47–49]. Mais les approches expérimentales ne conviennent pas aux processus de conception en raison des contraintes de coût et de temps.

Par conséquent, dans la phase de conception, les formules analytiques sont fortement préférées, permettant de relier de façon directe les propriétés des constituants, la microstructure et les performances attendues. De ce fait, les stratégies d'homogénéisation (quasi-)analytiques sont préférables pour les stades de conception.

Une considération supplémentaire est nécessaire pour étudier les SMC de façon pertinente. En effet, le comportement magnétique des matériaux ferromagnétiques est généralement sensible à l'application d'une contrainte mécanique [50–52]. Le couplage magnéto-mécanique peut être principalement décrit par deux aspects. L'un est la magnétostriction [53], décrivant la déformation de matériau sous l'effet d'un champ magnétique. L'autre est l'effet de la contrainte sur le comportement magnétique [54], représentant le changement de susceptibilité magnétique en fonction de la contrainte. Ces comportements peuvent être décrits par des approches phénoménologiques [55, 56] ou des modèles multi-échelles [57–59]. L'analyse des pertes dans les matériaux ferromagnétiques [60–62] ainsi que le couplage magnéto-mécanique [58, 63, 64] ont menés à de nombreuses études sur ces matériaux, tant d'un point de vue expérimental qu'en termes de modélisation. Un modèle analytique a été proposé pour décrire la dépendance de la susceptibilité magnétique à la contrainte [65]. Néanmoins, il n'existe pas de modèle précis pour prendre en compte l'effet des contraintes mécaniques sur les pertes.

Cette thèse est consacrée au développement de modèles analytiques ou semi-analytiques pour les pertes par courants de Foucault dans les composites magnétiques doux. L'examen détaillé de la distribution des champs magnétiques et électriques n'est pas la préoccupation principale. Dans la plupart des cas, on peut se contenter d'approximations raisonnables sur les champs pour déterminer les pertes par courants de Foucault d'un point de vue macroscopique. Les propriétés complexes peuvent être utilisées dans des applications électromagnétiques pour décrire les phénomènes dissipatifs. Un examen approfondi des modèles d'homogénéisation pour le comportement diélectrique utilisant la permittivité complexe peut être trouvé dans [42, 66]. Les cas 2D et 3D ont été explorés numériquement en détails. La permittivité complexe dépend des propriétés de chaque constituant, de leur fraction de volume et de leur répartition spatiale [67]. De manière analogue, la perméabilité complexe est un outil utile pour traiter les effets magnétiques à haute fréquence, par exemple dans les applications de transformateurs [68, 69]. La dissipation peut se refléter directement

dans la partie imaginaire de la perméabilité complexe [70, 71]. Dans le cas de SMC à basse fréquence, lorsque le champ magnétique induit peut être négligé, il n'y a pas de déphasage entre la densité de flux magnétique et le champ magnétique. À cet égard, la partie imaginaire de la perméabilité complexe doit être considérée comme nulle. Toutefois, les pertes EC sont présentes - tant que la fréquence n'est pas nulle. Ainsi, une partie imaginaire peut être introduite dans le tenseur de perméabilité magnétique de manière à refléter les pertes EC.

Le tenseur de perméabilité complexe peut être utilisé comme un outil mathématique pour représenter un matériau magnétique dissipatif. Dans cette étude, ce tenseur de perméabilité complexe est utilisé pour décrire les performances électromagnétiques des SMC. La partie réelle est la perméabilité effective, et la partie imaginaire reflète les pertes EC. Les modèles développés se basent sur l'étude de composites à microstructure périodique avec des inclusions circulaires ou sphériques excités par des champs magnétiques harmoniques. Si, comme c'est en général le cas, le champ dans l'inclusion n'est pas uniforme, on considère alors les champs moyens dans les différentes phases. La perméabilité complexe est une propriété matériaux, indépendante de la géométrie. Elle peut être utilisée comme une propriété constitutive dans la conception de machines utilisant des SMC. Sur la base de l'étude d'une seule inclusion dans un milieu infini, on déduit les propriétés de matériaux hétérogènes dilués et le cas général des composites est extrapolé à partir de cette approche. La densité de pertes EC dans les SMC est ensuite décrite à l'aide du tenseur de perméabilité complexe homogénéisé. L'approche est comparée aux résultats obtenus par un modèle éléments finis et les erreurs observées restent généralement inférieures à 5%. Il convient de noter que l'approche nécessite des estimations précises du tenseur de perméabilité magnétique statique efficace du matériau composite. C'est généralement la principale difficulté d'un tel modèle. On constate que l'approche tend à sous-estimer la densité de pertes EC par rapport aux résultats éléments finis et que les erreurs sont indépendantes de la fréquence sous l'hypothèse de basse fréquence.

La densité de pertes EC dans les SMC peut être approchée en estimant le champ magnétique soit à partir des moments de premier ordre (moyenne classique pour obtenir le champ moyen) soit à partir des moments du second ordre (moyenne des carrés du champ magnétique) du champ magnétique. Pour les SMC périodiques avec des inclusions circulaires ou sphériques, il a été prouvé dans cette étude que les deux approches permettent de borner les pertes EC. L'approche utilisant la moyenne du champ magnétique sous-estime la densité de pertes EC dans les SMC, fournissant ainsi une limite inférieure; alors qu'elle est surestimée dans l'approche utilisant les moments d'ordre deux, fournissant ainsi une limite supérieure. Les deux estimations sont généralement proches l'une de l'autre, fournissant

des valeurs précises pour les pertes EC tant que la perméabilité efficace est estimée avec une bonne précision. Les pertes EC peuvent ainsi être approchées, sans connaissance de la solution exacte de la distribution d'EC, ce qui simplifie l'approche par rapport à un calcul FEM complet. Quand la perméabilité effective n'est pas connue mais estimée, les pertes calculées perdent leur propriété de borne et sont simplement des estimations.

Comme exemple d'application, un circuit magnétique constitué de SMC est homogénéisé avec la méthode de la perméabilité complexe. Il est composé de SMC à haute concentration à microstructure périodique. Des calculs FEM ont été effectués sur la structure hétérogène et sur la structure avec le matériau homogène équivalent. Les répartitions du champ magnétique et des pertes EC ont été examinées et comparées entre les deux solutions. Un bon accord est observé entre la densité de pertes EC de référence (obtenue pour le transformateur hétérogène) et les valeurs calculées avec une perméabilité complexe. Les calculs montrent que l'erreur globale sur les pertes EC est très faible (moins de 0,5%) et les erreurs locales ne dépassent pas 3% généralement, sauf pour des zones très localisées du circuit (angles droits de la géométrie). On conclut alors que la méthode d'homogénéisation peut fournir une répartition des pertes EC avec une précision très satisfaisante.

En plus de cela, le comportement multi-physique des SMC est exploré. L'effet de la contrainte mécanique sur la performance magnétique et sur la densité des pertes EC est étudié pour les SMC à concentration d'inclusions ferromagnétiques élevée. A partir des perméabilités locales, et en négligeant la magnétostriction, une formule est dérivée pour la densité de pertes EC en fonction du champ magnétique macroscopique et de la contrainte mécanique. La contrainte a une influence sur la densité de pertes EC en raison de la variation du comportement magnétique du matériau ferromagnétique sous contrainte. Il est montré que la contrainte a peu d'effet sur les pertes EC dans les SMC (tout en affectant la perméabilité magnétique). On en tire une conclusion intéressante : le comportement magnétique des SMC semble être moins sensible à la contrainte mécanique que celui des matériaux ferromagnétiques homogènes habituels. Cette attente doit être confirmée par des mesures expérimentales. Dans cette étude, les pertes par hystérésis et la non linéarité du comportement ne sont pas prises en considération. Pour un comportement magnétique non-linéaire, le modèle serait bien plus complexe à mettre en œuvre. Puisque la perméabilité magnétique dépend dans ce cas du champ magnétique appliqué, une procédure itérative devrait être utilisée pour obtenir le champ moyen dans l'inclusion, puis le tenseur de perméabilité de l'inclusion, et enfin le tenseur de perméabilité effective du composite. En outre, le champ magnétique harmonique doit être échantillonné au fil du temps afin de déterminer le champ moyen final et la perméabilité de l'inclusion. La densité de pertes EC doit ensuite être intégrée sur une période de temps.

Les modèles développés ici proposent des approches directes pour déterminer les pertes EC dans les SMC à faible fréquence de travail. La perméabilité complexe contient le comportement magnétique ainsi que les pertes EC. Les approches menant aux bornes des pertes EC offrent un moyen simple de se rapprocher des pertes EC dans le composite. L'effet de la contrainte mécanique est également directement intégré dans la formule de densité de pertes EC. Les modèles sont adaptés à différents contrastes de perméabilité et sont discutés pour une gamme complète de fractions volumiques. Ils sont développés pour les SMC ayant une matrice diélectrique. Lorsque les courants de Foucault globaux dans la matrice ne peuvent plus être négligés, les modèles doivent être corrigés. Les formules de densité de pertes EC sont dérivées à partir des SMC à microstructure périodique. Pour des SMC avec des microstructures aléatoires, des estimations des pertes EC peuvent également être obtenues. Dans cette étude, la non-linéarité des matériaux ferromagnétiques, l'hystérésis et les pertes par excès ne sont pas pris en compte.

En conclusion, cette étude fournit une méthodologie pour obtenir une perméabilité complexe décrivant le comportement de matériaux ferromagnétiques linéaires. Cette méthodologie donne un accès simple aux pertes par courant de Foucault. Les perspectives à ces travaux seront de développer un modèle de perméabilité complexe générique intégrant la non-linéarité du comportement magnétique, ainsi que l'hystérésis et les pertes par excès. De plus, il serait intéressant d'intégrer un couplage magnétomécanique fort dans le modèle de la perméabilité magnétique complexe. Des expériences sont nécessaires pour valider les modèles. Le couplage magnétomécanique est souvent négligé dans les études sur les SMC, ces travaux montrent néanmoins que les contraintes mécaniques ont un effet sur le comportement des SMC. L'effet de la température sur les propriétés électromagnétiques pourrait également être pris en compte. Une formule générique pourrait être développée pour faire face aux comportements couplés des SMC en utilisant des techniques d'homogénéisation. Les travaux futurs pourraient également inclure l'application du modèle de perméabilité complexe dans les outils de dimensionnement de structure pour concevoir des moteurs et des transformateurs à base de SMC. Les dispositifs prototypes pourraient être développés et fabriqués et les performances électriques comparées à celles des machines traditionnelles. Promouvoir l'application de SMC en remplacement de l'acier stratifié dans les appareils électriques afin d'économiser de l'énergie sera une tâche difficile mais importante.

General Introduction

Industrial development relies a lot on lighter, stronger and more energy efficient devices. Motors and transformers are widely used in Electrical Engineering applications. The fundamental component of a static or rotating device is its magnetic core, designed to amplify and to control the direction of the magnetic flux that in turn determines a machine's performance. This function requires a high saturation magnetization. The magnetic core is designed with ferromagnetic materials, which, unfortunately, are generally highly conductive. When a conductor experiences an alternative magnetic field, eddy currents (EC) circulate, resulting in losses. In the design and analysis of electrical machines, magnetic performance and losses are the two dominant points to be taken into consideration.

Composite materials offer a balance between the two points. Composites combine the attributes of constituents to provide desired features which cannot readily be obtained from either of the individual components. Soft Magnetic Composites (SMC), typically composed of ferromagnetic inclusions embedded in a dielectric polymer matrix, possess the characteristics of low level of EC losses when they are subjected to electromagnetic loadings. SMC have the potential for widespread usage in aerospace, naval and automotive industries as a perspective replacement to traditional metal materials owing to designable magnetic and thermal properties and comparatively low EC losses [3–9].

In order to design electrical machines using SMC as the magnetic material, the optimization of material properties is crucial. First, a high magnetic permeability is required. Pure iron or Fe-alloys are then good candidates for the particle material. Second, low EC losses are needed and can be achieved thanks to the dielectric coating which significantly cuts down the induced EC. Epoxy is often chosen as the matrix material. These constituents exhibit a very high contrast both in electric conductivity and magnetic permeability. This high property contrast is a serious challenge for homogenization techniques developed in order to deduce the effective properties of heterogeneous materials. However, these homogenization techniques are required to design optimal electromagnetic devices based on SMC.

The study of the effective property of composite has been a large area of research [17–25]. Analytical and numerical models were proposed. Powerful computing capacity enabled the rapid development of numerical strategies. One of the most commonly employed is the Finite Element Method (FEM). FEM provides a full-field approach to electromagnetic problems. Effective properties and losses can then be post-processed. But in the case of SMC, the microstructure has to be finely meshed, which brings significant numerical burden and instabilities in FEM approach. FEM homogenization techniques [26–29] have been introduced to tackle electromagnetic problems with different scales. The main idea is to replace periodic microstructures of the composite by an equivalent homogeneous material, which can then be used in standard structural analysis tools, with a reduced numerical complexity. Various strategies derived from standard FEM have been proposed [30, 31]. These methods reduce the computational time and resources to a certain extent while maintaining accuracy. Nevertheless, these numerical methods still have the drawback of being not very flexible, for instance for parametric studies that require multiple numerical computations. Also, it is difficult to address the problem of high property contrast unless specific numerical techniques are used [31, 32]. Thus, it is crucial to develop new models for EC losses in SMC.

On the other hand, analytical and semi-analytical approaches are widely studied. Mean field methods have for instance been developed for the determination of the effective magnetic permeability of ferromagnetic polycrystals [33, 34]. Analytical homogenization strategies have also been used for the determination of the effective permittivity of composites for shielding applications [35–37]. These analytical or semi-analytical models pour attention only on the effective constitutive properties and do not provide an insight into losses characteristics of composites.

Among alternative methods, experiments on commercial SMC or prototypes have been conducted to study the magnetic properties and lossy characteristics [72–74]. But experimental approaches are not suitable for design processes due to the cost and time constraints.

Therefore, in the phase of design, analytical formulas are greatly required, by which the selection of constituents can be easily realized for the desired performance. Thus a constitutive study of SMC is critically important. In addition, at this stage, the overall performance and the balance between properties are the utmost concerns. Therefore homogenization strategy is thus a preferable choice for this constitutive study.

In addition, the magnetic behavior of ferromagnetic materials is usually sensitive to the application of mechanical stress [50–52]. Ferromagnetic material loss analysis [60–62] and magnetomechanical behavior [58, 63, 64] have attracted widely research attention in their

respective branches. An analytical model has been proposed to describe the dependence of the magnetic susceptibility to stress [65]. Still, there is no accurate model to take care of the loss characteristics under mechanical stress applications. For SMC, since the matrix is nonmagnetic and dielectric, the magneto-mechanical coupling in the ferromagnetic inclusion is of concern.

This thesis is devoted to developing analytical or semi-analytical models for eddy current loss in soft magnetic composites. Detailed examinations of the magnetic and electric field distributions are not the most crucial concern, and in most cases, some reasonable approximations of the field are enough to determine the eddy current loss from a macroscopic point of view. In this thesis, homogenization techniques are applied to determine the magnetic permeability and EC losses of SMC.

Outline of the manuscript

This present thesis is elaborated in five chapters:

The first chapter introduces Maxwell's equations, constitutive relations, the concept and characteristics of Soft Magnetic Composites, and homogenization strategies.

In chapter 2, a complex permeability is proposed to characterize both the magnetic behavior (real component) and loss characteristic (imaginary component). This complex permeability is deduced based on an average field approach.

In chapter 3, EC loss bounds are analytically derived for simple geometries.

Chapter 4 provides an application example. A transformer made of high concentration SMC is considered. The complex permeability model is applied to the calculation of the transformer.

Chapter 5 consists in a discussion of the effect of stress on the magnetic performance and EC losses of SMC. EC loss density as a function of macroscopic stress and magnetic field is presented.

In the end, some concluding remarks and perspectives are given.

Chapter 1

Basic Equations for the Modeling of Soft Magnetic Composites

Contents

1.1 Maxwell's Equations **7**

1.2 Constitutive Relations **8**

1.2.1 Magnetic Behavior 9

1.2.2 Mechanical Behavior 11

1.2.3 Magneto-Mechanical Behavior 12

1.3 Eddy Current Losses **13**

1.3.1 EC Loss Density Definition 13

1.3.2 EC Loss Density of Homogeneous Structures 14

1.4 Soft Magnetic Composites **15**

1.4.1 EC Loss Density of SMC 17

1.5 Homogenization Techniques **17**

1.6 Conclusion **20**

In order to understand the electromagnetic behavior of Soft Magnetic Composites (SMC), it is necessary to take into consideration the constitutive behavior of different phases of the composites.

The aim of this chapter is to synthesize the theoretical formulas to model the electromagnetic behavior of SMC. Maxwell's equations are first introduced. The boundary conditions are derived at the interface, which express the continuity of electromagnetic fields across the boundary between two media. Material constitutive relations are introduced in section 1.2. The eddy current (EC) loss density is then defined for conductive materials. Formulas for EC loss density are deduced for simple homogeneous structures and simplified at low frequency in section 1.3. An introduction on Soft Magnetic Composites is given in section 1.4. The final section presents homogenization techniques for the determination of effective properties of composite materials.

1.1 Maxwell's Equations

Electromagnetic (EM) theory can be regarded as the study of fields produced by electric charges at rest and in motion. Dynamic or time-varying fields are usually due to accelerated charges or time-varying currents [75]. Electromagnetism studies the coupling phenomenon between the electric field and magnetic field. The pioneering physicists, Ampère and Faraday, among others, conducted experiments on electricity and magnetism. These experimental observations were summed up by James Clerk Maxwell in four mathematical formulas [76–78]:

$$\nabla \times \mathbf{E} = -\frac{\partial \mathbf{B}}{\partial t} \qquad \text{Maxwell-Faraday} \tag{1.1a}$$

$$\nabla \times \mathbf{H} = \mathbf{J} + \frac{\partial \mathbf{D}}{\partial t} \qquad \text{Maxwell-Ampère} \tag{1.1b}$$

$$\nabla \cdot \mathbf{D} = \rho \qquad \text{Gauss electric} \tag{1.1c}$$

$$\nabla \cdot \mathbf{B} = 0 \qquad \text{Gauss magnetic} \tag{1.1d}$$

where ρ (C/m^3) represents the volume density of free electric charges. The four fields **E**, **H**, **B**, and **D** are respectively the electric field (V/m), the magnetic field (A/m), the magnetic flux density (T) and the displacement flux density (C/m^2). **J**(A/m^2) is the electric current density. Maxwell's equations are first-order linear coupled differential equations relating the vector field quantities to each other. They unify the four fields **E**, **H**, **B**, and **D** in a system of partial differential equations. The charge density ρ and the current density **J**

comply with the continuity equation,

$$\nabla \cdot \mathbf{J} + \frac{\partial \rho}{\partial t} = 0 \tag{1.2}$$

which expresses the conservation of the electric charge. Equations (1.1a)–(1.1d) are solved in a bounded subdomain Ω of the Euclidean space $\mathbb{R}^3$.

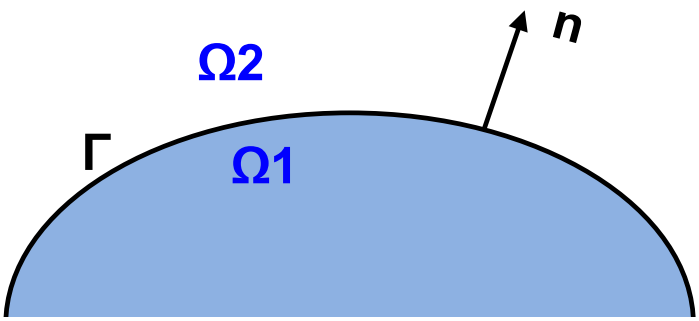

Fig. 1.1 Boundary condition at the interface between two material domains Ω_1 and Ω_2

The interface Γ separates two different materials Ω_1 and Ω_2, shown in Fig. 1.1. Electromagnetic fields can be discontinuous at the interface. The fields in Ω_1 and Ω_2 are distinguished by the subscript 1 and 2, respectively. A unit normal vector $\mathbf{n}$ is directed from Ω_1 to Ω_2. Denote the surface current density vector $\mathbf{K}$ and surface charge density ρ_S on the interface Γ. The boundary conditions can be easily deducted from the integral form of Maxwell equations. They are [75, 77]

$$\text{on } \Gamma, \quad \begin{cases} (\mathbf{E}_1 - \mathbf{E}_2) \times \mathbf{n} = 0 & \text{(1.3a)} \\ (\mathbf{H}_1 - \mathbf{H}_2) \times \mathbf{n} = \mathbf{K} & \text{(1.3b)} \\ (\mathbf{D}_1 - \mathbf{D}_2) \cdot \mathbf{n} = \rho_S & \text{(1.3c)} \\ (\mathbf{B}_2 - \mathbf{B}_1) \cdot \mathbf{n} = 0 & \text{(1.3d)} \end{cases}$$

These equations show the continuity of the tangential component of $\mathbf{E}$ (1.3a) and of the normal component of $\mathbf{B}$ (1.3d) whereas the tangential component of $\mathbf{H}$ (1.3b) and the normal component of $\mathbf{D}$ (1.3c) are discontinuous respectively by $\mathbf{K}$ and ρ_S on the boundary.

1.2 Constitutive Relations

The distribution of electromagnetic fields also depend on the medium properties characterized by the constitutive parameters: magnetic permeability μ (H/m), electric conductivity

$\mathbb{\sigma}$ (S/m) and dielectric permittivity $\mathbb{\epsilon}$ (F/m). These properties are generally in the form of second order tensor. These tensors are symmetric and therefore can be expressed with 6 coefficients:

$$\mathbb{\mu} = \begin{bmatrix} \mu_{11} & \mu_{12} & \mu_{13} \\ \mu_{12} & \mu_{22} & \mu_{23} \\ \mu_{13} & \mu_{23} & \mu_{33} \end{bmatrix} \tag{1.4}$$

for the magnetic permeability tensor (the same form for the conductivity and permittivity tensors). For the isotropic case, the magnetic behavior is described by a scalar μ:

$$\mathbb{\mu} = \mu \mathbb{I} \tag{1.5}$$

where $\mathbb{I}$ is the second order identity tensor.

The constitutive laws are the formulas that link the fields through the material properties:

$$\mathbf{B} = \mathbb{\mu} \cdot \mathbf{H} \tag{1.6a}$$

$$\mathbf{D} = \mathbb{\epsilon} \cdot \mathbf{E} \tag{1.6b}$$

$$\mathbf{J} = \mathbb{\sigma} \cdot \mathbf{E} \tag{1.6c}$$

These relations together with Maxwell equations (1.1) and well-posed boundary conditions close the electromagnetic problems.

1.2.1 Magnetic Behavior

In vacuum the constitutive magnetic law is:

$$\mathbf{B} = \mu_0 \mathbf{H} \tag{1.7}$$

with $\mu_0 = 4\pi \times 10^{-7}$ (H/m) the vacuum permeability. For linear magnetic materials with magnetic susceptibility tensor $\mathbb{\chi}$, the degree of magnetization $\mathbf{M}$ is proportional to the magnetic field $\mathbf{H}$ by:

$$\mathbf{M} = \mathbb{\chi} \cdot \mathbf{H} \tag{1.8}$$

so that the magnetic constitutive relation is:

$$\mathbf{B} = \mu_0(\mathbf{M} + \mathbf{H}) = \mu_0(\mathbb{I} + \mathbb{\chi}) \cdot \mathbf{H} = \mathbb{\mu} \cdot \mathbf{H} \tag{1.9}$$

In the case of isotropic materials, the magnetic susceptibility does not depend on the direction of the external field. Thus it becomes a scalar quality ($\chi = \chi\mathbb{I}$). In vacuum, $\chi = 0$. Materials with small positive susceptibility are called paramagnetic. In this case, the magnetic field in the material is strengthened by the induced magnetization. On the other hand, if $\chi < 0$, the material is diamagnetic. In this case, the magnetic field in the material is weakened by the induced magnetization. The susceptibility values of the paramagnetic and diamagnetic materials are small [52, 79, 80].

Ferromagnetic materials have a large positive susceptibility to an external magnetic field. They exhibit nonlinear behavior (susceptibility depends on the applied magnetic field) and possible hysteretic behavior, shown in Fig. 1.2.

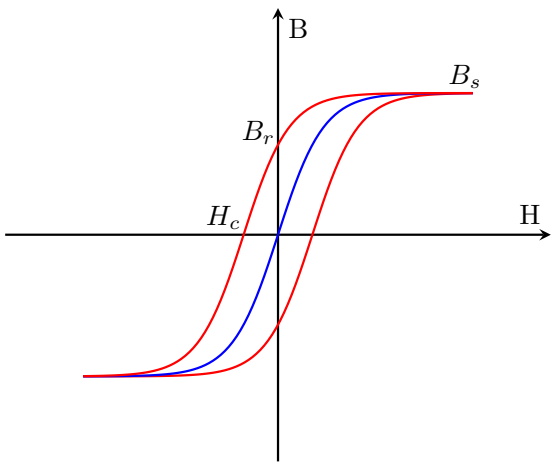

Fig. 1.2 Hysteresis loop (red curve) for a nonlinear irreversible magnetic material (the blue curve is the anhysteretic curve).

When a ferromagnetic material is magnetized in one direction, it will not relax back to zero magnetization when the imposed field is removed. The remaining flux density is called remanent induction B_r. It must be driven back to zero by the coercive magnetic field H_c in the opposite direction. As the imposed magnetic field increase, the flux density reaches saturation B_s. According to the values of their coercive magnetic field, ferromagnetic materials can be classified into two categories. Materials which maintain their magnetization and are difficult to demagnetize are called hard magnetic materials. These materials find their greatest use in permanent magnets. On the contrary, soft ferromagnetic materials have a small coercive magnetic field (typically less than 10^3A/m), which results in low amount of hysteresis loss. The constitutive relation for soft magnetic materials is roughly approximated by the anhysteretic curve [81, 82]. For low level of magnetic field, the soft magnetic material can be further approximated as linear, as shown in Fig. 1.3. In this manuscript, the magnetic materials will be considered linear.

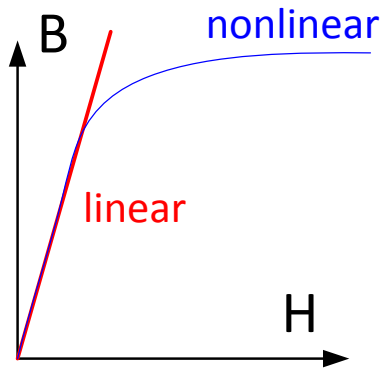

Fig. 1.3 *BH* curves for linear (red line) or nonlinear (blue curve) reversible magnetic material.

1.2.2 Mechanical Behavior

The mechanical behavior that links the strain tensor $\mathbb{S}$ (second-order) and the stress tensor $\mathbb{T}$ (second-order) has the form:

$$\mathbb{T} = \mathscr{C} : \mathbb{S} \tag{1.10}$$

where $\mathscr{C}$ is a fourth-order stiffness (elasticity) tensor. Using Einstein notation, (1.10) writes: $T_{ij} = C_{ijkl} S_{kl}$. The stiffness tensor $\mathscr{C}$ is a material property to represent the resistance to deformation in response to an applied force. It is constant in a linear elastic material. The stress tensor $\mathbb{T}$ is the force per unit area on a body [83].The intensity of distortion is known as strain tensor $\mathbb{S}$. It is a dimensionless tensor of rank 2.

Due to the inherent symmetries of $\mathscr{C}$ ($C_{ijkl} = C_{jikl} = C_{ijlk} = C_{jilk} = C_{klij}$), the stiffness tensor can be represented by a symmetric second order tensor. For orthotropic materials which have three orthogonal planes of symmetry, the stiffness tensor can be described by 9 independent parameters:

$$\mathbb{C}_{\text{orth}} = \begin{bmatrix} C_{11} & C_{12} & C_{13} & 0 & 0 & 0 \\ C_{12} & C_{22} & C_{23} & 0 & 0 & 0 \\ C_{13} & C_{23} & C_{33} & 0 & 0 & 0 \\ 0 & 0 & 0 & C_{44} & 0 & 0 \\ 0 & 0 & 0 & 0 & C_{55} & 0 \\ 0 & 0 & 0 & 0 & 0 & C_{66} \end{bmatrix} \tag{1.11}$$

For isotropic media (which have the same physical properties in any direction), the stiffness tensor $\mathbb{C}$ can be reduced to only two independent numbers, the bulk modulus κ and the shear modulus G, that quantify the material's resistance to changes in volume and to

shearing deformations, respectively.

$$\mathbb{C}_{\text{iso}} = \begin{bmatrix} \kappa + \frac{4}{3}G & \kappa - \frac{2}{3}G & \kappa - \frac{2}{3}G & 0 & 0 & 0 \\ \kappa - \frac{2}{3}G & \kappa + \frac{4}{3}G & \kappa - \frac{2}{3}G & 0 & 0 & 0 \\ \kappa - \frac{2}{3}G & \kappa - \frac{2}{3}G & \kappa + \frac{4}{3}G & 0 & 0 & 0 \\ 0 & 0 & 0 & 2G & 0 & 0 \\ 0 & 0 & 0 & 0 & 2G & 0 \\ 0 & 0 & 0 & 0 & 0 & 2G \end{bmatrix} \tag{1.12}$$

In this work, the elastic property of material will be considered isotropic.

1.2.3 Magneto-Mechanical Behavior

The magneto-mechanical coupling can be principally described by two aspects:

- Magnetostriction [53]: strain induced by magnetization.
- Effect of stress [54]: change of the magnetic susceptibility of a material when subjected to a mechanical stress.

The corresponding behaviors are generally described by phenomenological approaches [55, 56] or multi-scales models [57–59]. The magnetic behavior of ferromagnetic material is sensitive to the application of mechanical stress [51, 52]. Fig. 1.4 gives an example of mag-

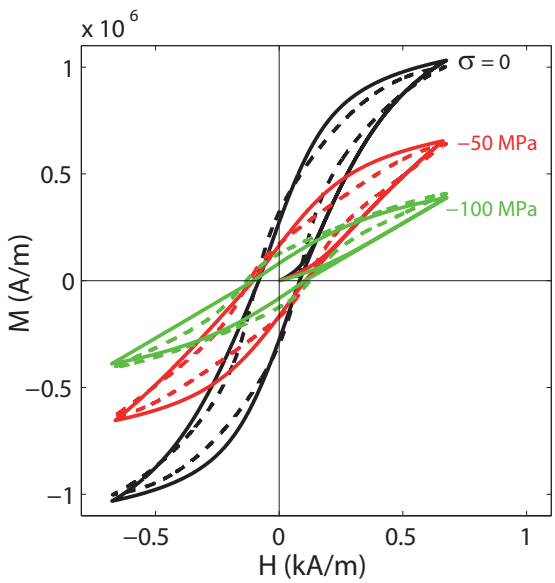

Fig. 1.4 Magnetization curves for a nonoriented Iron-Silicon alloy subjected to a uniaxial compression applied in the direction parallel to the magnetic field [84].

netization curves for a nonoriented Iron-Silicon alloy subjected to a uniaxial compression applied in the direction parallel to the magnetic field [84].

Consider a ferromagnetic material that is subjected to a magnetic field H in the direction $\mathbf{x}\,(\mathbf{H} = H\,\mathbf{x})$ and simultaneously a stress state $\mathbb{T}$:

$$\mathbb{T} = \begin{bmatrix} T_{11} & T_{12} & T_{13} \\ T_{12} & T_{22} & T_{23} \\ T_{13} & T_{23} & T_{33} \end{bmatrix} \tag{1.13}$$

An analytical magneto-elastic model has been proposed in [65]. The magnetization of the ferromagnetic core can be written in the form:

$$\mathbf{M} = \frac{A_1 \sinh(\kappa H)}{A_1 \cosh(\kappa H) + A_2 + A_3} M_s \mathbf{x} \tag{1.14}$$

with

$$A_i = \exp(\alpha T_{ii}),\ i = \{1, 2, 3\} \tag{1.15}$$

where M_s is the saturation of magnetization of the material. α and κ are material constants.

1.3 Eddy Current Losses

1.3.1 EC Loss Density Definition

Once the Maxwell's equations are solved with constitutive laws and boundary conditions, the distribution of electric field $\mathbf{E}$ and magnetic field $\mathbf{H}$ can be obtained. In a conductor Ω of conductivity σ there arises eddy current $\mathbf{J}_{\text{eddy}} = \sigma \cdot \mathbf{E}$, which results in EC losses in the material. In a harmonic electromagnetic problem, the EC loss density U is defined as the Joule losses dissipated per unit volume during a wave period:

$$U = \frac{\langle \mathbf{E}^* \cdot \sigma \cdot \mathbf{E} \rangle}{2f} \tag{1.16}$$

where f is the working frequency. The superscript "*" refers to the conjugate transpose operator and the operator $\langle \cdot \rangle$ denotes a volume average over the domain Ω by $\langle \cdot \rangle = \frac{1}{V} \int_V \cdot \, \mathrm{d}V$, where V is the volume of Ω.

The EC losses increase the temperature of the magnetic material. On the one hand, EC can be used in the case of induction heating. On the other hand, the heat represents a major source of energy loss in AC machines like transformers, generators, and motors. The

heat must be safely dissipated otherwise it would deteriorate the working performance or cause a risk of failure due to local overheating or thermal cycling.

1.3.2 EC Loss Density of Homogeneous Structures

Consider an isotropic, homogeneous and linear material of permeability μ, electric conductivity σ, and permittivity ϵ. The material is submitted to a harmonic magnetic field $\mathbf{H}$ of frequency f (angle frequency: $\omega = 2\pi f$). Combining Maxwell's equations with constitutive laws of material, the problem becomes a Poisson equation,

$$\nabla \times \nabla \times \mathbf{H} = -j\omega\mu(j\omega\epsilon + \sigma)\mathbf{H} \tag{1.17}$$

The definition of EC loss density in (1.16) is a general one. It applies for any frequency. Nevertheless, in the following formula derivation, quasistatics is assumed meaning that the frequency is low enough so that the induced magnetic field generated by the electric field can be ignored.

When a structure is homogeneous, Maxwell's equations (1.1) can be analytically solved for some basic 2D shapes, for instance, a plate, a circle, and a square, as shown in Fig. 1.5.

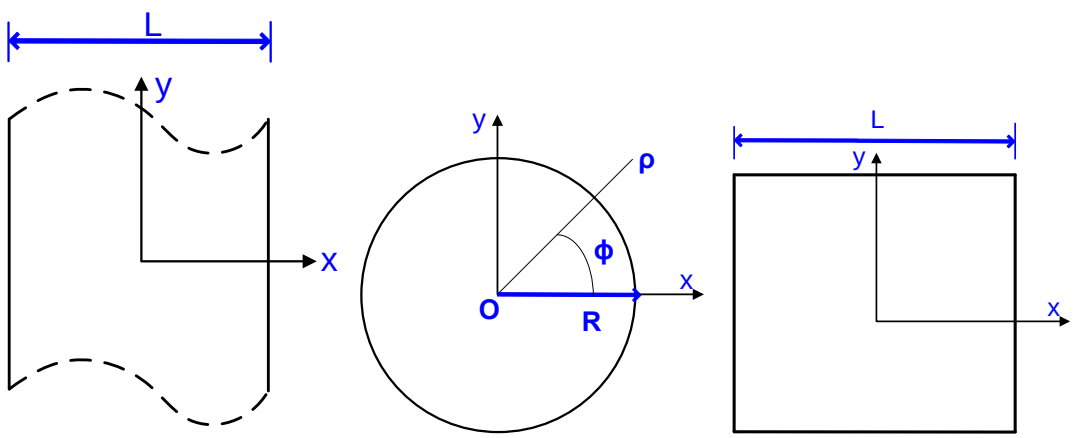

(a) Plate (b) Circle (c) Square

Fig. 1.5 Sketch of homogeneous structures

Since the domain is cut from 3D structure with infinite dimension along the z-axis, the magnetic field and the induced electric field are z-invariant,

$$\frac{\partial \mathbf{H}}{\partial z} = 0 \quad \text{and} \quad \frac{\partial \mathbf{E}}{\partial z} = 0 \tag{1.18}$$

Let's apply a magnetic field $\mathbf{H} = [0, 0, H_z]^t$ on the domain Ω, where the superscript t indicates a matrix transpose, and consider a low frequency such that $\omega\epsilon \ll \sigma$. Denoting $k^2 = -j\omega\mu\sigma$, the Poisson equation (1.17) becomes,

$$\nabla^2 H + k^2 H = 0 \tag{1.19}$$

subject to the Dirichlet boundary condition $H|_{\partial\Omega} = H_z$ with $\partial\Omega$ denoting the boundary of the domain. According to the boundary condition and z-invariance, and considering null current flow in the fiber, we have,

$$E_z = 0 \quad \text{and} \quad J_z = 0 \tag{1.20}$$

To solve (1.19) in a domain of one of the basic shapes, shown in Fig. 1.5, the magnetic field and electric field can be obtained. Therefore, the eddy current density has the form:

$$U_{\text{plate}} = \frac{1}{6}\pi^2 f\,\sigma\,\mu^2 H_z^2 L^2 \tag{1.21a}$$

$$U_{\text{circle}} = \frac{1}{4}\pi^2 f\,\sigma\,\mu^2 H_z^2 R^2 \tag{1.21b}$$

See Appendix A for detailed derivations. As for the square-shaped material, a simple form as (1.21) can not be directly obtained. Nevertheless, since the proportional relationship holds [85, 86]:

$$U \propto f\,\sigma\,\mu^2 H_z^2 L^2, \tag{1.22}$$

the EC loss density of a square-shaped material can be approximated as:

$$U_{\text{square}} = \frac{9}{128}\pi^2 f\,\sigma\,\mu^2 H_z^2 L^2 \tag{1.23}$$

See the detailed steps and the errors of this approximation in Appendix A.

1.4 Soft Magnetic Composites

Soft Magnetic Composites (SMC) consist of ferromagnetic inclusions embedded in a dielectric polymer matrix, as shown in Fig. 1.6. The unique properties of SMC materials include magnetic and thermal isotropy [1, 2], making them suitable for constructions of electrical devices with complex structure and three-dimensional magnetic flux path. SMC have the advantages of low core losses and high magnetic permeability at various frequency ranges.

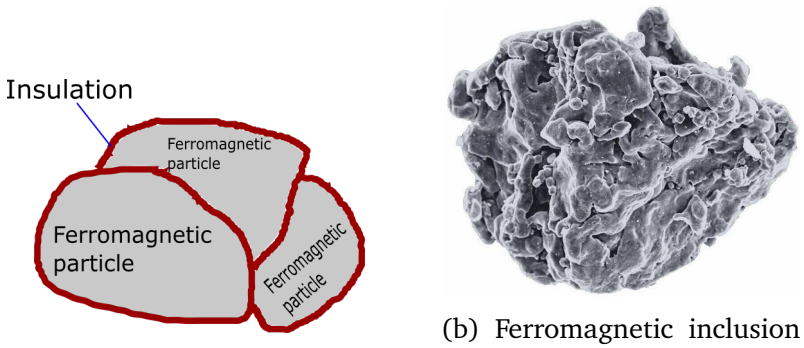

(a) SMC sketch

(b) Ferromagnetic inclusion (Courtesy of Höganäs)

Fig. 1.6 Schematic diagram of SMC and a ferromagnetic inclusion

Continuous research on SMC has shown a wide range of applications in motor design [10], such as PM transverse flux motor [11–13], axial flux PM motor [14] for hybrid electric vehicles, and induction motor [15]. An example of the benefits by switching laminated steel to SMC is indicated in Fig. 1.7. It is a BDC-motor for Anti-lock Braking Systems (ABS).

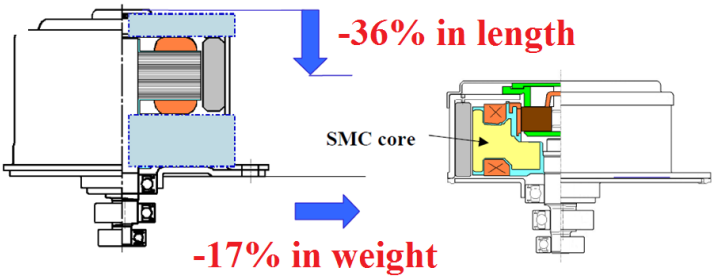

Fig. 1.7 Commercial ABS motor: (left) original laminated motor; (right) improved new SMC design (Courtesy of Aisin Seiki Co Ltd). The application of SMC core brings 17% in weight reduction and a more compact design (36% shorter in length) [87].

SMC are normally fabricated by conventional Power Metallurgy (P/M) techniques combined with secondary operations followed by an annealing procedure to control grain size and to increase the magnetic permeability [16]. The powder cores have to be coated with a dielectric matrix to reduce global eddy currents and to confine them within each particle. The powder particles are generally in irregular shapes but roughly globular particles ranging in an average diameter from about 50 to 250 μm. The commonly selected ferromagnetic materials are pure iron or iron-based alloys, such as Fe-Ni alloys (high permeability), Fe-Si alloys (high electrical resistivity) and Fe-Co alloys (high magnetization saturation) [3]. High concentration of magnetic inclusions yields higher density, mechanical strength, and magnetic permeability of the composite. The coating materials can be inorganic or organic. Higher volume fraction of coatings will significantly decrease the

EC losses, whereas the density and overall magnetic performance will be simultaneously sacrificed. The balance of these properties should be considered in designing SMC.

1.4.1 EC Loss Density of SMC

Eddy currents occur in the ferromagnetic inclusions when the applied magnetic field changes with time. Since the matrix is dielectric, EC occurs only in the inclusions, the macroscopic EC (flowing in the matrix) being negligible. Denote U_{inc} the EC loss density of the inclusions. From the perspective of the whole composite materials, the EC loss density U_{SMC} is then

$$U_{\text{SMC}} = \xi_{\text{inc}} U_{\text{inc}} \tag{1.24}$$

with ξ_{inc} the volume fraction of the inclusions.

1.5 Homogenization Techniques

In mathematical terms, a material is homogeneous if its constitutive parameters are independent of space variables. Homogenization theory is a mathematical formalism widely applied in the study of composite materials. The aim of homogenization is to replace the highly heterogeneous material by an Equivalent Homogeneous Material (EHM), as shown in Fig. 1.8. The EHM should provide the same macroscopic response as the composite when

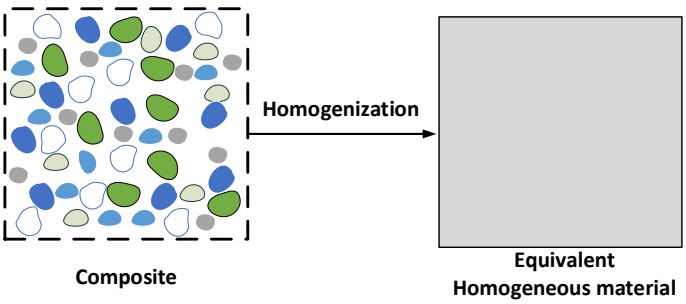

Fig. 1.8 Homogenization principle

the macroscopic loadings are the same. In electromagnetics, homogenization techniques are used to determine the effective electric and magnetic properties of materials. Sihvola's monograph [23] gives a useful overview of homogenization techniques in quasistatics.

Constitutive relations (1.6) are local, meaning that each equality holds at each point in space. The material can be homogeneous but not the field inside it. The effective

magnetic permeability, $\tilde{\mathbb{\mu}}$, is defined to build the relationship between the macroscopic average magnetic field, $\overline{\mathbf{H}}$ and flux density, $\overline{\mathbf{B}}$,

$$\overline{\mathbf{B}} = \tilde{\mathbb{\mu}} \cdot \overline{\mathbf{H}} \tag{1.25}$$

Likewise, effective conductivity and effective permittivity can be defined. The effective properties can be obtained by homogenization strategy with a limited quantity of microstructure information.

In the general case, a complete knowledge of the microstructure of composites is not provided, so that exact effective properties for EHM cannot be determined. In that case, certain bounds can be derived for the effective properties. Consider a biphase composite with inclusions of permeability μ_2 embedded in a matrix of permeability μ_1. Denote ξ the filling factor of the inclusion and a tilde symbol indicates the effective property of the composite. The effective permeability $\tilde{\mu}$ necessarily lies between Wiener lower and upper bounds [19]:

$$\tilde{\mu}_{\mathrm{W}-} = \frac{1}{\frac{\xi}{\mu_2} + \frac{1-\xi}{\mu_1}} \tag{1.26a}$$

$$\tilde{\mu}_{\mathrm{W}+} = \xi\,\mu_2 + (1-\xi)\,\mu_1 \tag{1.26b}$$

Tighter bounds on $\tilde{\mu}$ for isotropic composites are given by the Hashin–Shtrikman bounds. For the case of three-dimensional composite, the bounds have the forms (assuming $\mu_1 < \mu_2$) [20, 38]:

$$\tilde{\mu}_{\mathrm{HS}-} = \frac{(1+2\xi)\mu_2 + 2(1-\xi)\mu_1}{\xi\mu_2 + (2+\xi)\mu_1}\mu_1 \tag{1.27a}$$

$$\tilde{\mu}_{\mathrm{HS}+} = \frac{2\xi\mu_2 + (3-2\xi)\mu_1}{(3-\xi)\mu_2 + \xi\mu_1}\mu_2 \tag{1.27b}$$

which were derived on the basis of energy considerations, using a variational method for isotropic composites.

For composites with fiber inclusions, the composite can be viewed as two-dimensional. The perpendicular (to the cross-section) component of the effective permeability tensor can be obtained by Wiener upper bound:

$$\tilde{\mu}_z = \tilde{\mu}_{\mathrm{W}+} = \xi\,\mu_2 + (1-\xi)\,\mu_1 \tag{1.28}$$

This model works for fiber inclusion case (the length is much greater than the cross-section size) and provides an exact effective permeability value.

Maxwell-Garnett (MG) formalism was presented in 1904 to estimate the effective permittivity of an isotropic dielectric EHM for a composite material made from a dispersal of spherical particles in a host material [18]. This model is suitable for composites with low volume fraction ξ. It is one of the most widely used methods for calculating the macroscopic properties of inhomogeneous materials [39–44]. The effective permeability has the form:

$$\tilde{\mu}_{\mathrm{MG}} = \mu_1 + \frac{\xi\mu_1(\mu_2 - \mu_1)}{\mu_1 + N(1-\xi)(\mu_2 - \mu_1)} \tag{1.29}$$

where N is depolarization coefficient: $N = \frac{1}{3}$ for spherical inclusion. In this case, MG estimate is equivalent to Hashin–Shtrikman lower bound. MG model can also be applied to retrieve the parallel component (in-plane) of effective permeability tensor of composite with fiber inclusion, using a depolarization coefficient $N = \frac{1}{2}$, and even the perpendicular component with $N = 0$.

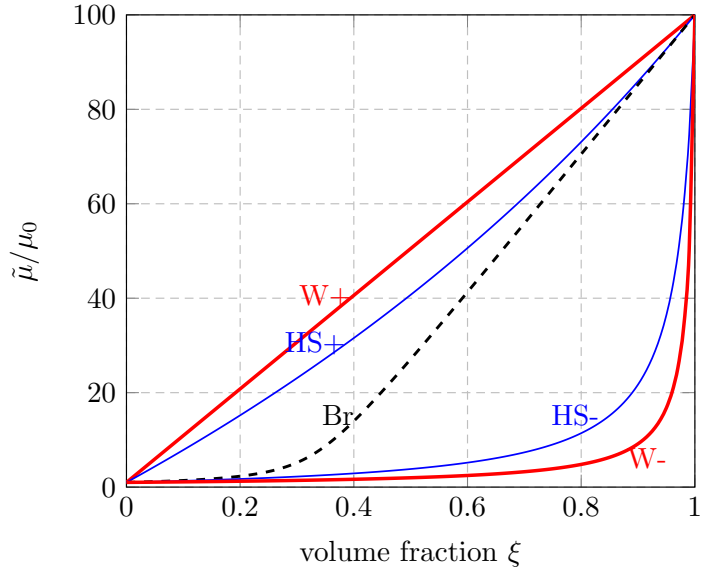

Fig. 1.9 Effective permeability estimated by Wiener bounds (W+ and W-), Hashin– Shtrikman bounds (HS+ and HS-) and Bruggeman's model (Br). Parameters: $\mu_1 = \mu_0$, $\mu_2 = 100\,\mu_0$.

Bruggeman's model [45] is not limited to low concentration of inclusions. The two constituent materials in a composite material play the same role and they are symmetrically treated either as the inclusion or the matrix. Actually, in the Bruggeman's model, particles of all constituent materials are assumed to be dispersed in the EHM itself. The formula for spherical scatters has the form:

$$\xi \frac{\mu_2 - \tilde{\mu}}{\mu_2 + 2\tilde{\mu}} + (1-\xi)\frac{\mu_1 - \tilde{\mu}}{\mu_1 + 2\tilde{\mu}} = 0 \tag{1.30}$$

The effective property estimates (bounds) depend on the constitutive properties of the constituent materials and their volume fractions. The main advantage of these models lies in their relative simplicity. Calculations of effective permeability by these estimates as a function of volume fraction are plotted in Fig. 1.9.

In addition to these analytical homogenization approaches, numerical homogenization techniques [26–29, 46] have been introduced to tackle electromagnetic problems with different scales. In the case of periodic microstructures, the asymptotic expansion technique [47–49] can also be used.

1.6 Conclusion

The Maxwell's equations and constitutive relations presented in this chapter characterize the electromagnetic problem. When boundary conditions are imposed on a SMC, the electromagnetic behavior in SMC can theoretically be determined. However, the complexity of such an approach is usually too high. Homogenization approaches can provide solutions analytically with reasonable approximations. The effective properties and loss features can be obtained, which allow for the optimization in the design of structures using SMC.

Chapter 2

EC Losses Modeling of Periodic Soft Magnetic Composites with Cylindrical or Spherical Inclusions Using a Complex Magnetic Permeability

Contents

2.1 EC Loss Density of Single Inclusion **23**

2.1.1 Cylindrical Inclusion 24

In-plane field 24

Perpendicular field 25

2.1.2 Spherical Inclusion 25

2.2 EC Loss Density of SMC **27**

2.3 Effective Permeability of SMC **29**

2.3.1 MG Estimate 29

2.3.2 Series Expansion Estimate 30

2.4 Complex Permeability Definition **30**

2.4.1 Complex Permeability of Single Inclusion 32

2.4.2 Complex Permeability of SMC 32

2.5 Validation using FEM computations **33**

2.5.1 Microstructure 33

2.5.2 Parameters 34
2.5.3 Effective Permeability Comparison 36
2.5.4 EC Loss Density Comparison 37
2.5.5 EC Loss Density by Average Field Assumption 39
2.5.6 EC Loss Density by Effective Complex Permeability Tensor 39
Errors versus Volume Fraction 40
Errors from Effective Permeability 41
Errors versus Permeability Contrast 41
Errors versus Inclusion Size 43
2.6 Discussion 44
2.6.1 Square Microstructure 45
Perpendicular Field 45
In-plane Field 45
2.6.2 Cube Microstructure 46
2.6.3 Complex Permeability 46
2.7 Conclusion 47

This chapter presents a homogenization technique to estimate EC losses in composite materials with high contrast in constituent properties. It is based on the use of a complex magnetic permeability. It reflects magnetic behavior including EC losses (through the imaginary part of the permeability). The work focuses on the estimate of EC losses for SMC with linear behavior. Other components of losses such as hysteresis losses and excess losses are not considered.

In this chapter, the equations of EC loss density are first derived for a single cylindrical or spherical inclusion in free space with initially uniform magnetic field. In such case, the magnetic field in the inclusion being uniform, there exist simple equations for EC loss density. In SMC, the magnetic field in each inclusion is disturbed by the surrounding ones. The EC loss density cannot readily be deduced into the same simple equations as in single inclusion cases. Nevertheless, it is assumed that the EC loss density can still be obtained by the same equations by replacing the uniform field in the single inclusion case with the average field in the inclusion of SMC.

The working condition is quasi-statics. The frequency of applied field is low such that the skin effect is negligible. The effect of induced magnetic field upon the exciting field is also ignored.

2.1 EC Loss Density of Single Inclusion

If a magnetic ellipsoidal inclusion is placed in an infinite free space with initially uniform magnetic field, the magnetic field inside the ellipsoid is also uniform [78]. A cylinder can be viewed as an ellipsoid with an infinite axis. When the magnetic field in the domain is uniform, for certain shapes of inclusions such as an ellipsoid and a cylinder with circular or square cross-section, it is possible to obtain analytically the equations of eddy current density in the inclusion. EC loss density can be further deduced.

The cylindrical particle is assumed to have infinite length. Thus the problem is reduced to two-dimensional (2D). Two conditions of magnetic field loading are deduced separately. One case is the exciting field normal to the domain (along cylinder axis); the other is the exciting field in-plane. Finally, a generic formula combines these two cases.

As for the case of spherical inclusion, an exciting field along one axis is first derived. Further, a general formula is generated with arbitrary magnetic field loading.

In the end, a general EC loss density formula is given with a shape factor distinguishing the different shapes.

2.1.1 Cylindrical Inclusion

Consider that a cylindrical inclusion is placed in infinite space. Set up Cartesian coordinates $Oxyz$ by putting the cylinder axis along the z direction and centering the cross-section of the cylinder at O. The cross-section Ω is a disk of radius R, as shown in Fig. 2.1.

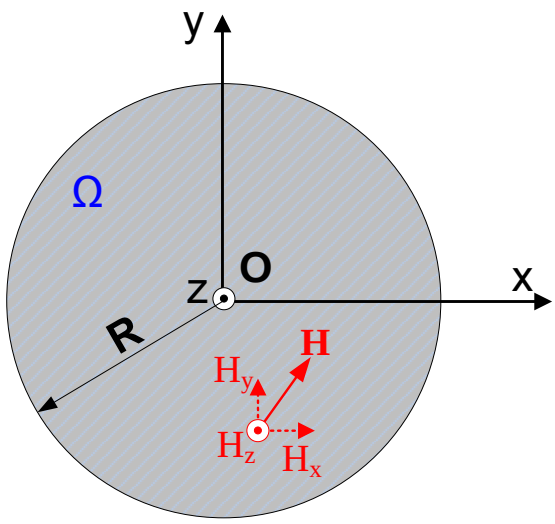

Fig. 2.1 A 2D sketch of cylindrical inclusion.

Because the cylinder length is infinite, the problem has the property of z-invariance, for instance, $\partial_z \mathbf{E} = 0$ and $\partial_z \mathbf{H} = 0$.

The magnetic field in the inclusion, $\mathbf{H} = [H_x, H_y, H_z]^t$, can be firstly decomposed into two components: in-plane one, $[H_x, H_y, 0]^t$, and perpendicular one, $[0, 0, H_z]^t$, where the superscript t is the transpose operator.

In-plane field

Consider the field is exclusively in-plane, *i.e.*, $H_z = 0$. Solving Maxwell-Ampère (1.1b) in Cartesian coordinates and applying z-invariance leads to,

$$\begin{cases} J_x = \dfrac{\partial H_z}{\partial y} - \dfrac{\partial H_y}{\partial z} = 0 \\ J_y = \dfrac{\partial H_x}{\partial z} - \dfrac{\partial H_z}{\partial x} = 0 \end{cases} \tag{2.1}$$

so that,

$$\begin{cases} E_x = 0 \\ E_y = 0 \end{cases} \tag{2.2}$$

Therefore, the induced electric field only has a normal component. Substituting (2.2) and $H_z = 0$ into Maxwell-Faraday (1.1a), by imposing the boundary condition, $E_z(0,0) = 0$, gives

$$E_z(x,y) = j\omega\mu(H_y \cdot x - H_x \cdot y) \tag{2.3}$$

Since the inclusion is isotropic, substituting (2.3) into the EC loss density definition (1.16) results in

$$U_{x,y} = \frac{\pi^2}{2} f R^2 \sigma \mu^2 \left(H_x^2 + H_y^2\right) \tag{2.4}$$

Perpendicular field

The previous configuration is kept, but the loading field is now normal to the plane (along the z-axis). The magnetic field $\mathbf{H} = [0,0,H_z]^t$ inside the circle is still uniform. The equation $\nabla \times \mathbf{E} = -j\omega\mu\mathbf{H}$ is solved in the circle to obtain the following expression for the electric field:

$$\mathbf{E}(\rho,\phi,z) = -\frac{1}{2} j\omega\mu H_z \rho \vec{u}_\phi \tag{2.5}$$

where $\vec{u}_\phi$ represents the unit vector in the ϕ direction in the cylindrical coordinates. Hence, the loss density is

$$U_z = \frac{\langle \sigma \mathbf{E}^* \cdot \mathbf{E} \rangle}{2f} = \frac{\pi^2}{4} R^2 f \sigma \mu^2 H_z^2 \tag{2.6}$$

In brief, if the magnetic field in the inclusion is uniform and denoted as $\mathbf{H} = [H_x, H_y, H_z]^t$, by combining (2.4) and (2.6), the EC loss density is,

$$U = \pi^2 f R^2 \sigma \mu^2 \mathbf{H}^* \cdot \begin{bmatrix} \frac{1}{2} & 0 & 0 \\ 0 & \frac{1}{2} & 0 \\ 0 & 0 & \frac{1}{4} \end{bmatrix} \cdot \mathbf{H}. \tag{2.7}$$

2.1.2 Spherical Inclusion

The magnetic field is applied along the z-axis. The magnetic field in the inclusion is uniform, noted $\mathbf{H} = [0,0,H_z]^t$. It is supposed that the sphere consists of disks of varying radii as shown in Fig. 2.2.

The electromagnetic problem is solved first in the domain Ω based on cylindrical coordinates (ρ,ϕ,z), as shown in Fig. 2.3.

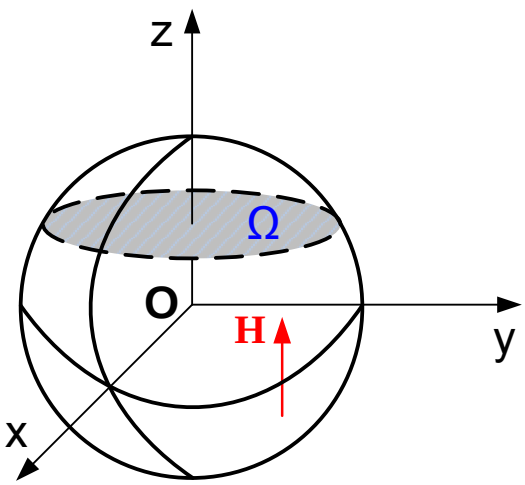

Fig. 2.2 A cross-section Ω in the spherical inclusion.

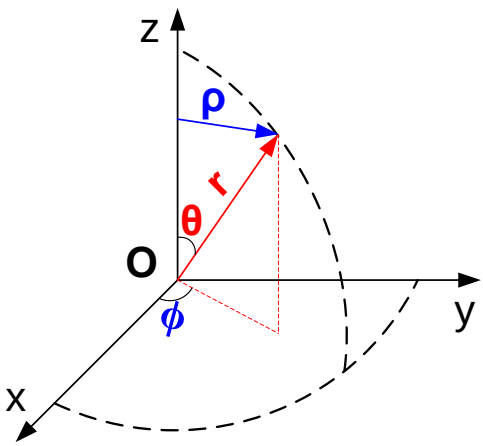

Fig. 2.3 Cylindrical coordinates (ρ, ϕ, z) and spherical coordinates (r, θ, ϕ).

The Maxwell-Faraday equation (1.1a) becomes,

$$\frac{1}{\rho}\frac{\partial(\rho E_\phi)}{\partial \rho} = -j\omega\mu H_z \tag{2.8}$$

Then, considering $E_\phi = 0$ at the center of Ω, the electric field in the domain has the form,

$$E_\phi(\rho, \phi, z) = -\frac{1}{2} j\,\omega\,\mu\,H_z\,\rho \tag{2.9}$$

This field $\mathbf{E}(\rho,\phi,z)$ is then transformed from the cylindrical coordinates to the spherical coordinates (r,θ,ϕ) as indicated in Fig. 2.3. The electric field is then expressed as,

$$\mathbf{E}(r,\theta,\phi) = -\frac{1}{2} j\,\omega\,\mu H_z\, r\,\sin\theta\,\vec{u}_\phi \tag{2.10}$$

Therefore, the loss density can be expressed as

$$U_z = \frac{\langle \sigma \mathbf{E}^* \cdot \mathbf{E}\rangle}{2f} = \frac{\pi^2}{5} R^2 f\,\sigma\,\mu^2 H_z^2 \tag{2.11}$$

Because of symmetry, for arbitrary magnetic field excitation $\mathbf{H} = [H_x, H_y, H_z]^t$, the EC loss density has the form,

$$U = \frac{\pi^2}{5} R^2 f\,\sigma\,\mu^2 \mathbf{H}^2 \tag{2.12}$$

where $\mathbf{H}^2 = \mathbf{H}^* \cdot \mathbf{H}$. This result can also be found in [51].

To summarize from both the cylindrical and the spherical inclusion cases, the EC loss density is proportional to the loading frequency, conductivity of the inclusion, and the squared magnitude of the magnetic flux density ($\mathbf{B} = \mu\mathbf{H}$), and also depends on the size and shape of the inclusion.

To synthesize both the cylindrical and spherical cases, a shape factor tensor $\mathbb{K}$ is defined as

$$\mathbb{K} = \begin{cases} \begin{bmatrix} \frac{1}{2} & 0 & 0 \\ 0 & \frac{1}{2} & 0 \\ 0 & 0 & \frac{1}{4} \end{bmatrix} & \text{(cylindrical)} \\ \begin{bmatrix} \frac{1}{5} & 0 & 0 \\ 0 & \frac{1}{5} & 0 \\ 0 & 0 & \frac{1}{5} \end{bmatrix} & \text{(spherical)} \end{cases} \tag{2.13}$$

so that

$$U = \pi^2 R^2 f\,\sigma\,\mu^2 \mathbf{H}^* \cdot \mathbb{K} \cdot \mathbf{H} \tag{2.14}$$

is the generic formula for the EC loss density of a single inclusion with uniform magnetic field.

2.2 EC Loss Density of SMC

SMC can be viewed microscopically as a periodical layout of inclusions embedded in a dielectric host matrix. Consider now the SMC material as a representative elementary

cell containing an inclusion and its surrounding matrix. This cell is supposed to have spatial periodicity. The properties of the inclusion are denoted with the subscript 2 and the properties of the matrix with the subscript 1.

For periodic SMC containing cylindrical or ellipsoidal inclusions, when the filling factor of the inclusion is sufficiently low, each inclusion can be regarded as a single one in the previous section. For biphasic composite, given the effective permeability, $\mathbb{\mu}^r$, the average field in the inclusion is given by (2.15) [88],

$$\langle \mathbf{H} \rangle_2 = \frac{1}{\xi_2(\mu_2 - \mu_1)} (\mathbb{\mu}^r - \mu_1 \mathbb{I}) \cdot \langle \mathbf{H} \rangle \tag{2.15}$$

where $\langle \mathbf{H} \rangle$ is the average magnetic field over the whole cell. $\mathbb{I}$ is the second order identity tensor. And ξ_2 is the volume fraction (filling factor) of the inclusions.

The EC loss density U_2 in the inclusion can be written as a function of the 'uniform' magnetic field in the inclusion ($\mathbf{H}_2 = \langle \mathbf{H} \rangle_2$):

$$U_2 = \pi^2 R^2 f \, \sigma_2 \mu_2^2 \mathbf{H}_2^* \cdot \mathbb{K} \cdot \mathbf{H}_2 \tag{2.16}$$

Since the matrix is dielectric, EC occurs only in the inclusion, the macroscopic EC (flowing in the matrix) being negligible. From the perspective of the whole composite material, the EC loss density U is then

$$U = \xi_2 U_2 \tag{2.17}$$

As the filling factor increases, the magnetic field in the inclusion becomes nonuniform. Equation (2.16) cannot be readily deduced as in the single inclusion case. Nevertheless, the assumption that (2.16) is still applicable is made, replacing $\mathbf{H}_2$ with the average $\langle \mathbf{H} \rangle_2$ within the inclusions. Therefore, the EC loss density estimate for the whole composite becomes:

$$U = \xi_2 \pi^2 R^2 f \, \sigma_2 \, \mu_2^2 \, \langle \mathbf{H} \rangle_2^* \cdot \mathbb{K} \cdot \langle \mathbf{H} \rangle_2 \tag{2.18}$$

Equation(2.15) still holds to calculate $\langle \mathbf{H} \rangle_2$. Therefore, the EC loss density of SMC is linked to the macroscopic average magnetic field by (2.19),

$$U = \frac{\pi^2 R^2 f \, \sigma_2 \, \mu_2^2}{\xi_2 (\mu_2 - \mu_1)^2} \langle \mathbf{H} \rangle^* \cdot (\mathbb{\mu}^r - \mu_1 \mathbb{I})^* \cdot \mathbb{K} \cdot (\mathbb{\mu}^r - \mu_1 \mathbb{I}) \cdot \langle \mathbf{H} \rangle \tag{2.19}$$

According to (2.19), it is clear that an accurate estimate of the effective magnetic permeability $\mathbb{\mu}^r$ is a key requirement for the approximation of EC losses of SMC.

2.3 Effective Permeability of SMC

The effective permeability of SMC is critical in EC losses modeling. Various approaches are introduced in the previous chapter(1.5). In the following discussion, Maxwell-Garnett (MG) estimate and Series Expansions are used.

2.3.1 MG Estimate

The Maxwell-Garnett(MG) approximation is useful when one of the components can be considered as a host in which inclusions of the other components are embedded. For dilute SMC where the volume fraction of inclusion is sufficiently small, the effective magnetic permeability obtained with MG estimate has the tensor form [23],

$$\mathbb{\mu}^r = \mu_1\mathbb{I} + \xi_2\mu_1(\mu_2-\mu_1)[\mu_1\mathbb{I} + (1-\xi_2)(\mu_2-\mu_1)\mathbb{N}]^{-1} \tag{2.20}$$

where $\mathbb{N}$ is the depolarization tensor:

$$\mathbb{N} = \begin{cases} \begin{bmatrix} \frac{1}{2} & 0 & 0 \\ 0 & \frac{1}{2} & 0 \\ 0 & 0 & 0 \end{bmatrix} & \text{(cylindrical)} \\ \begin{bmatrix} \frac{1}{3} & 0 & 0 \\ 0 & \frac{1}{3} & 0 \\ 0 & 0 & \frac{1}{3} \end{bmatrix} & \text{(spherical)} \end{cases} \tag{2.21}$$

There is a special case of cylindrical inclusion with loading field along length (for instance, in z-direction). The corresponding depolarization factor is $N = 0$. MG estimate is equivalent to the Wiener upper bound (see 1.28 and 1.29). In such case, the magnetic field in the domain is always uniform so long as the frequency is low,

$$\langle H_z \rangle_2 = \langle H_z \rangle = H_z \tag{2.22}$$

The effective permeability formula by MG is simple and straightforward. Nevertheless, it is only valid when the volume fraction is low. As the volume fraction ξ_2 increases, MG estimate brings unacceptable inaccuracy for the definition of the effective permeability (see Fig. 2.7 later in this chapter). This definition must then be revisited. In other cases, $\mathbb{\mu}^r$ has to be calculated either by FEM computation or, if the structure is periodic, by series

expansions [22, 25]. The latter provides a high precision estimate if sufficiently high order terms are computed.

2.3.2 Series Expansion Estimate

For cubic lattice of spherical inclusions or square lattice of circular inclusions, the effective magnetic permeability can be accurately determined using series expansions. The accuracy depends on the order of the terms of the series used for the practical calculation. In the case of spherical or circular inclusions, because of spatial symmetries, the effective magnetic permeability is isotropic. It is denoted μ^r. The approximation used in this chapter leads to the following expressions for μ^r:

$$\mu^r_{\text{sphere}} = \left(1 + \frac{3\xi_2}{\gamma(\xi_2)}\right)\mu_1 \tag{2.23a}$$

$$\mu^r_{\text{circle}} = \frac{1+\lambda(\xi_2)\xi_2}{1-\lambda(\xi_2)\xi_2}\mu_1 \tag{2.23b}$$

where

$$\begin{aligned}\gamma(\xi_2) = &-1/R_1 - \xi_2 + 1.3045R_3\xi_2^{10/3} + 0.0723R_5\xi_2^{14/3} \\ &- 0.5289R_3^2\xi_2^{17/3} + 0.1526R_7\xi_2^6 + O(\xi_2^7)\end{aligned} \tag{2.24}$$

with

$$R_n = \frac{n(\mu_1-\mu_2)}{(n+1)\mu_1 + n\mu_2} \tag{2.25}$$

and

$$\begin{aligned}\lambda(\xi_2) = &\alpha + 0.305827\alpha^3\xi_2^4 + \alpha^3\left(0.0935304\alpha^2 + 0.0133615\right)\xi_2^8 \\ &+ \alpha^3\left(0.0286042\alpha^4 + 0.437236\alpha^2 + 0.000184643\right)\xi_2^{12} + O(\xi_2^{16})\end{aligned} \tag{2.26}$$

with

$$\alpha = \frac{\mu_2-\mu_1}{\mu_2+\mu_1} \tag{2.27}$$

The theoretical foundations for these expressions can be found in references [22] and [25].

2.4 Complex Permeability Definition

Complex properties can be used in electromagnetic applications to describe dissipation. A thorough review of homogenization models for dielectric behavior using complex permit-

tivity can be found in [42, 66]. 2D and 3D cases have been numerically explored in details. The complex effective permittivity depends on the properties of each constituent, on their volume fraction and on their spatial arrangement [67]. In an analogous way, complex permeability is a useful tool to handle high frequency magnetic effects, for instance in transformer applications [68, 69]. Power dissipation is directly reflected in the imaginary part of the complex permeability [70, 71]. In the case of SMC at low frequency, when the induced magnetic field can be neglected, there is no time lag between magnetic flux density and magnetic field. In this respect, the imaginary part of complex permeability should be considered as zero. However, EC losses are present - as long as the frequency is not zero. Thus, an imaginary part, noted μ^i, can be introduced into the magnetic permeability tensor so as to reflect EC losses.

The complex permeability tensor $\tilde{\mu}$ ($\tilde{\mu} = \mu^r - j\mu^i$) can be used as a mathematical tool to represent a dissipative magnetic material. In this study, this complex permeability tensor is used to describe the effective properties of SMC. The real part is the usual magnetic permeability, and the imaginary part reflects the EC losses. In what follows, $\tilde{\mu}$ denotes the (effective) complex permeability while μ^r is still called the effective permeability.

Consider a homogeneous and linear material of permeability tensor $\tilde{\mu}$ excited by a harmonic magnetic field $\mathbf{H}(t) = \mathbf{H}_0 e^{j\omega t}$ ($\mathbf{H}_0$ is the magnetic field magnitude and ω the angle frequency). The induction flux is $\mathbf{B}(t) = \tilde{\mu}\,\mathbf{H}_0 e^{j\omega t}$. As in the case of transformers at high frequency range [71], the energy loss density in a period of time T is,

$$S = \frac{1}{2}\Re\left(\int_0^T \mathbf{H}^*(t)\cdot\frac{\mathrm{d}\mathbf{B}(t)}{\mathrm{d}t}\,\mathrm{d}t\right) \tag{2.28}$$

where the operator $\Re(\cdot)$ is the real part of a complex number. This equation can be simplified into,

$$S = \pi\,\mathbf{H}_0^*\cdot\mu^i\cdot\mathbf{H}_0 \tag{2.29}$$

Proof of this equation is detailed in Appendix B.

Applying successively the magnetic field in different directions, and $U = S$, the components of tensor μ^i can be obtained. Thus heterogeneous anisotropic materials can be homogenized as a virtual homogeneous material. This material has a complex permeability tensor containing effective magnetic behavior and lossy features of SMC. In the next section, the tensor μ^i is built for single inclusion and for SMC.

2.4.1 Complex Permeability of Single Inclusion

Consider that the magnetic field is uniform in the single inclusion: $\mathbf{H} = \mathbf{H}_{\text{inc}}\, e^{j\omega t}$. The EC loss density can be obtained by the shape-related equation (2.14) or by complex permeability (2.29). Equaling the Setting $U = S$ gives,

$$\begin{aligned} \pi\, \mathbf{H}^*_{\text{inc}} \cdot \mathbb{\mu}^i_{\text{inc}} \cdot \mathbf{H}_{\text{inc}} &= \pi^2 R^2 f\, \sigma\, \mu^2\, \mathbf{H}^*_{\text{inc}} \cdot \mathbb{K} \cdot \mathbf{H}_{\text{inc}} \\ \Longrightarrow \mathbb{\mu}^i_{\text{inc}} &= \pi R^2 f\, \sigma\, \mu^2 \mathbb{K} \end{aligned} \tag{2.30}$$

Therefore, the complex permeability has the form,

$$\tilde{\mathbb{\mu}}_{inc} = \mu\, \mathbb{I} - j\pi R^2 f\, \sigma\, \mu^2\, \mathbb{K} \tag{2.31}$$

which depends on the material properties, working frequency, shape and size (radius).

2.4.2 Complex Permeability of SMC

Applying successively the magnetic field in different directions, each element of tensor $\mathbb{\mu}^i$ can be obtained. Equaling (2.29) to (2.19), tensor $\mathbb{\mu}^i$ can be deduced as,

$$\mathbb{\mu}^i = \frac{\pi R^2 f\, \sigma_2\, \mu_2^2}{\xi_2 (\mu_2 - \mu_1)^2} (\mathbb{\mu}^r - \mu_1 \mathbb{I})^* \cdot \mathbb{K} \cdot (\mathbb{\mu}^r - \mu_1 \mathbb{I}) \tag{2.32}$$

Tensor $\mathbb{\mu}^i$ is proportional to the frequency f, to the inclusion conductivity σ_2 and depends also on the magnetic permeabilities μ_1 and μ_2 of the constituents, on the volume fraction ξ_2, and the shape factor tensor $\mathbb{K}$ of the inclusions.

Finally, the complex permeability tensor $\tilde{\mu}$ for a SMC material is defined as

$$\tilde{\mathbb{\mu}} = \mathbb{\mu}^r - j \frac{\pi R^2 f\, \sigma_2\, \mu_2^2}{\xi_2 (\mu_2 - \mu_1)^2} (\mathbb{\mu}^r - \mu_1 \mathbb{I})^* \cdot \mathbb{K} \cdot (\mathbb{\mu}^r - \mu_1 \mathbb{I}) \tag{2.33}$$

The real part represents the magnetic behavior of the composite, and the imaginary part offers an immediate approach to the EC loss density, by (2.29). It must be noticed that an accurate estimate of the effective magnetic permeability $\mathbb{\mu}^r$ is required to define the effective complex permeability tensor $\tilde{\mathbb{\mu}}$.

In order to determine the EC losses with the complex permeability (imaginary part), a precise estimate of the effective permeability (real part) is essential. The analytical approaches for the effective property of composites with elliptic or ellipsoidal inclusions prove to be arduous. But simple inclusion shapes such as circular cylinder or sphere have

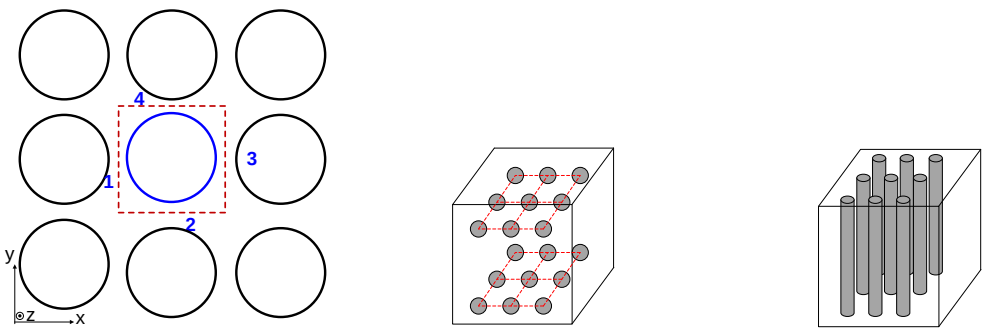

(a) (b) (c)

Fig. 2.4 (a) 2D sketch of cubic lattice of spherical inclusions or square lattice of fiber inclusions. The domain confined by dashed lines 1-4 forms an elementary cell of periodic pattern. (b) 3D view of cubic lattice of spherical inclusions (case 1). (c) 3D view of square lattice of fiber inclusions (case 2).

been widely studied [17, 21, 22, 25]. Thus, in the following, focus is limited on SMC with circular cylindrical or spherical inclusions to verify the application of the complex permeability model with the average field assumption.

2.5 Validation using FEM computations

2.5.1 Microstructure

SMC consists of inclusions surrounded by an insulating film. In this work, attention is focused on two simple microstructures: cubic lattice of spherical inclusions and square lattice of fiber inclusions, as shown in Fig. 2.4. The fiber inclusion problem can be reduced to 2D. Only circular cross-section of fiber is considered.

The problem of 2D SMC with a magnetic field applied in the normal direction has been discussed in the Appendix A as well as in [86]. At low frequency, the magnetic field is uniform in the domain, so that (2.19) is an exact formula for EC losses. In that simple case, the effective magnetic permeability (real part) is obtained from the Wiener estimate, which also provides in that case an exact value. Therefore, the required validations concern the spherical inclusion case (later referred to as case 1), and the case of cylindrical inclusions with in-plane loading (later referred to as case 2). These two cases are associated to more complex field distributions, and require more advanced homogenization techniques.

2.5.2 Parameters

To carry out this validation, FEM simulations have been performed on a unit cell of SMC as described in Fig. 2.4a for different volume fractions ξ_2 at different frequencies. The cell size L_1 (lattice length) is fixed to $50\,\mu$m. The average flux density over a cell is imposed at $B_0 = 1\,$T. Vector magnetic potential $\mathbf{A}$ is employed here to impose the flux density.

$$\mathbf{B} = \nabla \times \mathbf{A} \tag{2.34}$$

For case 1 computations, as denoted in Fig. 2.4a, a rotating vector potential is imposed on the four surfaces of the cube cell to form a flux density in one direction, for instance, in the z-direction.

$$\mathbf{A}_1 = -A_0\vec{u}_y, \quad \mathbf{A}_2 = A_0\vec{u}_x, \quad \mathbf{A}_3 = A_0\vec{u}_y, \quad \mathbf{A}_4 = -A_0\vec{u}_x \tag{2.35}$$

A 2D sketch of the boundary condition is plotted in Fig. 2.5.

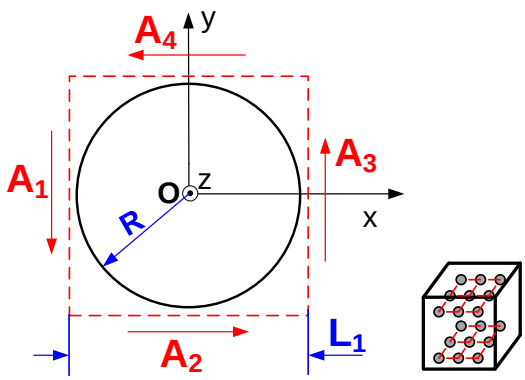

Fig. 2.5 Rotating vector potential to generate a flux density in the z direction.

The remaining two horizontal surfaces are imposed by Perfect Magnetic Conductor (PMC),

$$\begin{cases} \mathbf{n} \times \mathbf{H} = 0 \\ \mathbf{n} \cdot \mathbf{J} = 0 \end{cases} \tag{2.36}$$

Therefore, the flux density is,

$$B_z = \frac{\oint \mathbf{A} \cdot \mathrm{d}\vec{l}}{S} = \frac{4A_0 L_1}{L_1^2} = \frac{4A_0}{L_1} \tag{2.37}$$

In order to maintain $B_z = B_0 = 1\,\mathrm{T}$ and given $L_1 = 50\,\mu\mathrm{m}$, then $A_0 = 1.25 \times 10^{-5}$ Wb/m. For symmetry reasons, only half of the unit cell is modeled. The magnetic field is directed along the z-axis. A 3D mesh made of hexahedral elements has been used. The mesh is constituted of approximately one million elements and the computation time is about 300 seconds.

Similarly, for case 2 computations, a rotating vector potential directing z-axis is necessary to form a flux density, for example, in y direction. The two boundary lines are imposed with vector potential,

$$\mathbf{A}_1 = A_0 \vec{u}_z, \quad \mathbf{A}_3 = -A_0 \vec{u}_z \tag{2.38}$$

and the remaining two boundary lines (2 and 4) are imposed with PMC by (2.36), shown in Fig. 2.6.

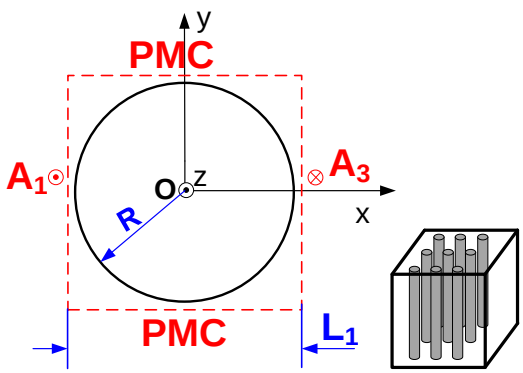

Fig. 2.6 Vector potential boundary condition to generate a flux density in the y direction.

Therefore, the average flux density imposed on the cell is:

$$B_y = \frac{\oint \mathbf{A} \cdot \mathrm{d}\vec{l}}{S} = \frac{2A_0}{L_1} \tag{2.39}$$

In order to maintain $B_y = B_0 = 1\,\mathrm{T}$ and given $L_1 = 50\,\mu\mathrm{m}$, then $A_0 = 2.5 \times 10^{-5}$ Wb/m. For case 2 computations, the magnetic field is applied along the y-axis. A 2D mesh made of triangular elements has been used. The mesh is constituted of approximately 3×10^4 elements and the computation time is about 2 seconds.

The material properties used for the constituents are given in Table 2.1.

Table 2.1 Material parameters used in the calculations for SMC

	Conductivity (S/m)	Relative Permeability	Relative Permittivity
Iron	1.12×10^{7}	4000	1
Epoxy	1.7×10^{-13}	1	9

2.5.3 Effective Permeability Comparison

As stated before, the Wiener estimate provides an exact effective permeability for cylinder inclusion with normal magnetic loading. Therefore, only in-plane effective permeability is examined, which can be degenerated to be a scalar, as well as for the case of spherical inclusion. This scalar effective permeability is denoted μ^r. To be consistent with the notation of EC loss density, μ^r_{FEM}, μ^r_{SE} and μ^r_{MG} are the effective permeability obtained from FEM, series expansion and MG estimate, respectively. The value μ^r_{SE} is calculated to the order ξ_2^6 in (2.24) for the case 1 and to the order ξ_2^{12} in (2.26) for the case 2.

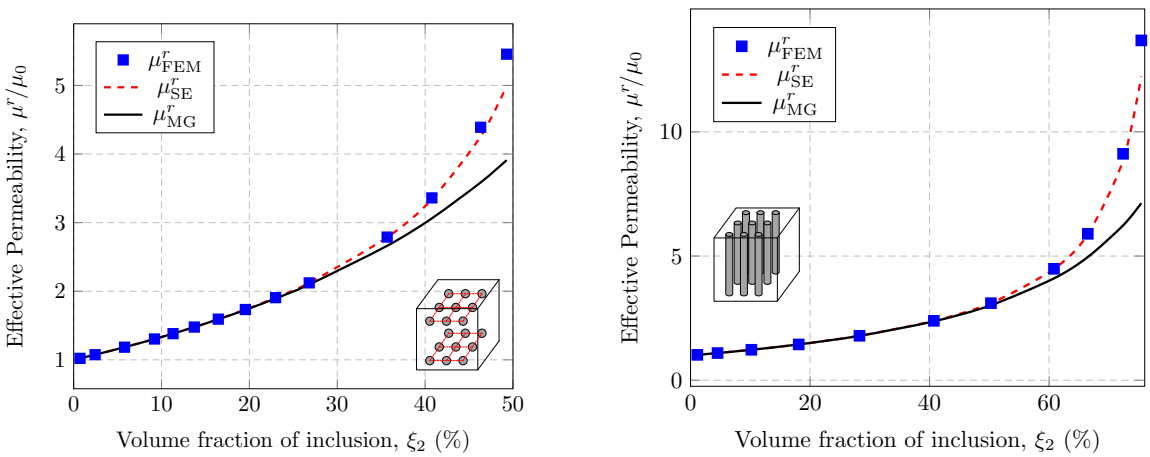

(a) Cubic lattice of spheres

(b) Square lattice of fibers

Fig. 2.7 Effective permeability obtained from FEM (blue squares), series expansion (red dashed line) and MG estimate (black line). (a) case 1: Cubic lattice of spheres: magnetic field loading along z-direction, (b) case 2: Square lattice of fibers: in-plane loading field along y-direction. For all calculations: lattice size $L_1 = 50\,\mu$m, $\mu_2 = 4000\mu_0$, $\mu_1 = \mu_0$, $\sigma_2 = 1.12 \times 10^7$ S/m, average flux density $B_0 = 1$ T.

Fig. 2.7 indicates that the effective permeability increases with the volume fraction of the inclusion. That is because the inclusion permeability is bigger than the matrix one. The plots also show that series expansion provides a better estimate of the effective permeability than MG estimate.

In order to check the discrepancies, using the FEM results as the reference values, errors are defined,

$$\begin{cases} \eta^{\mu}_{\mathrm{SE}} = \dfrac{\mu^{r}_{\mathrm{SE}} - \mu^{r}_{\mathrm{FEM}}}{\mu^{r}_{\mathrm{FEM}}} \times 100\% \\ \eta^{\mu}_{\mathrm{MG}} = \dfrac{\mu^{r}_{\mathrm{MG}} - \mu^{r}_{\mathrm{FEM}}}{\mu^{r}_{\mathrm{FEM}}} \times 100\% \end{cases} \tag{2.40}$$

The plots of the effective permeability errors are shown in Fig. 2.8.

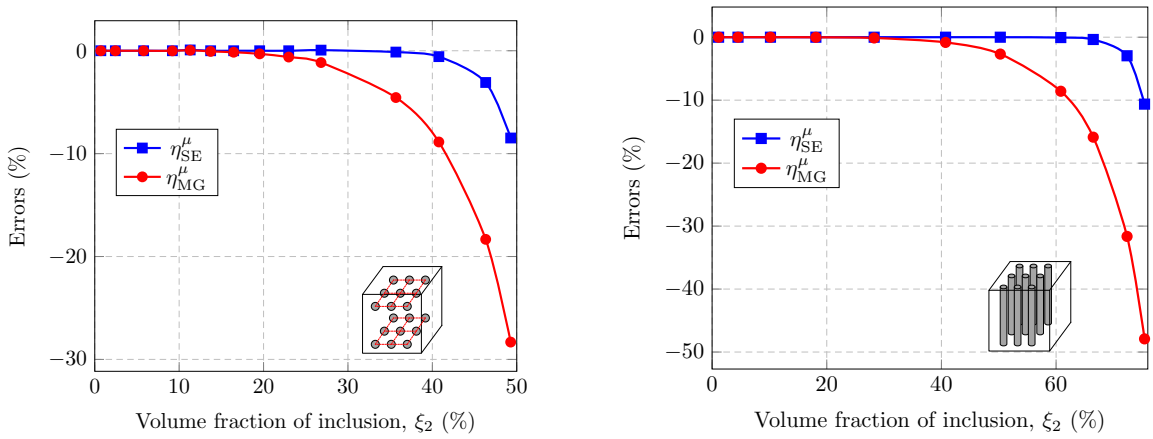

(a) Cubic lattice of spheres (b) Square lattice of fibers

Fig. 2.8 Errors of the effective permeability generated by series expansion and MG estimate by comparing with the reference values (FEM). Configuration: the same as Fig. 2.7.

Fig. 2.8 shows that series expansion and MG estimate invariably underestimate the effective permeability both in case 1 and case 2. When the filling factor is low, series expansion and MG estimate agree well with FEM results. As the filling factor increases, errors grow for both estimates. To conclude from cases 1 and 2, series expansion provides a better approximation than MG estimate. In addition, theoretically, the series expansion has the potential of arriving at the exact value if all the infinite series are calculated.

2.5.4 EC Loss Density Comparison

The total EC loss density U_{FEM}, and the average value $\langle \mathbf{H}_{\mathrm{FEM}} \rangle_2$ of the magnetic field in the inclusion are post-processed. $\langle \mathbf{H}_{\mathrm{FEM}} \rangle_2$ is substituted into (2.18) to get the EC loss density approximation, noted U_a.

$$U_a = \xi_2 \pi^2 R^2 f \, \sigma_2 \, \mu_2^2 \, \langle \mathbf{H}_{\mathrm{FEM}} \rangle_2^* \cdot \mathbb{K} \cdot \langle \mathbf{H}_{\mathrm{FEM}} \rangle_2 \tag{2.41}$$

The comparison between U_a and U_{FEM} indicates the validity of the average field assumption in (2.18).

SMC is homogenized by the complex permeability. The effective permeability (real part) is determined by series expansion. The EC loss density estimated by the homogenization model is noted U_{SE}. It is obtained analytically from (2.29) after the complex permeability model has been used. The comparison between U_{FEM} and U_{SE} indicates the validity of the proposed model. This comparison has been performed for different concentrations of inclusions and different values of magnetic permeability for the inclusions.

Fig. 2.9 plots the EC loss density as a function of the volume fraction ξ_2 of the inclusions, in both case 1 (spherical inclusions) and case 2 (fiber inclusions and in-plane magnetic field).

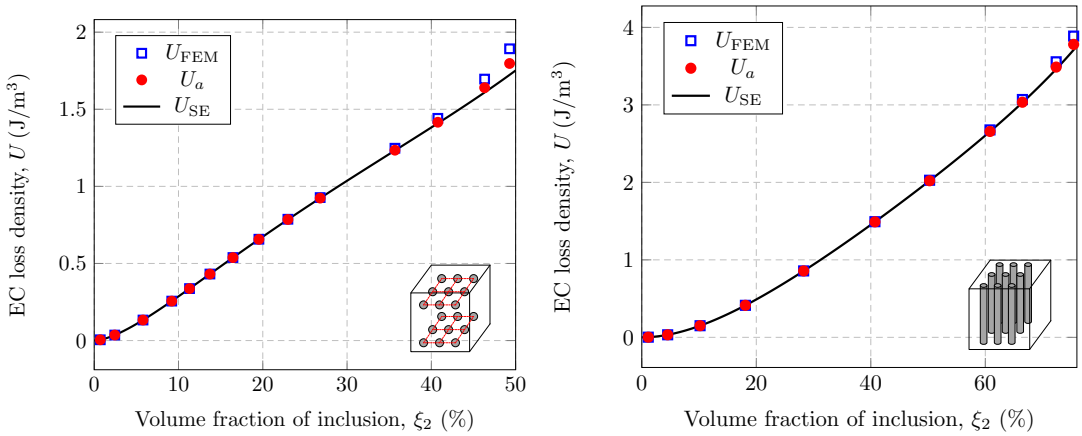

(a) Cubic lattice of spheres (b) Square lattice of fibers

Fig. 2.9 EC loss density as a function of inclusion volume fraction evaluated by full FEM computation (squares), by approximation (2.18) using the average magnetic field obtained by FEM (circles) and by the proposed analytical formulation (line). (a) case 1: Cubic lattice of spheres: magnetic field loading along z-direction, (b) case 2: Square lattice of fibers: in-plane loading field along y-direction. For all calculations: frequency $f = 100$ Hz, lattice size $L_1 = 50\,\mu$m, $\mu_2 = 4000\,\mu_0$, $\mu_1 = \mu_0$, $\sigma_2 = 1.12 \times 10^7$ S/m, average flux density $B_0 = 1$ T.

As expected - since the flux is imposed - EC losses increase when the volume fraction of inclusions becomes higher. At low volume fraction, the average field assumption, and the analytical formulation are consistent with the FEM results. As the volume fraction increases, the discrepancy arises. These discrepancies can be attributed to two main causes. The first is the assumption used in relation (2.18) that the average magnetic field within the inclusions can be used to estimate the EC losses. The second is the definition of the complex permeability $\tilde{\mu}$ based on the proposed homogenization model. These causes can

be studied separately by considering successively the estimates U_a and U_{SE} for EC losses in the following.

2.5.5 EC Loss Density by Average Field Assumption

The error related to the average field assumption is defined as

$$\eta_a = \frac{U_a - U_{\text{FEM}}}{U_{\text{FEM}}} \times 100\% \tag{2.42}$$

Fig. 2.11 plots the evolution of η_a as a function of the volume fraction ξ_2 for the two studied cases at frequencies from 10Hz to 10kHz. According to the low frequency criterion discussed in Appendix A, using (A.28), the low frequency range is $f < 5$ kHz. Below this value, the results are frequency independent. When the frequency is greater than 5 kHz, the skin effect cannot be neglected. The case of frequency 10 kHz is calculated as an example of higher frequency.

The error level increases with the volume fraction ξ_2. At low volume fraction, the errors tend towards zero, which is consistent with the dilute approximation with quasi-uniform field inside the inclusions. On the other hand, as the volume fraction increases, the field distortion in the inclusions becomes severe, and the error η_a increases. Fig. 2.11 also shows that for the studied cases, (2.18) underestimates the losses. At low frequency (lower than 5 kHz), the error does not depend on frequency. For higher frequencies, the induced magnetic field cannot be neglected anymore. The induced magnetic field reduces the level of the whole magnetic field leading to a reduction of the losses in the numerical computation. This reduces the difference between U_a and U_{FEM} because the average field approximation tends to underestimate the loss level. This effect explains the reduction of the error observed at high frequency.

Overall, the average field approximation brings errors lower than 5% on the EC losses estimate for the proposed volume fractions, which validates the applicability of (2.18).

2.5.6 EC Loss Density by Effective Complex Permeability Tensor

Another source of error in the full homogenization approach is the definition of the complex permeability, which adds up to the error discussed in the previous section. The total error of the model is defined as

$$\eta_{\text{SE}} = \frac{U_{\text{SE}} - U_{\text{FEM}}}{U_{\text{FEM}}} \times 100\% \tag{2.43}$$

Errors versus Volume Fraction

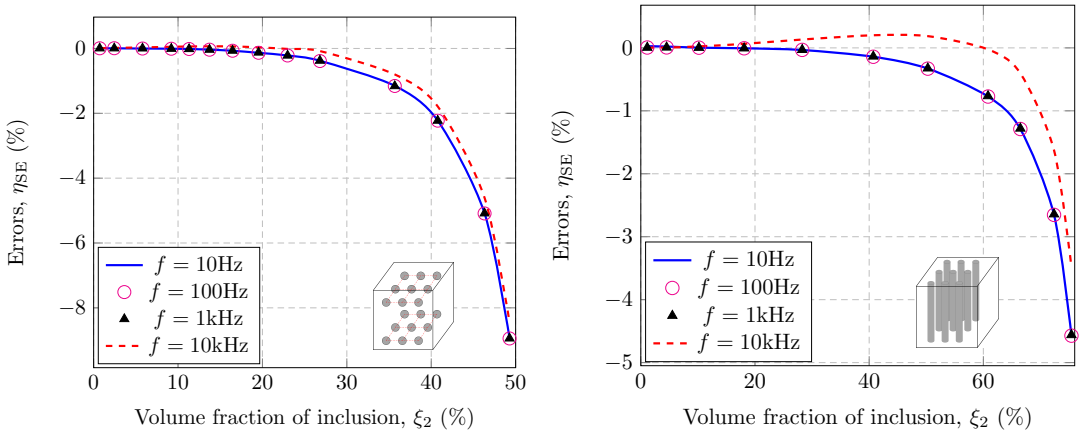

(a) Cubic lattice of spheres (b) Square lattice of fibers

Fig. 2.10 Errors on EC losses of the proposed homogenization model as a function of volume fraction ξ_2 for different frequencies. (a) case 1: Cubic lattice of spheres: magnetic field loading along z-direction, (b) case 2: Square lattice of fibers: in-plane loading field along y-direction. For all calculations: lattice size $L_1 = 50\,\mu$m, $\mu_2 = 4000\mu_0$, $\mu_1 = \mu_0$, $\sigma_2 = 1.12 \times 10^7$ S/m, average flux density $B_0 = 1$ T .

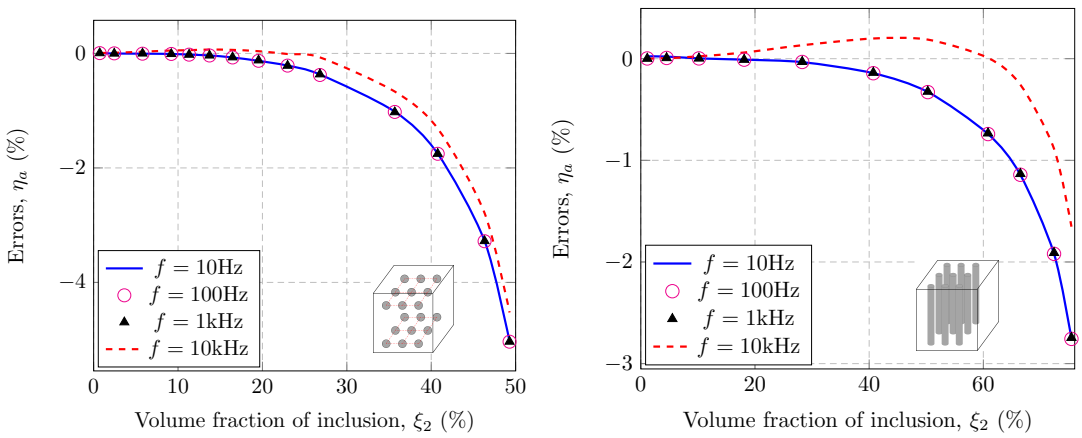

(a) Cubic lattice of spheres (b) Square lattice of fibers

Fig. 2.11 Errors on EC losses attributed to the average field assumption in equation (2.18) as a function of volume fraction ξ_2 for different frequencies. (a) case 1: Cubic lattice of spheres: magnetic field loading along z-direction, (b) case 2: Square lattice of fibers: in-plane loading field along y-direction. For all calculations: lattice size $L_1 = 50\,\mu$m, $\mu_2 = 4000\mu_0$, $\mu_1 = \mu_0$, $\sigma_2 = 1.12 \times 10^7$ S/m, average flux density $B_0 = 1$ T.

Fig. 2.10 plots the evolution of η_{SE} as a function of the volume fraction ξ_2 for the two studied cases at frequencies from 10Hz to 10kHz.

The trend on the error η_{SE} is very similar to that of η_a. The definition of the effective complex permeability just increases the general level of error, approximately by a factor 2. This increase in the error level could be reduced to almost zero by increasing the order of the series expansion used to calculate the effective permeability. But this comes to a higher computation cost.

Errors from Effective Permeability

Since only certain terms are employed in the series expansion calculations, there exist discrepancies in estimating the effective permeability. These discrepancies give rise to errors for the effective complex permeability, which further add up to the approximations of the EC loss estimates.

If we only consider the spherical case and circular case with in-plane excitation, SMC would have isotropic effective magnetic property, μ^r. Substituting the magnetic constitutive relationship $\langle \mathbf{B} \rangle = \mu^r \langle \mathbf{H} \rangle$ into (2.19), the EC loss density leads to:

$$U = \pi^2 R^2 f \, \sigma_2 \frac{\mu_2^2 (\mu^r - \mu_1)^2}{\xi_2 (\mu^r)^2 (\mu_2 - \mu_1)^2} \langle \mathbf{B} \rangle^* \cdot \mathbb{K} \cdot \langle \mathbf{B} \rangle \tag{2.44}$$

Since the flux density $\langle \mathbf{B} \rangle$ is a constant, the EC loss density has the relationship with μ^r:

$$U \propto \left(1 - \frac{\mu_1}{\mu^r}\right)^2 \tag{2.45}$$

The EC loss density is a monotonically increasing function of μ^r as indicated in (2.45). The effective permeability by series expansion (to the order ξ_2^6 in (2.24) for the case 1 and to the order ξ_2^{12} in (2.26) for the case 2) is underestimated, as shown in Figs. 2.7 and 2.8: $\mu^r_{\mathrm{SE}} \leq \mu^r_{\mathrm{FEM}}$. It gives rise to: $U_{\mathrm{SE}} \leq U_a$. From the previous section, the average field assumption always underestimates the EC loss density at low frequency: $U_a \leq U_{\mathrm{FEM}}$. Therefore,

$$U_{\mathrm{SE}} \leq U_a \leq U_{\mathrm{FEM}} \tag{2.46}$$

It leads to $\eta_{\mathrm{SE}} \geq \eta_a$. That clarifies the difference between Fig. 2.11 and 2.10 at low frequency ($f < 5\,\mathrm{kHz}$).

Errors versus Permeability Contrast

The level of error is also a function of the permeability contrast between matrix and inclusions. The matrix magnetic permeability is kept at μ_0. The error being frequency-

independent at low frequency (see Fig. 2.11 and 2.10), the frequency is fixed at $f = 100$ Hz. The radius R for the inclusions is also fixed at $R = 24\,\mu$m corresponding to a volume fraction of 46.3% for spherical inclusions (case 1) and 72.4% for cylindrical inclusions (case 2).

The EC loss density as a function of the permeability contrast between matrix and inclusions is given in Fig. 2.12. The corresponding error η_{SE} is given in Fig. 2.13. The EC loss density increases with the permeability of the inclusions. It reaches a saturation value when the permeability contrast is greater than 100. For this level of contrast, the magnetic flux is fully concentrated in the inclusions. A further increase of the permeability contrast then causes only slight variation of the magnetic flux distribution, which can be neglected. For the same reasons, EC losses also reach a saturation value.

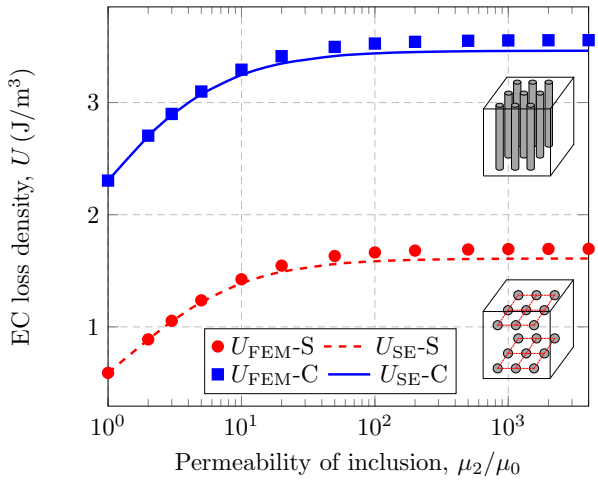

Fig. 2.12 EC loss density U_{SE} evaluated with the proposed approach (lines) for cases 1 and 2 and corresponding FEM results U_{FEM} (dots) as a function of the permeability contrast between matrix and inclusions. For all calculations: $f = 100$Hz, lattice size $L_1 = 50\,\mu$m, $R = 24\,\mu$m, $\mu_1 = \mu_0$, $\sigma_2 = 1.12 \times 10^7$ S/m, average flux density $B_0 = 1$ T.

These results show that, when the permeability contrast is high, greater than a few hundreds, the error remains at a very stable level, lower than 6 % and 3 % for case 1 and case 2, respectively. As the contrast decreases, the error decreases, which is expected because the distortion of the magnetic field inside the inclusions is higher when the contrast is higher. In other words, the average field assumption is getting more and more appropriate when the contrast is low.

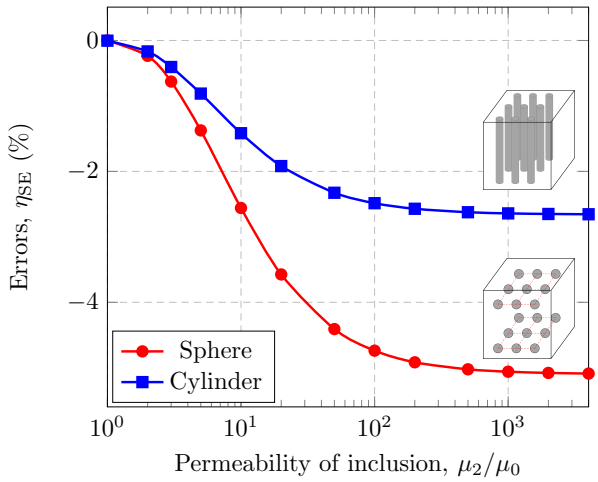

Fig. 2.13 Errors on EC losses of the proposed homogenization model as a function of the permeability contrast between matrix and inclusions for cases 1 and 2. Configuration: the same as Fig. 2.12.

Errors versus Inclusion Size

If the filling factor is fixed, there is a proportional relationship between the elementary cell size and the radius of the inclusion. Meanwhile, the permeability of each component is kept constant. The effective permeability would remain, in principle, invariable.

It is known that the EC loss density increases with the inclusion size. Therefore, in designing SMC, in order to reduce EC loss density, small inclusion size is desired. By (2.44) the relationship between the EC loss density and the inclusion size is:

$$U \propto R^2 \tag{2.47}$$

It explains the parabolic curves of EC loss density in Fig. 2.14. The corresponding errors are plotted in Fig. 2.15. It is clear from Fig. 2.15 that the errors are independent of the inclusion size. The errors come from the average field assumption and the definition of the effective permeability. When the filling factor and magnetic property are fixed, the effective permeability is invariable according to (2.23). It is not affected by the inclusion size. Moreover, by (2.15) the average field in the inclusion does not rely on the inclusion size.

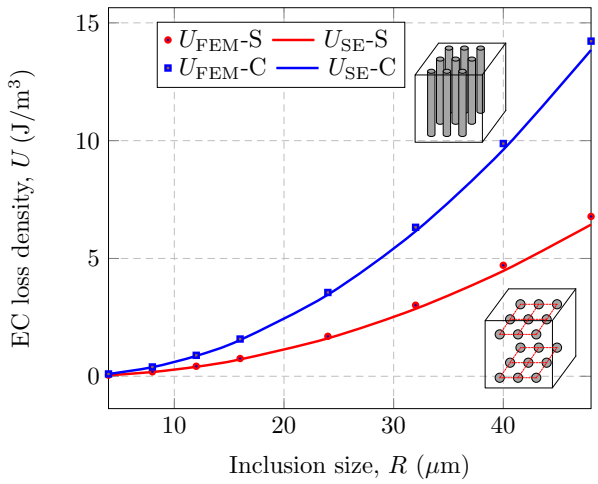

Fig. 2.14 EC loss density versus different inclusion size. The filling factor is fixed for each case: 46.32 % for case 1 and 72.38% for case 2. For all calculations: $f = 100$Hz, $\mu_1 = \mu_0$, $\mu_2 = 4000\mu_0$, $\sigma_2 = 1.12 \times 10^7$ S/m, average flux density $B_0 = 1$ T.

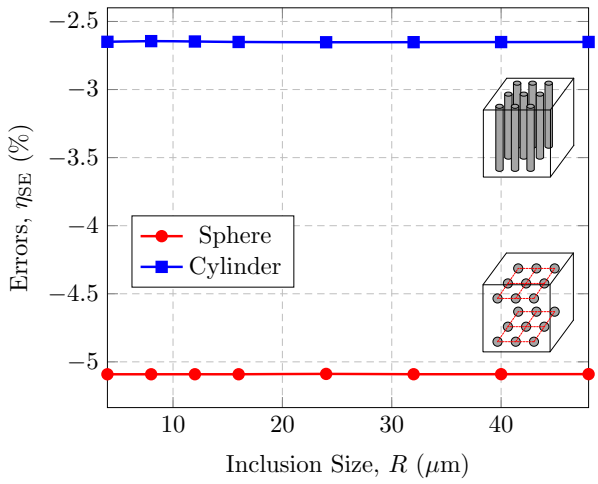

Fig. 2.15 Errors on EC losses of the proposed homogenization model as a function of the inclusion size for cases 1 and 2. Configuration: the same as Fig. 2.14.

2.6 Discussion

The microstructures considered in this study are not fully representative for real SMC, and limit the filling factors that can be achieved. Higher filling factors hence more complex shapes for the inclusions must be considered. The same approach remains applicable, the key-point lying in the determination of the effective magnetic permeability and of the average magnetic field in the inclusion.

For SMC with high concentration of inclusions (greater than 90%), the magnetic field in the inclusion can also be viewed uniform. MG estimate provides acceptable approximation for the effective magnetic permeability of the composite (The higher inaccuracies for the MG estimate arise for mid-range filling factors).[1]

In order to realize high concentration of inclusions, SMC with fiber or cubic inclusions are considered. The fiber particle is assumed to have infinite length and a square cross-section. This problem can be simplified as two-dimensional, denoted as 'square microstructure'. Similarly, the problem of SMC with cubic inclusion is denoted as 'cube microstructure'.

2.6.1 Square Microstructure

Perpendicular Field

The applied magnetic field is perpendicular to the square domain. Substituting the EC loss density in the domain (A.24) in Appendix A into (2.17), the EC loss density of square microstructure has the form,

$$U_z = \frac{9\pi^2}{128}\xi_2 f\, \sigma_2 \mu_2^2 \langle H_z\rangle_2^2 L_2^2 \tag{2.48}$$

where L_2 is the size of the inclusion.

In-plane Field

Now the magnetic field is applied in-plane. Denote $\langle \mathbf{H}\rangle_2$ the 'uniform' magnetic field in the inclusion. Neglecting the induced fields and considering there is no initial current flow through the fiber, the electric field in the inclusion can be solved from Maxwell-Faraday equation which further leads to the EC loss density of SMC,

$$U_{xy} = \frac{1}{6}\pi^2 \xi_2 f\, L_2^2 \sigma_2 \mu_2^2 \left(\langle H_x\rangle_2^2 + \langle H_y\rangle_2^2\right) \tag{2.49}$$

To combine both the perpendicular and in-plane field discussions, a shape factor tensor can be determined as,

$$\mathbb{K} = \begin{bmatrix} \frac{1}{6} & 0 & 0 \\ 0 & \frac{1}{6} & 0 \\ 0 & 0 & \frac{9}{128} \end{bmatrix} \tag{2.50}$$

[1] An example of comparison between MG estimate and FEM results is given later in Fig. 4.4 for 2D case and in Fig. 5.6 for 3D case.

The complete EC loss density formula is,

$$U = \xi_2 \pi^2 L_2^2 f \, \sigma_2 \mu_2^2 \, \langle \mathbf{H} \rangle_2^* \cdot \mathbb{K} \cdot \langle \mathbf{H} \rangle_2 \tag{2.51}$$

2.6.2 Cube Microstructure

If the magnetic field **H** in the cube-shaped inclusion can be considered uniform, the EC losses of the cube can be determined from the cross-section perpendicular to the field. According to the discussion of the square case in Appendix A, the EC loss density formula of SMC with cubic inclusions has the form:

$$U = \frac{9}{128} \pi^2 \xi_2 f \, L_2^2 \sigma_2 \mu_2^2 \, \langle \mathbf{H} \rangle_2^2 \tag{2.52}$$

where L_2 is the size of the cubic inclusion. A shape factor tensor can be determined as (see Appendix A),

$$\mathbb{K} = \frac{9}{128} \mathbb{I} \tag{2.53}$$

so that the EC loss density formula is,

$$U = \xi_2 \pi^2 L_2^2 f \, \sigma_2 \mu_2^2 \, \langle \mathbf{H} \rangle_2^* \cdot \mathbb{K} \cdot \langle \mathbf{H} \rangle_2 \tag{2.54}$$

2.6.3 Complex Permeability

The effective magnetic permeability $\mathbb{\mu}^r$ is obtained by MG estimate (2.20). According to Inclusion Based Problem (IBP) approaches [34, 89], the shape of the inclusion placed in the infinite medium for the inclusion problem is only related to the spatial distribution of the phase in the composite. It is not determined by the shape of the phase in the real microstructure. Therefore, the depolarization tensor (2.21) defined previously remains valid for high concentration SMC with square-shaped inclusions or with cubic inclusions.

Similar to (2.32), the imaginary component of complex permeability has the form

$$\mathbb{\mu}^i = \frac{\pi L_2^2 f \, \sigma_2 \mu_2^2}{\xi_2 (\mu_2 - \mu_1)^2} (\mathbb{\mu}^r - \mu_1 \mathbb{I}) \cdot \mathbb{K} \cdot (\mathbb{\mu}^r - \mu_1 \mathbb{I}) \tag{2.55}$$

Finally, the complex permeability is determined,

$$\tilde{\mathbb{\mu}} = \mathbb{\mu}^r - j \mathbb{\mu}^i \tag{2.56}$$

The discussion on the complex permeability of high concentration SMC is expanded in the following chapters.

2.7 Conclusion

In this chapter, a homogenization strategy for Soft Magnetic Composites is proposed. The purpose is to define an effective complex permeability tensor representative for the behavior of the material. The real part of this tensor reflects the quasi-statics magnetic behavior of the composite, while the imaginary part reflects the eddy current losses. The latter is proportional to the loading frequency and depends on the material properties. It also relies on the spatial arrangement of inclusions, which eventually determines the magnetic field distribution within the structure.

Based on the study of a single inclusion in an infinite medium, the case of dilute heterogeneous materials is deduced, and the general case of composites is extrapolated from this approach. It is crucial to determine the effective permeability, which leads to the determination of the average field in the inclusions. As a result, EC loss density in SMC is described using a homogenized complex permeability tensor. The approach is compared to finite element results and the observed errors are of the order of 5%. It is worth noting that the approach requires accurate estimates of the effective static magnetic permeability tensor of the composite material. That is usually the main difficulty of such a model. It is found that the approach tends to underestimate the EC loss density compared to finite element results and that the errors are frequency-independent for low frequency ranges.

Chapter 3

Bounds and Estimates on Eddy Current Losses in Soft Magnetic Composites

Contents

3.1 EC Loss Density in SMC **51**

3.2 Bounds **52**

3.2.1 Cylinder Microstructure 52

3.2.2 Sphere Microstructure 55

3.2.3 Extension to More Generic Microstructures 57

3.3 EC Loss Density Estimates **60**

3.3.1 Cylinder Microstructure 61

EC Loss Density as a Function of the Filling Factor 61

EC Loss Density as a Function of Permeability Contrast 63

3.3.2 Sphere Microstructure 65

EC Loss Density as a Function of the Filling Factor 65

EC Loss Density as a Function of Permeability Contrast 66

3.4 Discussion **67**

3.4.1 Numerical Calculations on EC Losses Estimates 67

3.4.2 Model Validation 69

3.5 Conclusion **71**

In this chapter, upper and lower bounds for eddy current loss density are analytically deduced for SMC periodic pattern of circular fibers or spherical particles. First and second order moment of the magnetic field in the inclusions are used to build the bounds. Homogenization strategy is applied to determine the effective permeability which links the microscopic field to the macroscopic one. Series expansion can provide an exact formula for the effective permeability, which leads to the determination of first and second order moment of the magnetic field within the inclusions. In the cases where the effective permeability is approximated, bounds approaches are used to estimate the EC loss density. The bounds estimates are compared with Finite Element calculations and then with experimental data from the literature.

3.1 EC Loss Density in SMC

Magnetic field $\mathbf{H}$ can be mathematically split into two contributions $\mathbf{H} = \mathbf{H}_{qs} + \mathbf{H}_{EC}$. $\mathbf{H}_{qs}$ represents the magnetic field in quasistatics and $\mathbf{H}_{EC}$ denotes the induced magnetic field due to EC. At low frequency, $\mathbf{H}_{EC}$ can be neglected, simplifying Maxwell's equations (1.1) into:

$$\nabla \times \mathbf{E} = -j\omega\mu\mathbf{H}_{qs} \tag{3.1}$$

As shown in Fig. 2.4, consider a periodic layout of biphasic SMC with linear, isotropic constituents. Cylindrical (fiber) or spherical inclusions with conductivity σ_2 and permeability μ_2 are considered. The fiber inclusion problem can be reduced to a 2D study and only circular cross-section for fibers is considered.

If the magnetic field $\mathbf{H}_2$ in the inclusion is uniform, as is discussed in the previous chapter, the EC loss density has the form,

$$U = \xi_2\, \pi^2 R^2 f\, \sigma_2\, \mu_2^2 \mathbf{K}^t \cdot \begin{bmatrix} H_{2x}^2 \\ H_{2y}^2 \\ H_{2z}^2 \end{bmatrix} \tag{3.2}$$

where ξ_2 is the volume fraction of the inclusion (filling factor) and R is the radius of cylinder or sphere. Shape factor vector $\mathbf{K}$ value depends on the shape of the inclusion,

$$\mathbf{K}^t = \begin{cases} \left[\frac{1}{2}, \frac{1}{2}, \frac{1}{4}\right] & \text{(cylindrical inclusion)} \\ \left[\frac{1}{5}, \frac{1}{5}, \frac{1}{5}\right] & \text{(spherical inclusion)} \end{cases} \tag{3.3}$$

For SMC, the magnetic field in the inclusion is usually nonuniform and (3.2) is not valid anymore. Then, EC loss density cannot be expressed as a function of the magnetic field distribution in such a simple manner. The norm of the magnetic field, $[H_{2x}^2, H_{2y}^2, H_{2z}^2]^t$, in the inclusion in (3.2) is replaced by first or second order moment of the magnetic field:

$$H_{2m}^2 \simeq \langle H_m \rangle_2^2 \quad \texttt{with} \quad m = x, y, z \tag{3.4}$$

or

$$H_{2m}^2 \simeq \left\langle H_m^2 \right\rangle_2 \quad \texttt{with} \quad m = x, y, z \tag{3.5}$$

where $\langle \cdot \rangle_2$ is the average operator over the inclusion. It leads to the following two estimates for EC loss density:

$$U^- = \xi_2 \, \pi^2 R^2 f \, \sigma_2 \, \mu_2^2 \mathbf{K}^t \cdot \begin{bmatrix} \langle H_x \rangle_2^2 \\ \left\langle H_y \right\rangle_2^2 \\ \langle H_z \rangle_2^2 \end{bmatrix} \tag{3.6}$$

and

$$U^+ = \xi_2 \, \pi^2 R^2 f \, \sigma_2 \, \mu_2^2 \mathbf{K}^t \cdot \begin{bmatrix} \left\langle H_x^2 \right\rangle_2 \\ \left\langle H_y^2 \right\rangle_2 \\ \left\langle H_z^2 \right\rangle_2 \end{bmatrix} \tag{3.7}$$

The following section provides the proof that the exact value of EC loss density lies between these two estimates for square lattice of cylinders or cube lattice of spheres.

3.2 Bounds

Under the low frequency assumption, the magnetic field distribution can be deduced similarly to magnetostatics conditions. EC loss density bounds are discussed separately for SMC in cylinder microstructure and sphere microstructure.

3.2.1 Cylinder Microstructure

The case of cylinder Microstructure can be simplified into a 2D problem. Magnetic field can be decomposed into two parts. One is the tangent component (in-plane part); the other is the normal component. As discussed in the previous chapter, when the field is imposed perpendicularly to the domain, at low frequency, the magnetic field in the domain

is uniform so (3.2) still holds:

$$U_z = \frac{1}{4}\xi_2 \pi^2 R^2 f \sigma_2 \mu_2^2 H_z^2 \tag{3.8}$$

The effective magnetic permeability can also be exactly determined by the upper Wiener bound (1.28).

Consider now only the in-plane magnetic field loading, as indicated in Fig. 3.1. The problem is solved in polar coordinates (r, θ) and Cartesian coordinates (x, y).

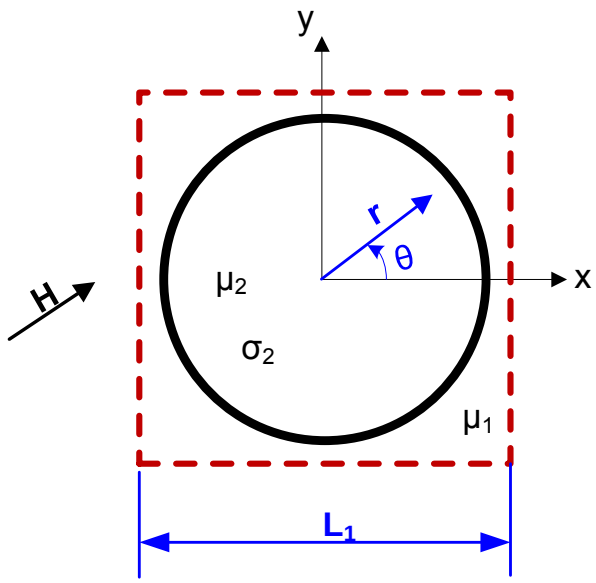

Fig. 3.1 Sketch of SMC in a 2D problem with in-plane magnetic field loading.

For a square lattice of circular inclusions excited by an average magnetic field $\overline{\mathbf{H}}$ (with $\overline{H_z} = 0$) over the cell (and denoting $H = \|\overline{\mathbf{H}}\|$), the general magnetic scalar solution for the potential Φ (with $\mathbf{H} = -\nabla\Phi$) in the inclusion can be determined from the following equation in polar coordinates [25],

$$\Phi_2(r,\theta) = H R \sum_{n=0}^{\infty} (A_n \cos[(2n+1)\theta] + B_n \sin[(2n+1)\theta]) \left(\frac{r}{R}\right)^{2n+1} \tag{3.9}$$

where A_n, B_n are real dimensionless coefficients depending on the applied magnetic field direction, constituent properties and relative size of the inclusion. The magnetic field in

the inclusion in polar coordinates is then,

$$\begin{aligned}\mathbf{H}_2(r,\theta) = &-H\sum_{n=0}^{\infty}(A_n\cos[(2n+1)\theta]+B_n\sin[(2n+1)\theta])(2n+1)\left(\frac{r}{R}\right)^{2n}\vec{u}_r \\ &+H\sum_{n=0}^{\infty}(A_n\sin[(2n+1)\theta]-B_n\cos[(2n+1)\theta])(2n+1)\left(\frac{r}{R}\right)^{2n}\vec{u}_\theta\end{aligned} \tag{3.10}$$

where $\vec{u}_r$ and $\vec{u}_\theta$ indicate unit vectors in polar coordinates.

The induced electric field in the inclusion can be determined. Considering null current flow through the cylinder:

$$E_z(r,\theta) = j\omega\mu_2 HR\sum_{n=0}^{\infty}(A_n\sin[(2n+1)\theta]-B_n\cos[(2n+1)\theta])\left(\frac{r}{R}\right)^{2n+1} \tag{3.11}$$

with ω the working angular frequency: $\omega = 2\pi f$. The in-plane electric field is zero (with $E_r = E_\theta = 0$).

Applying the definition of EC loss density $U = \frac{\langle\sigma\mathbf{E}^2\rangle}{2f}$, the exact value can be determined (while considering no loss in the dielectric matrix surrounding the inclusion):

$$U_{x,y} = \frac{1}{2}\xi_2\pi^2R^2f\,\sigma_2\mu_2^2H^2\sum_{n=0}^{\infty}\frac{1}{n+1}(A_n^2+B_n^2) \tag{3.12}$$

Now, let consider the two estimates for EC loss density given by (3.6) and (3.7). Using (3.10), the first and second order moment in the inclusion are respectively:

$$\begin{cases}\langle\mathbf{H}\rangle_2 = -H(A_0\vec{u}_x+B_0\vec{u}_y) \\ \langle\mathbf{H}^2\rangle_2 = H^2\sum_{n=0}^{\infty}(2n+1)(A_n^2+B_n^2)\end{cases} \tag{3.13}$$

Substituting them into (3.6) and (3.7) leads to the following EC loss density estimates:

$$\begin{cases}U_{x,y}^- = \frac{1}{2}\xi_2\pi^2R^2f\,\sigma_2\mu_2^2H^2(A_0^2+B_0^2) \\ U_{x,y}^+ = \frac{1}{2}\xi_2\pi^2R^2f\,\sigma_2\mu_2^2H^2\sum_{n=0}^{\infty}(2n+1)(A_n^2+B_n^2)\end{cases} \tag{3.14}$$

Comparing (3.12) to (3.14), the two estimates clearly define bounds for EC loss density:

$$U_{x,y}^- \leq U_{x,y} \leq U_{x,y}^+. \tag{3.15}$$

When the magnetic field in the inclusion is uniform, $\mathbf{H}_2(r,\theta)$ in (3.10) should be r-independent, which gives ,

$$A_n = 0, B_n = 0 \quad \forall n \in \mathbb{N}^+. \tag{3.16}$$

Substituting (3.16) into (3.12) to (3.14) lead to the equality in (3.15). This is the case of dilute approximation.

EC loss density is also exact for the component of the magnetic field in z-direction, that is,

$$U_z^- = U_z = U_z^+ \tag{3.17}$$

Combining the cases of perpendicular field and in-plane field, the following generic bounding equation holds for SMC with cylinder microstructure:

$$U^- \leq U \leq U^+ \tag{3.18}$$

3.2.2 Sphere Microstructure

For cubic lattice of spherical inclusions, magnetic field is applied along z-direction first. The general case can be obtained using symmetries (see Appendix C for detailed proof). In spherical coordinates (r,θ,ϕ), shown in Fig. 3.2, the magnetic scalar potential Φ (with

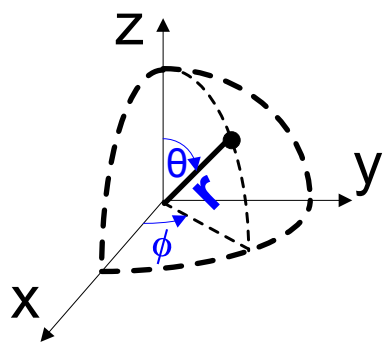

Fig. 3.2 Spherical coordinates (r,θ,ϕ).

$\mathbf{H} = -\nabla\Phi$) can be solved by Laplace's equation $\nabla^2\Phi = 0$. The general solution has the form [77]:

$$\Phi(r,\theta,\phi) = \sum_{l=0}^{\infty}\sum_{m=-l}^{l}\left[A_{lm}r^l + B_{lm}r^{-(l+1)}\right]Y_{lm}(\theta,\phi) \tag{3.19}$$

where A_{lm} and B_{lm} are coefficients to be determined by the boundary conditions and also depend on R. $Y_{lm}(\theta,\phi)$ is the normalized spherical harmonic function:

$$Y_{lm}(\theta,\phi)=\sqrt{\frac{2l+1}{4\pi}\frac{(l-m)!}{(l+m)!}}P_l^m(\cos\theta)e^{jm\phi} \tag{3.20}$$

with $P_l^m(\cos\theta)$ the Legendre polynomials.

If it concerns only the sphere (the inclusion), $B_{lm}=0$. In addition, l is restricted to odd integers ($l=1,3,5,\ldots$) and m to non-negative integer multiples of 4 ($m=0,4,8,\ldots$) [22, 90]. Denote $H=\|\overline{\mathbf{H}}\|$. The potential equation can be rewritten as:

$$\Phi_2(r,\theta,\phi)=HR\sum_{n=0}^{\infty}\sum_{m=0}^{\lfloor\frac{2n+1}{4}\rfloor}C_{2n+1,4m}\left(\frac{r}{R}\right)^{2n+1}Y_{2n+1,4m}(\theta,\phi) \tag{3.21}$$

with $\lfloor\cdot\rfloor$ representing the floor operator. $C_{n,m}$ are real dimensionless coefficients.

Apply

$$\mathbf{H}=-\nabla\Phi=-\frac{\partial\Phi}{\partial r}\vec{u}_r-\frac{1}{r}\frac{\partial\Phi}{\partial\theta}\vec{u}_\theta-\frac{1}{r\sin\theta}\frac{\partial\Phi}{\partial\phi}\vec{u}_\phi \tag{3.22}$$

where $\vec{u}_r$, $\vec{u}_\theta$ and $\vec{u}_\phi$ are unit vectors in spherical coordinates. And then the magnetic field distribution in the inclusion can be obtained.

Given the magnetic field distribution in the sphere, the induced electric field can be analytically deduced. Numerical calculations show that azimuthal induced electric field is negligible. This is also discussed in [21]. Finally, the expression for E_ϕ is:

$$E_\phi(r,\theta,\phi)=-j\,\omega\,\mu\,HR\sum_{n=0}^{\infty}\frac{C_{2n+1,0}}{2n+2}\left(\frac{r}{R}\right)^{2n+1}\frac{\partial}{\partial\theta}Y_{2n+1,0}(\theta,\phi) \tag{3.23}$$

with $E_r=E_\theta=0$.

Substituting (3.23) into the definition $U=\frac{\langle\sigma\mathbf{E}^2\rangle}{2f}$ leads to the exact EC loss density formula:

$$U_z=\frac{3}{4}\xi_2\,\pi R^2 f\,\sigma_2\mu_2^2H^2\sum_{n=0}^{\infty}\frac{2n+1}{(n+1)(4n+5)}C_{2n+1,0}^2. \tag{3.24}$$

The average magnetic field $\langle\mathbf{H}\rangle_2$ and the second order moment $\left\langle\mathbf{H}^2\right\rangle_2$ in the sphere are obtained from (3.22):

$$\begin{cases}\langle\mathbf{H}\rangle_2=-\sqrt{\dfrac{3}{4\pi}}H\,C_{1,0}\\ \left\langle\mathbf{H}^2\right\rangle_2=\dfrac{3}{4\pi}H^2\displaystyle\sum_{n=0}^{\infty}(2n+1)C_{2n+1,0}^2\end{cases} \tag{3.25}$$

Substituting them into (3.6) and (3.7) leads to:

$$\begin{cases} U_z^- = \dfrac{3}{20}\xi_2 \pi R^2 f \sigma_2 \mu_2^2 H^2 C_{1,0}^2 \\ U_z^+ = \dfrac{3}{20}\xi_2 \pi R^2 f \sigma_2 \mu_2^2 H^2 \sum_{n=0}^{\infty}(2n+1)C_{2n+1,0}^2 \end{cases} \tag{3.26}$$

Again, comparing to (3.24), it can be concluded that:

$$U_z^- \leq U_z \leq U_z^+ \tag{3.27}$$

Due to symmetry, the inequality also holds when the magnetic field is applied along x- or y-axis separately. The corresponding EC loss density is U_x or U_y, respectively. As discussed in Appendix C, the final EC loss density can be directly obtained by the addition:$U = U_x + U_y + U_z$. The same for the first and second order moment of the magnetic field. Therefore, if the magnetic field is in arbitrary direction, we still have:

$$U^- \leq U \leq U^+ \tag{3.28}$$

which demonstrates that estimates for EC loss density using average magnetic field and second order moment ((3.6) and (3.7)) are bounds in the case of cubic lattice of spheres.

3.2.3 Extension to More Generic Microstructures

It has been proved that, for periodic SMC with circular or spherical inclusions, first and second order moment of magnetic field provide bounds for EC loss density. Consider that the constituents of a biphasic composite are linear and isotropic and the domain is excited by a macroscopic flux density $\|\overline{\mathbf{B}}\| = B_0$. Given the effective permeability $\tilde{\mu}$, the average magnetic field $\langle \mathbf{H} \rangle_2$ and the second order moment of magnetic field $\langle \mathbf{H}^2 \rangle_2$ in the inclusion can be retrieved [88],

$$\langle \mathbf{H} \rangle_2 = \frac{\tilde{\mu} - \mu_1}{\xi_2(\mu_2 - \mu_1)}\overline{\mathbf{H}} = \frac{\tilde{\mu} - \mu_1}{\xi_2 \tilde{\mu}(\mu_2 - \mu_1)}\overline{\mathbf{B}} \tag{3.29}$$

and

$$\langle \mathbf{H}^2 \rangle_2 = \frac{1}{\xi_2}\frac{\partial \tilde{\mu}}{\partial \mu_2}\overline{\mathbf{H}}^2 = \frac{1}{\xi_2 \tilde{\mu}^2}\frac{\partial \tilde{\mu}}{\partial \mu_2}\overline{\mathbf{B}}^2 \tag{3.30}$$

where μ_1 is the permeability of the dielectric matrix.

For an arbitrary composite, if enough geometry information, noted Ξ, is given, the effective permeability can be obtained as a function of the geometry information and the properties of the constituents: $\tilde{\mu}(\mu_1, \mu_2, \Xi)$. The shape factor $K(\Xi)$ can be obtained analytically, as in Appendix A, or semi-analytically [86], with the geometries of the inclusion simplified as basic simple shapes. Substituting $\tilde{\mu}(\mu_1, \mu_2, \Xi)$ into (3.29) and (3.30), the first and second order moment of magnetic field can be obtained, which lead to the upper and lower EC loss density bounds (U^+ and U^-), respectively. The bounds as a function of volume fraction of inclusions ξ_2 is plotted in Fig. 3.3 in a schematic way. The EC loss density values are normalized by the value at $\xi_2 = 1$. At very low or very high volume

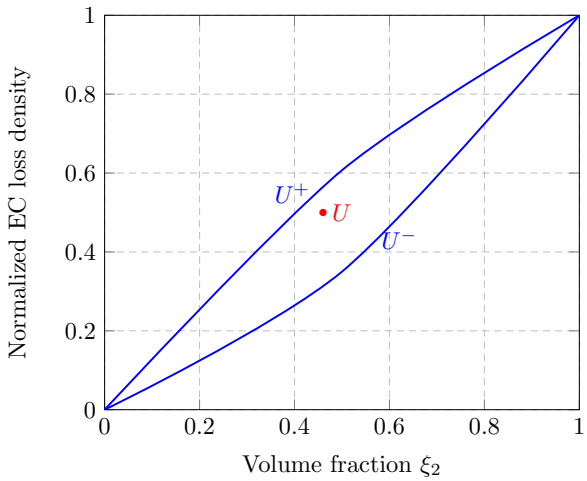

Fig. 3.3 A schematic plot of EC loss density bounds as a function of volume fraction of the inclusion.

fraction, the magnetic field in the inclusion can be considered uniform, so that,

$$\left\langle \mathbf{H}^2 \right\rangle_2 \approx \langle \mathbf{H} \rangle_2^2 \tag{3.31}$$

At the middle range of volume fraction, the magnetic field in the inclusion is distorted, so that,

$$\left\langle \mathbf{H}^2 \right\rangle_2 > \langle \mathbf{H} \rangle_2^2 \tag{3.32}$$

Therefore, there is a gap between the two bounds.

The EC loss density bounds depend on the permeability contrast, as shown in Fig. 3.4. At low permeability contrast, the magnetic field in the inclusion can be considered uniform, so that the two bounds have the same value. As the permeability contrast increases, the magnetic field become distorted. The two bounds separate. When the permeability contrast is big enough, the change of the field distribution brought by the increase of the permeability

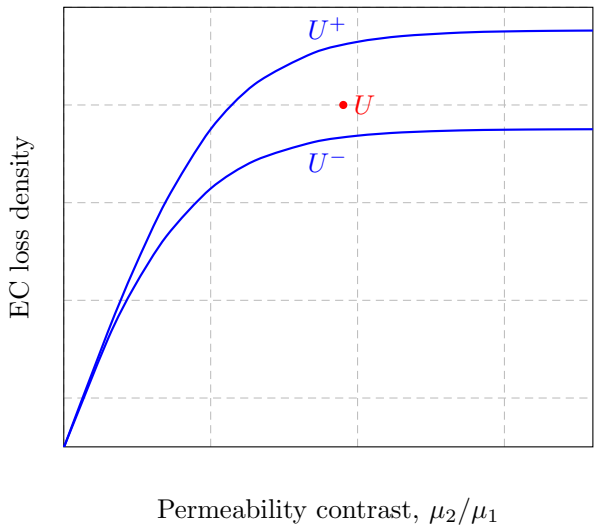

Fig. 3.4 A schematic plot of EC loss density bounds as a function of permeability contrast.

is negligible. Therefore, the space between the two bounds remains unchanged when the permeability contrast is high enough.

The EC loss density bounds also vary as a function of frequency, as shown in Fig. 3.5. At low frequency, the contribution of the induced magnetic field is neglected. The field

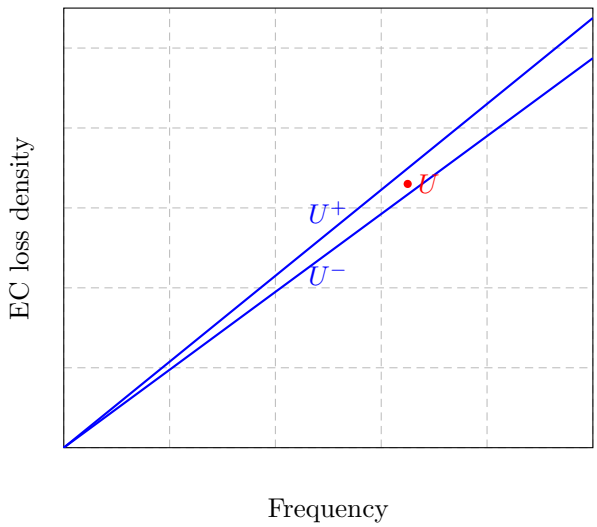

Fig. 3.5 A schematic plot of EC loss density bounds as a function of frequency.

distribution is independent of frequency. The two bounds are proportional to frequency just as the EC loss density. Therefore, the gap between the two bounds is also proportional to frequency.

To conclude, if the effective permeability $\tilde{\mu}(\mu_1, \mu_2, \Xi)$ and the shape factor $K(\Xi)$ are correctly determined, the upper and lower bounds for EC loss density can be obtained. Nevertheless, in most cases, the microstructure information is not sufficiently provided. Usually, with limited geometry information, the effective permeability can only be estimated and the form of the inclusions can be approximated into basic shapes. If an estimate for effective permeability is used, then, U^- and U^+ cannot be considered as bounds anymore.

3.3 EC Loss Density Estimates

The upper and lower bounds depend greatly on the determination of the effective permeability of the composite. In most cases, the effective permeability cannot be exactly obtained; the value has to be approximated. The upper and lower bounds approaches can only be used as estimates.

Maxwell Garnett (MG) estimate is a simple and popular approach for the effective property of composite. The effective permeability is obtained by MG estimate (1.29). Substituting (1.29) into (3.29) and (3.30) leads to

$$\left\langle \mathbf{H}^2 \right\rangle_2 = \langle \mathbf{H} \rangle_2^2 \tag{3.33}$$

Therefore, there is only one EC loss density estimate, denoted as U_{MG}. MG estimate provides a satisfying approximation for dilute SMC with circular or spherical inclusions. An alternative effective permeability estimate can be obtained using series expansions [22, 25], which can attain high precision by calculating high order terms even for high volume fractions ξ_2. Therefore, (3.29) and (3.30) can be determined and provide EC loss density bounds estimates by substitution into (3.6) and (3.7). It should be noted that series expansion is carried out to compute the infinite sum of coefficients. In principle, for composite with square lattice of circular inclusion or with cubic lattice spherical inclusions, the effective permeability can be exactly determined and exact values of average magnetic field and second order moment are obtained.

In the following, EC loss density estimates for periodic SMC with circular inclusion or spherical inclusions are obtained with series expansions. For SMC with high volume fraction of inclusions (greater than 78.54% for 2D case, or greater than 52.36% for 3D case), the inclusions cannot be considered circular or spherical without overlapping. The inclusions are then taken as squares or cubes. The estimates are compared with numerical simulations. Finite Element Method (FEM) calculations have been performed on a unit cell of SMC as described in Fig. 2.4a for different volume fractions at different frequencies.

Thus, EC loss density U_{FEM}, is post-processed in FEM calculations and is considered as a reference value.

The cell size L_1 (lattice length) is fixed to 50 μm. The average flux density over a cell B_0 is fixed to 1 T. The material properties used for the constituents are given in Table 2.1 in the previous chapter. In the following calculations, only one parameter can vary at a time.

3.3.1 Cylinder Microstructure

The effective permeability can be determined by MG estimate, denoted as $\tilde{\mu}_{\text{MG2}}$ [1]. $\tilde{\mu}_{\text{MG2}}$ as a function of volume fraction is plotted in Fig. 2.7b. $\tilde{\mu}_{\text{MG2}}$ is used to obtain EC loss density estimate, U_{MG} (because $\left\langle \mathbf{H}^2 \right\rangle_2 = \langle \mathbf{H} \rangle_2^2$, the two estimates have the same value).

On the other hand, for circular inclusions, as shown in Fig.2.7b, series expansion approaches provide more accurate approximations of effective properties than the MG estimates. The effective permeability is obtained using series expansion with the Godin's formula (2.23b).

In the following results, U_{G}^{-} and U_{G}^{+} are determined by using the effective permeability given by Godin's formula (2.23b). The effective permeability is calculated to the order ξ_2^{12} in (2.26).

EC Loss Density as a Function of the Filling Factor

Numerical EC loss density U_{FEM} and analytical bounds U_{G}^{-} and U_{G}^{+} varying according to the filling factor ξ_2 of cylinders are plotted in Fig. 3.6. In the plots, the 'cir' indicates the results for cylinders with circular cross section, while the 'squ' for cylinders with square cross section.

This figure indicates that EC losses increase when the volume fraction of inclusions becomes higher. For square-shaped inclusions, the EC loss density estimate writes,

$$\begin{aligned} U_{\text{MG}}^{\text{squ}} &= \frac{1}{6}\xi_2\,\pi^2\,L_2^2\,f\,\sigma_2\,\mu_2^2\,\langle \mathbf{H} \rangle_2^2 \\ &= \frac{1}{6}\,\pi^2\,L_1^2\,f\,\sigma_2\,B_0^2\left(\frac{2\mu_2\,\xi_2}{\mu_1+\mu_2+(\mu_2-\mu_1)\xi_2}\right)^2 \end{aligned} \tag{3.34}$$

$U_{\text{MG}}^{\text{squ}}$ is a monotonically increasing function of ξ_2.

For the case of circular inclusions, given $\mu_2 > \mu_1$, (2.27) satisfies $0 < \alpha < 1$, which results in $\tilde{\mu}_{\text{G}}$ in (2.23b) being a monotonically increasing function of ξ_2. The EC loss density

[1] 'MG2' refers to the 2D case in (1.29).

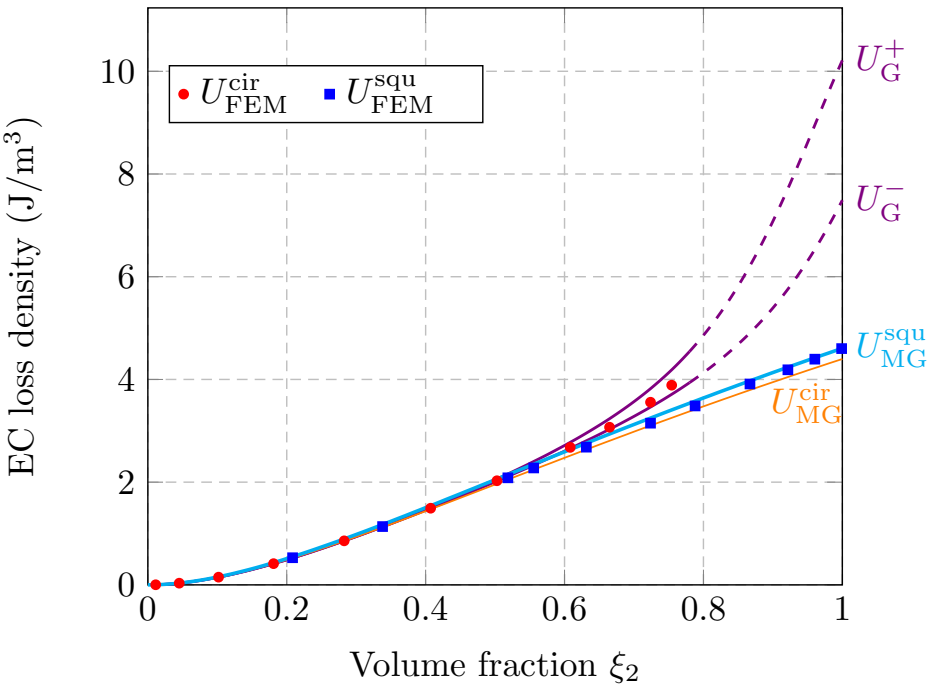

Fig. 3.6 EC loss density as a function of filling factor of the inclusion. For all calculations: $f = 100$ Hz, lattice size $L_1 = 50\,\mu$m, $\mu_2 = 4000\,\mu_0$, $\mu_1 = \mu_0$, $\sigma_2 = 1.12 \times 10^7$ S/m, average flux density $B_0 = 1$ T.

estimate from the average magnetic field approach has the form,

$$\begin{aligned} U_{\mathrm{G}}^{-} &= \frac{1}{2}\xi_2\,\pi^2 R^2 f\,\sigma_2\,\mu_2^2\,\langle \mathbf{H}\rangle_2^2 \\ &= \frac{1}{2}\pi\,L_1^2 f\,\sigma_2 B_0^2 \left(\frac{1}{1-\mu_1/\mu_2}\right)^2 \left(1-\frac{\mu_1}{\tilde{\mu}}\right)^2 \end{aligned} \tag{3.35}$$

Therefore, U^{-} increases monotonically with the volume fraction ξ_2, which was expected.

At low volume fraction, the bounds approximations (U_{G}^{-} and U_{G}^{+}) and MG estimate (U_{MG}) agree very well with the FEM results. The reason is that, at low volume fraction, the magnetic field in the inclusion is uniform (dilute approximation). The uniformity of the magnetic field provides the condition of equality in (3.15). Also for a given low volume fraction, the numerical results and estimates are the same no matter the cross section is a circle or square.

At the middle range of volume fraction ($0.5 < \xi_2 < 0.75$), the bounds approximations (U_{G}^{-} and U_{G}^{+}) still work for circle-shaped inclusions. And the space between the two bounds is getting bigger with the volume fraction, which is physically meaningful. That is because the magnetic field is distorted severely as the volume fraction increases. MG estimate is

not valid for the circular case at high volume fraction. Nevertheless, for the case of SMC with square-shaped inclusions, MG estimate can provide acceptable approximations.

For high volume fraction ($\xi_2 > 0.79$), the inclusion shapes cannot be circular without overlapping. But square inclusions can reach these high volume fractions. MG estimate still provides reliable approximations of EC loss density.

It can also be observed that, using MG estimate, SMC with circular inclusion have nearly the same level of EC losses as SMC with square inclusions for the same volume fraction. According to (2.4) and (2.49), we have,

$$\frac{U_{\mathrm{MG}}^{\mathrm{squ}}}{U_{\mathrm{MG}}^{\mathrm{cir}}} = \frac{\pi}{3} \tag{3.36}$$

As a summary, for SMC with circular inclusions, Godin's formula is used to bound the EC losses. For SMC with square-shaped inclusions, MG estimate is a good choice to obtain the EC losses. It is expected that for high volume fraction inclusion-matrix type composites, the MG estimate is a good approximation for the effective permeability as long as the distribution of the inclusions can be considered random. In the following discussion on the effect of permeability contrast, MG estimate is examined for SMC with square-shaped inclusions.

EC Loss Density as a Function of Permeability Contrast

EC loss density also depends on the permeability contrast, $c_\mu = \mu_2/\mu_1$. The matrix material is nonmagnetic, that is, $\mu_1 = \mu_0$. Results are plotted in Fig. 3.7. For all the calculations, the filling factor of inclusions is fixed to $\xi_2 = 72.38\%$. For circular inclusions, the radius is $R = 24\,\mu$m and for square-shaped inclusions, the size is $L_2 = 42.5\,\mu$m.

When the permeability contrast is high (greater than a few hundred), EC loss density values saturate. Actually, if $\mu_2 \gg \mu_1$, then (2.27) becomes $\alpha \approx 1$, which results in λ and $\tilde{\mu}_{\mathrm{G}}$ roughly independent of μ_2. For the case of circular inclusion, the bounds estimates have the forms,

$$\begin{aligned} U_{\mathrm{G}}^{-} &= \frac{1}{2}\xi_2\,\pi^2 R^2 f\,\sigma_2 B_0^2 \left(\frac{1}{1-\mu_1/\mu_2}\right)^2 \left(\frac{2}{1+\lambda\,\xi_2}\right)^2 \lambda^2 \\ &\approx \frac{1}{2}\xi_2\,\pi^2 R^2 f\,\sigma_2 B_0^2 \left(\frac{2}{1+\lambda\,\xi_2}\right)^2 \lambda^2 \quad \text{as} \quad \mu_2 \gg \mu_1 \end{aligned} \tag{3.37}$$

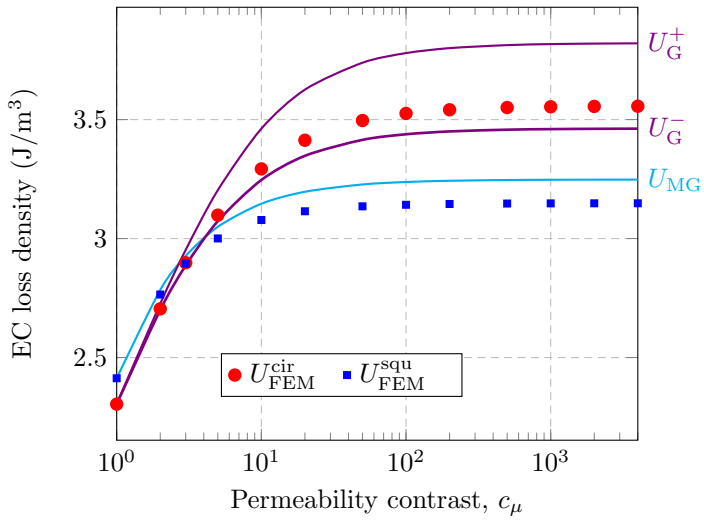

Fig. 3.7 EC loss density as a function of the permeability contrast. Parameters: $f = 100\,\text{Hz}$, lattice size $L_1 = 50\,\mu\text{m}$, $\xi_2 = 72.38\%$, $\mu_1 = \mu_0$, $\sigma_2 = 1.12 \times 10^7\,\text{S/m}$, average flux density $B_0 = 1\,\text{T}$.

and

$$\begin{aligned} U_G^+ &= \frac{1}{2}\xi_2\,\pi^2 R^2 f\,\sigma_2 B_0^2 \left(\frac{1}{1+\mu_1/\mu_2}\right)^2 \left(\frac{2}{1+\lambda\,\xi_2}\right)^2 \left(1+0.9175\alpha^2\xi_2^4+\ldots\right) \\ &\approx \frac{1}{2}\xi_2\,\pi^2 R^2 f\,\sigma_2 B_0^2 \left(\frac{2}{1+\lambda\,\xi_2}\right)^2 \left(1+0.9175\alpha^2\xi_2^4+\ldots\right) \quad \text{as} \quad \mu_2 \gg \mu_1 \end{aligned} \tag{3.38}$$

so that U^- and U^+ are also c_μ-independent and the inequality $U^- < U^+$ holds.

For the case of square-shaped inclusions, the effective permeability is determined by MG estimate, the EC loss density formula writes,

$$\begin{aligned} U_{MG} &= \frac{1}{6}\pi^2 L_1^2 f\,\sigma_2 B_0^2 \left(\frac{2\xi_2\,c_\mu}{1-\xi_2+(1+\xi_2)c_\mu}\right)^2 \\ &\approx \frac{1}{6}\pi^2 L_1^2 f\,\sigma_2 B_0^2 \left(\frac{2\xi_2}{1+\xi_2}\right)^2 \quad \text{as} \quad c_\mu \gg 1 \end{aligned} \tag{3.39}$$

For low contrast, the differences between estimates and the reference values are very low. It was expected since the magnetic field is almost uniform in the inclusions for low permeability contrast even for high filling factors. Because the volume fraction is fixed, when $c_\mu \gg 1$, $\tilde{\mu}$ approaches a constant (judging either from series expansion (2.23) or from MG estimate (2.20)). Thus, the variation of the magnetic field distribution can be neglected. Finally the discrepancy between the MG approach and the FEM results remains

constant as c_μ increases (when $c_\mu > 100$ in Fig. 3.7). This discrepancy is attributed to the approximation on the effective permeability estimate.

3.3.2 Sphere Microstructure

Similar to the case of cylinder microstructure, for cubic inclusions, $\tilde{\mu}_{\text{MG3}}$ ('MG3' means the 3D case in (1.29), see the plot of $\tilde{\mu}_{\text{MG3}}$ as a function of volume fraction in Fig. 2.7a) is used to obtain EC loss density estimate, U_{MG}. For spherical inclusions, the effective permeability is obtained using series expansion with Lam's formula (2.23a). In the following results, U^-_{Lam} and U^+_{Lam} are determined by using the effective permeability given by Lam's formula (2.23a). The effective permeability is calculated to the order ξ_2^6 in (2.24).

EC Loss Density as a Function of the Filling Factor

EC loss density varying with filling factor ξ_2 of inclusions is plotted in Fig. 3.8. In the plots, the superscript 'sph' represents the case of SMC with 'spherical' inclusions, and 'cub' stands for 'cubic'.

Similar conclusions can be drawn for SMC with spherical inclusions as for SMC with cylindrical inclusions. At low volume fraction (dilute assumption), MG estimate provides a reliable approximation for EC loss density. That is because the magnetic field can be considered uniform. At middle volume fraction, when the inclusions are assumed spherical and the microstructure periodic, MG estimate is unacceptable, while the bounds estimates (U^-_{Lam} and U^+_{Lam}) are valid. And the space between two bounds is getting bigger with the volume fraction.

By comparison, when the inclusions are cube-shaped, MG estimate provides relatively good approximation of EC loss density for all the volume fraction range.

Combining (2.12) with (2.52) for the same volume fraction leads to,

$$\frac{U^{\text{cub}}_{\text{MG}}}{U^{\text{sph}}_{\text{MG}}} \approx 0.91 \tag{3.40}$$

The ratio in (3.40) does not depend on the volume fraction. When the inclusions are spherical, and therefore the filling factor small, Lam's approach is a better option. If the inclusions are cubic, MG estimate gives acceptable results. For any microstructure, if the filling factor is high, MG estimate seems a good option if the distribution of the inclusions can be considered random. In the following permeability contrast discussion, MG estimate is calculated for SMC with cubic inclusions.

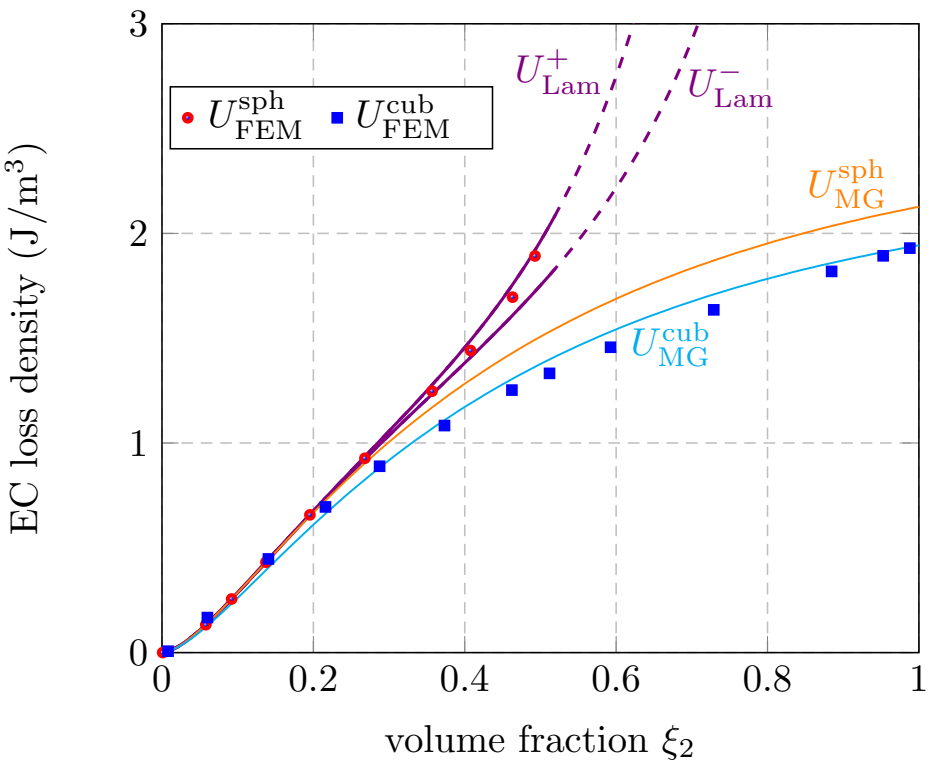

Fig. 3.8 EC loss density as a function of the filling factor of the inclusions. Parameters: $f = 100\,\mathrm{Hz}$, lattice size $L_1 = 50\,\mu\mathrm{m}$, $\mu_2 = 4000\,\mu_0$, $\mu_1 = \mu_0$, $\sigma_2 = 1.12 \times 10^7\,\mathrm{S/m}$, average flux density $B_0 = 1\,\mathrm{T}$.

EC Loss Density as a Function of Permeability Contrast

EC loss density depends also on the permeability contrast,c_μ. The matrix material is nonmagnetic, that is, $\mu_1 = \mu_0$. Fig. 3.9 presents EC loss density as a function of permeability contrast for a fixed filling factor $\xi_2 = 46.32\%$. For spherical inclusions, the radius is $R = 24\,\mu\mathrm{m}$ and for cubic inclusions, the size is $L_2 = 38.69\,\mu\mathrm{m}$.

Again, similar conclusions can be drawn for SMC with spherical inclusions (see conclusions for cylindrical inclusions). A similar formula can be obtained for U^- which is shown to be c_μ-independent at high permeability contrast:

$$\begin{aligned} U^-_{\mathrm{Lam}} &= \frac{1}{5}\xi_2\,\pi^2 R^2 f\,\sigma_2 B_0^2 \left(\frac{1}{1-\mu_1/\mu_2}\right)^2 \left(\frac{3}{\gamma+3\xi_2}\right)^2 \xi_2^2 \\ &\approx \frac{1}{5\xi_2}\pi^2 R^2 f\,\sigma_2 B_0^2 \left(\frac{3}{\gamma+3\xi_2}\right)^2 \quad \text{as} \quad \mu_2 \gg \mu_1 \end{aligned} \tag{3.41}$$

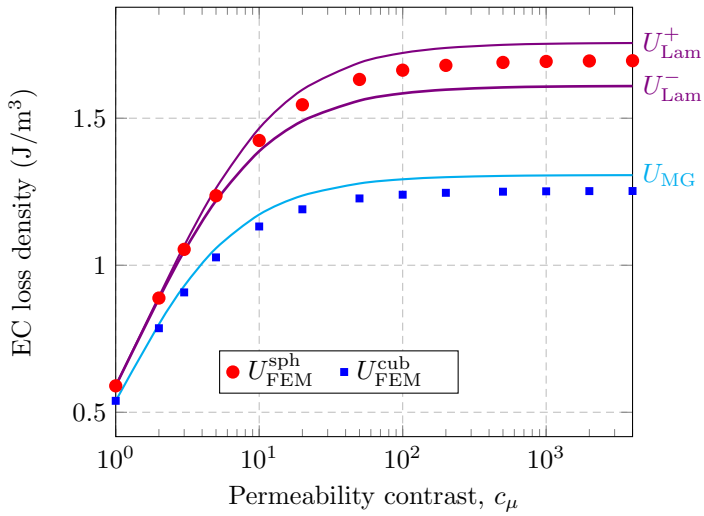

Fig. 3.9 EC loss density as a function of the permeability contrast. For all calculations: $f = 100\,\mathrm{Hz}$, lattice size $L_1 = 50\,\mu\mathrm{m}$, $\xi_2 = 46.32\%$, $\mu_1 = \mu_0$, $\sigma_2 = 1.12 \times 10^7\,\mathrm{S/m}$, average flux density $B_0 = 1\,\mathrm{T}$.

For the case of cubic inclusions, the effective permeability is determined by MG estimate, the EC loss density writes,

$$\begin{aligned} U_{\mathrm{MG}} &= \frac{9}{128}\pi^2 L_1^2 f\,\sigma_2 B_0^2 \left(\frac{3\xi_2 c_\mu}{2(1-\xi_2)+(1+2\xi_2)c_\mu}\right)^2 \\ &\approx \frac{9}{128}\pi^2 L_1^2 f\,\sigma_2 B_0^2 \left(\frac{3\xi_2}{1+2\xi_2}\right)^2 \quad \text{as} \quad c_\mu \gg 1 \end{aligned} \tag{3.42}$$

3.4 Discussion

3.4.1 Numerical Calculations on EC Losses Estimates

EC losses bounds hold for composite with square lattice of cylinders or cubic lattice of spheres. In this section, the possibility to extend these bounds to other microstructures is explored. In the following, microstructures are generated from randomly located cylinders which cannot overlap.

Different distributions of cylinders will lead to different EC losses since field distribution highly depends on microstructure. A square structure of length $L_1 = 200\,\mu\mathrm{m}$ is considered, containing 16 inclusions of the same radius. The following constraints have been used to generate the microstructures: the distance from a cylinder to the boundary satisfies $D_1 \geq 1\,\mu\mathrm{m}$ and the distance between two cylinders respects $D_2 \geq 2\,\mu\mathrm{m}$. One realization of random microstructure is shown in Fig. 3.10.

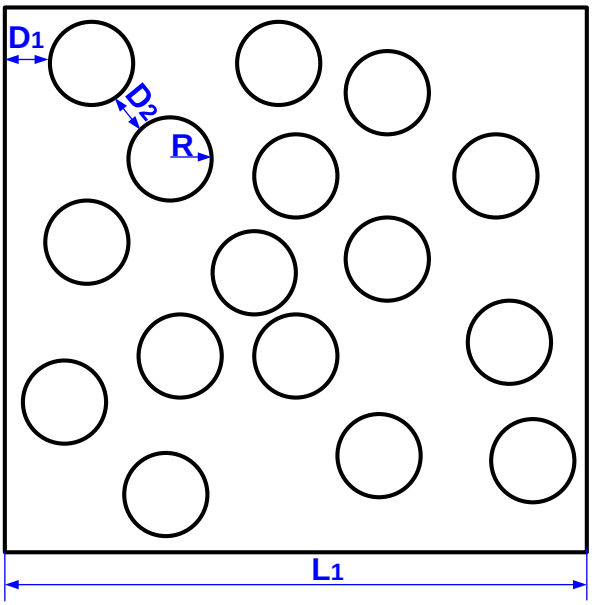

Fig. 3.10 An example of SMC with random distribution of same-size cylinders.

One thousand realizations of microstructures have been generated for each filling factor and the average magnetic field in the inclusions have been post-processed $\left(\langle H_x\rangle_{2,\mathrm{FEM}}, \langle H_y\rangle_{2,\mathrm{FEM}}\right)$, as well as second order moment of the magnetic field $\left(\left\langle H_x^2\right\rangle_{2,\mathrm{FEM}}, \left\langle H_y^2\right\rangle_{2,\mathrm{FEM}}\right)$, and the EC loss density values of the structure U_{FEM}.

(3.6) and (3.7) have then been computed using the post-processed average and second order moment of magnetic field in order to build numerical estimates for EC loss density:

$$\begin{cases} U^{-}_{\mathrm{FEM}} = \dfrac{1}{2}\xi_2\,\pi^2 R^2 f\,\sigma_2\,\mu_2^2\left(\langle H_x\rangle^2_{2,\mathrm{FEM}} + \langle H_y\rangle^2_{2,\mathrm{FEM}}\right) \\ U^{+}_{\mathrm{FEM}} = \dfrac{1}{2}\xi_2\,\pi^2 R^2 f\,\sigma_2\,\mu_2^2\left(\left\langle H_x^2\right\rangle_{2,\mathrm{FEM}} + \left\langle H_y^2\right\rangle_{2,\mathrm{FEM}}\right) \end{cases} \tag{3.43}$$

Each realization has been checked independently and it has been found that the following inequality was verified every time:

$$U^{-}_{\mathrm{FEM}} \leq U_{\mathrm{FEM}} \leq U^{+}_{\mathrm{FEM}} \tag{3.44}$$

One hundred of copies of EC loss density and the corresponding bounds for $R = 18\,\mu$m are plotted in Fig.3.11 as an example. This plot shows that the EC loss density (red line) lies well in between the upper and lower bounds for each of the 100 calculations.

For a composite with a matrix-inclusion microstructure, and supposing the effective permeability is known (or estimated with a certain accuracy), EC loss density can be easily

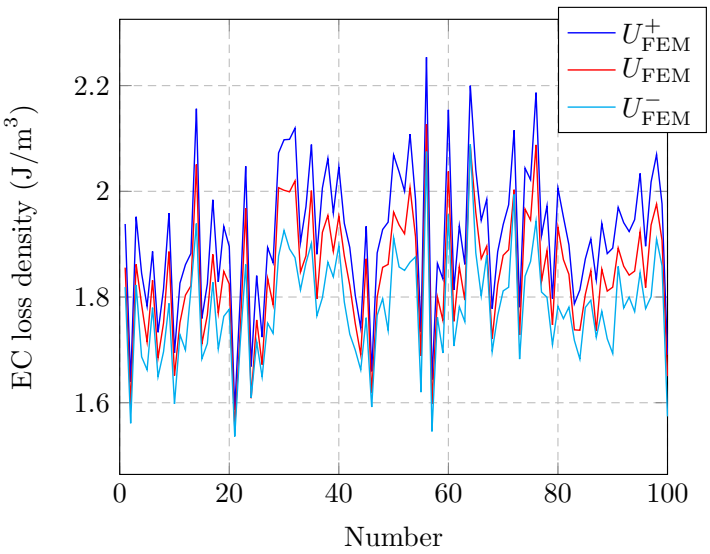

Fig. 3.11 EC loss density and the corresponding bounds. Disk size: $R = 18\,\mu$m, Disk count: 16. $L_1 = 200\,\mu$m, $f = 100\,$Hz, $\mu_2 = 4000\mu_0$, $\mu_1 = \mu_0$, $\sigma_2 = 1.12 \times 10^7\,$S/m, average flux density $B_0 = 1\,$T

estimated at the same time (using (3.43) with (3.29) and (3.30)). The two estimates may even bound the real EC loss density as long as the effective permeability $\tilde{\mu}$ and the derivative $\frac{\partial \tilde{\mu}}{\partial \mu_2}$ are determined.

3.4.2 Model Validation

In this section, the EC loss density estimates are compared with (semi-)analytical models and experimental approaches from the literature. In [91], O. de la Barrière *et al.* conducted experiments on two types of commercial SMCs. EC losses were separated from the total losses. And then they developed a (semi-)analytical model to predict the EC losses [73, 86]. The microscopic view of the two SMCs are shown in Fig. 3.12. The material parameters are detailed in Tab. 3.1. The mean size represents the size of particles assuming the grains as square. The ferromagnetic inclusion material is pure iron, with density $\delta_{\mathrm{Fe}} = 7870\,\mathrm{Kg/m^3}$ and conductivity $\sigma_{\mathrm{Fe}} = 9.93 \times 10^6\,$S/m.

The above parameters are put in the EC losses estimates. In calculating, the volume fraction is calculated from the density ratio $\delta/\delta_{\mathrm{Fe}}$, $\xi_{\mathrm{A}} \approx 94.7\%$ and $\xi_{\mathrm{B}} \approx 92.3\%$. Since the volume fraction is high, the inclusions are considered as cubic and the effective permeability is determined using MG estimate. The corresponding EC loss density estimate is denoted U_{MG}. The results are plotted in Fig. 3.13.

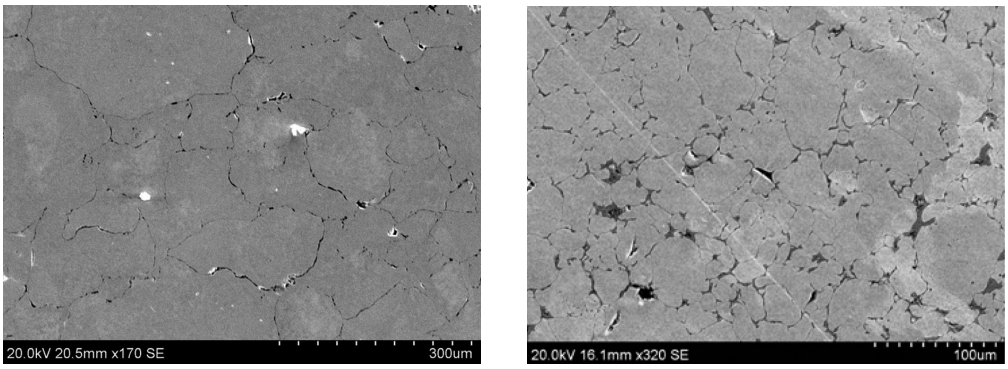

(a) Type A SMC [73] (b) Type B SMC [91]

Fig. 3.12 Cross-sectional microscopic view of SMCs

Table 3.1 Parameters for SMC A and B [73, 91]

		SMC A	SMC B
Relative permeability	μ_r	450	110
Electrical resistivity	$\rho(\Omega \cdot \mathrm{m})$	280×10^{-6}	7600×10^{-6}
Density	$\delta(\mathrm{Kg/m^3})$	7450	7260
Mean size	$\langle s \rangle\,(\mu\mathrm{m})$	114	29.5

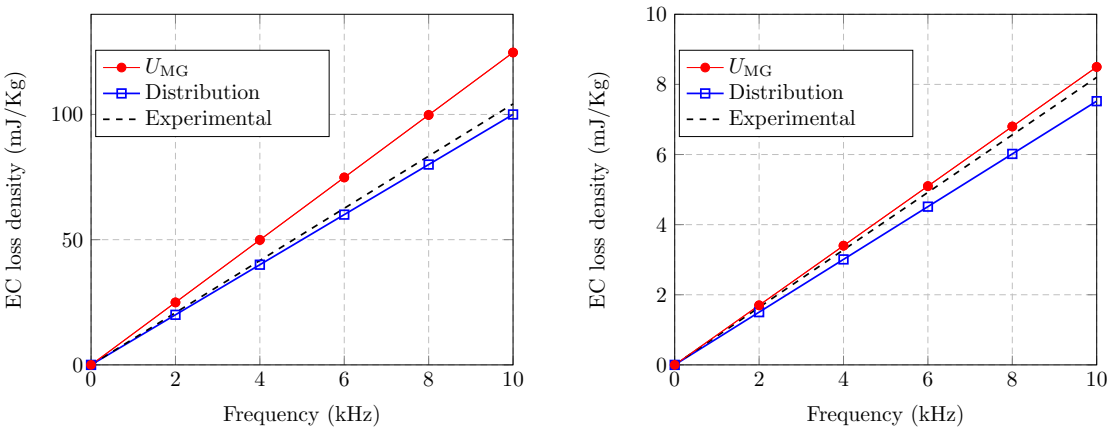

(a) Type A SMC (b) Type B SMC

Fig. 3.13 Comparison of EC loss density from different models with experimental results. (Sinusoidal polarization, peak value: 1 T). 'Experimental' results are from [91]; 'distribution' results are the prediction from [73] considering the distributions of cross sections.

From the comparisons, the EC loss estimate model is validated. The advantage of this model lies in the simplification. For geometry information, this model does not require a

detailed microstructure analysis. The EC losses can be directly calculated with a simple formula. Besides, this model considers the inclusions from the viewpoint of three-dimensions and thus has the potential to correctly predict the EC losses at low volume fractions. The model proposed in [73] uses statistical tools to deal with the micrographs. It considers only the two-dimensional view of the composite. An image software has to be used to carry out an extensive micrographic analysis and to find out experimental distribution functions on the geometry information, which requires more time for data acquisition and processing.

3.5 Conclusion

It is demonstrated in this chapter that average and second order moment of magnetic field can be used to bound EC losses in composite materials with square lattice of cylindrical inclusions or cubic lattice of spherical inclusions, for low frequencies. Generic bounds are predicted from the average and second order moment of magnetic field approaches.

A generalization attempt for a random distribution of (non-overlapping) cylinders shows that average and second order moment of the magnetic field seem to still provide bounds on EC losses.

The key point for evaluating these bounds is to know accurately the effective permeability which enables to retrieve easily the average and second order moment of the magnetic field. However, this effective permeability is usually estimated only. It means that the estimated values for average and second order moment of the magnetic field can only be considered as estimates for EC losses in that case.

A useful feature of this model is that EC distribution is not needed to estimate EC losses which makes this model very simple since it only relies on a homogenization model for the effective permeability. The two bounds estimates obtained in the case of periodic microstructures of spherical (3D) or circular (2D) inclusions are usually close to each other, providing accurate values for EC losses as long as the effective permeability is estimated with good accuracy.

The model presented in this chapter has been first examined by comparison to FEM results. It was then validated by comparing with models and experimental results from the literature.

Chapter 4

Complex Permeability for Soft Magnetic Composites: Application to Magnetic Circuit

Contents

4.1 EC Loss Density of High Concentration SMC **75**

4.1.1 Perpendicular field 76

4.1.2 In-plane field 76

4.1.3 Complex permeability for SMC 78

4.2 Magnetic Circuit Application **80**

4.2.1 Magnetic Behavior 83

4.2.2 EC Loss Density 84

4.3 Conclusion **86**

As discussed in Chapter 2, the complex permeability of SMC contains both the magnetic behavior and lossy characteristics of SMC. The two features can be approximated through an equivalent material with the complex permeability. The model has been comprehensively discussed on SMC with circular or spherical inclusions. It has been found that if the real component of the effective permeability is well estimated, the imaginary part would approximate the EC losses correctly. For high concentration SMC which can be considered as square lattice of square inclusions, MG estimate provides a good approximation of the real component of the complex effective permeability.

In this chapter, the complex permeability model is firstly extended to high filling factor SMC. Secondly, a magnetic circuit made of high concentration SMC is homogenized. Field and loss distributions are examined on an equivalent homogeneous magnetic circuit. And the results are compared with the heterogeneous one.

4.1 EC Loss Density of High Concentration SMC

SMC have 3D microstructures, and when the length of the inclusion grains is much greater than the size of the cross-section, SMC problems can be solved from the viewpoint of a 2D structure. High concentration SMC are simplified as periodic and square-shaped inclusions. The sketch of SMC is shown in Fig. 4.1. Because of periodicity, an elementary cell containing an inclusion and its corresponding matrix is enough to represent the whole structure.

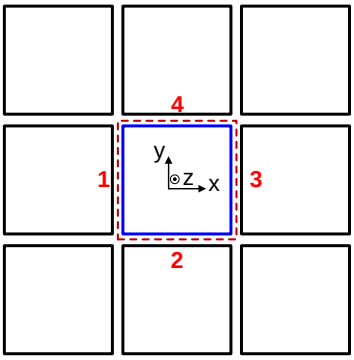

Fig. 4.1 Sketch of periodic high concentration SMC. The domain confined by dashed lines 1-4 forms an elementary cell of the periodic pattern.

This sketch represents both the 2D SMC and a cut plane of 3D SMC (for instance, cutting through the middle of an inclusion from the viewpoint of z direction).

For 2D SMC with perpendicular magnetic field excitation, at low frequency, the magnetic field in the inclusion as well as in the matrix is uniform. The EC loss density has been derived as in appendix A. On the other hand, for SMC with in-plane magnetic field, the

magnetic field in the inclusion is not uniform. Nevertheless, when the filling factor is big enough, an approaching uniformity can be observed in the inclusion.

In order to check the variance of flux density over the inclusion, a standard deviation is introduced as a function of the field and the domain studied:

$$\varsigma(\mathbf{B},\Omega) = \left\langle \|\mathbf{B} - \langle \mathbf{B} \rangle_\Omega\|^2 \right\rangle_\Omega^{\frac{1}{2}} \tag{4.1}$$

where $\langle \cdot \rangle_\Omega$ is the averaging operator over the domain Ω as $\langle \cdot \rangle_\Omega = \frac{1}{\Omega}\int_\Omega \cdot \, \mathrm{d}\Omega$.

The 2D SMC problem can then be separated into two different cases depending on the direction of the magnetic field excitation. The first case considers the magnetic field perpendicular to the cell. The second case considers in-plane magnetic field.

4.1.1 Perpendicular field

When the magnetic field is applied perpendicular to the domain, the magnetic field is uniform all over the domain, both in the inclusion and in the insulating matrix. As discussed in Appendix A, EC loss density formula is recalled as,

$$U = \frac{9}{128}\pi^2 \xi_2 f \, L_2^2 \sigma_2 \mu_2^2 H_z^2 \tag{4.2}$$

where ξ_2, L_2, σ_2, μ_2 are the volume fraction, the length of the inclusion, its electrical conductivity and magnetic permeability respectively.

4.1.2 In-plane field

When the magnetic field is applied in-plane, for instance, along y direction, the magnetic field and the eddy current density distribution in the inclusion are shown in the Fig. 4.2.

For different filling factors, the average flux density in the inclusion, $\langle \mathbf{B} \rangle_2$, and the standard deviation of flux density in the inclusion, $\varsigma(\mathbf{B},2)$, are post-processed from a FEM calculations (see chapter 2). The ratio, $\varsigma(\mathbf{B},2)/\|\langle \mathbf{B} \rangle_2\|$, as a function of the filling factor is plotted in Fig. 4.3.

By comparing the value of standard deviation with the average value, it is justified to conclude that the variance is negligible. In other words, the flux density can be globally

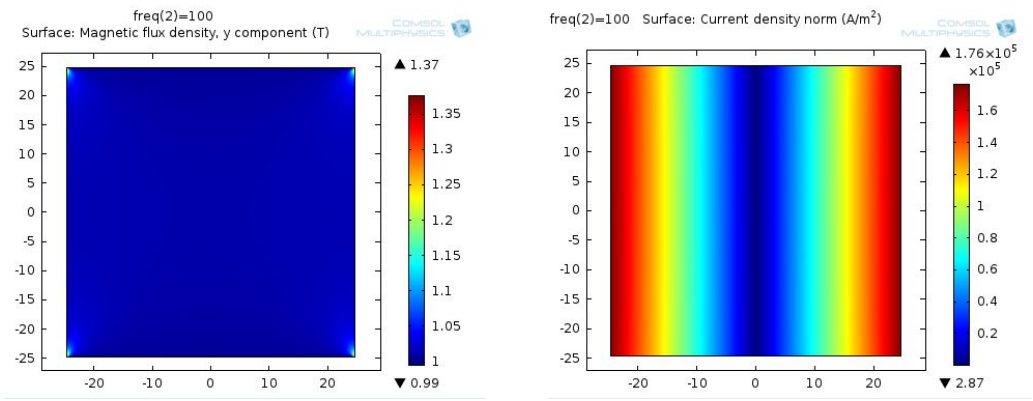

(a) B_y (b) $\|\mathbf{J}\|$

Fig. 4.2 Flux density and eddy current density norm distribution in the inclusion. Lattice size $L_1 = 50\,\mu$m, volume fraction $\xi_2 = 97.6\%$, $\mu_2 = 4000\mu_0$, $\mu_1 = \mu_0$, $\sigma_2 = 1.12 \times 10^7$ S/m, average flux density $B_0 = 1$ T, frequency $f = 100$ Hz.

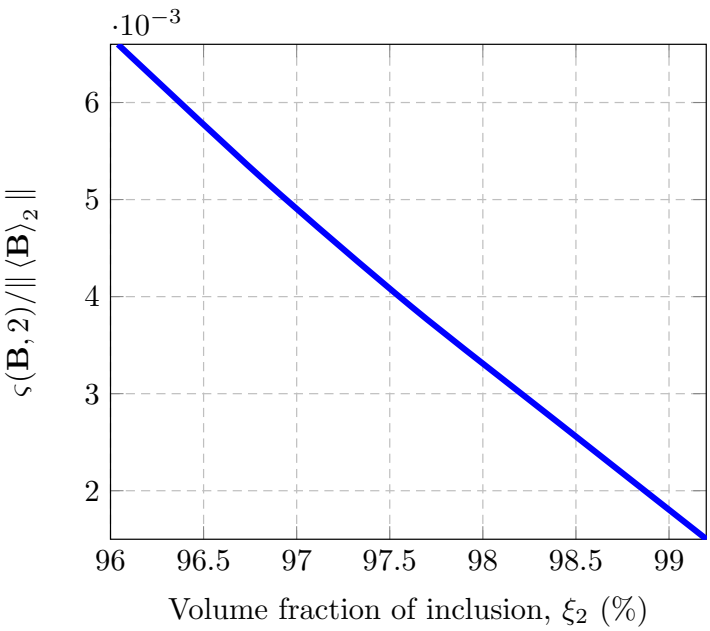

Fig. 4.3 Ratio of standard deviation of flux density to the average flux density norm in the inclusion as a function of the filling factor. Lattice size $L_1 = 50\,\mu$m, $\mu_2 = 4000\mu_0$, $\mu_1 = \mu_0$, $\sigma_2 = 1.12 \times 10^7$ S/m, average flux density $B_0 = 1$ T, frequency $f = 100$ Hz.

considered uniform over the inclusion. Denote $\mathbf{B}_2$ the 'uniform' flux density in the inclusion,

$$\mathbf{B}_2 = \begin{bmatrix} B_{2x} \\ B_{2y} \\ 0 \end{bmatrix} \tag{4.3}$$

Neglecting the induced fields and considering null current flow through the fiber, the electric field in the inclusion can be solved from Maxwell-Faraday equation as:

$$\mathbf{E}_2 = j2\pi f\,(B_{2y}\,x - B_{2x}\,y)\vec{u}_z \tag{4.4}$$

where $\vec{u}_z$ is the unit vector in the direction z for the chosen coordinate system.

Substituting (4.4) into the EC loss density definition (1.16) and considering that EC losses occur only in the inclusion, the EC loss density of SMC becomes,

$$U = \frac{1}{6}\pi^2 \xi_2 f\, L_2^2 \sigma_2 \mathbf{B}_2^2 \tag{4.5}$$

To combine both the perpendicular and in-plane field discussions, for 2D SMC with arbitrary field excitation, the average field in the inclusion writes,

$$\mathbf{B}_2 = \begin{bmatrix} B_{2x} \\ B_{2y} \\ B_{2z} \end{bmatrix} \tag{4.6}$$

The complete EC loss density formula is,

$$\begin{aligned} U &= \xi_2\,\pi^2\,L_2^2\,f\,\sigma_2\,\mathbf{B}_2^* \cdot \mathbb{K} \cdot \mathbf{B}_2 \\ &= \xi_2\,\pi^2\,L_2^2\,f\,\sigma_2\,\mu_2^2 \mathbf{H}_2^* \cdot \mathbb{K} \cdot \mathbf{H}_2 \end{aligned} \tag{4.7}$$

with the shape factor tensor $\mathbb{K}$,

$$\mathbb{K} = \begin{bmatrix} \frac{1}{6} & 0 & 0 \\ 0 & \frac{1}{6} & 0 \\ 0 & 0 & \frac{9}{128} \end{bmatrix} \tag{4.8}$$

4.1.3 Complex permeability for SMC

Using the definition of complex permeability in Chapter 2, setting $\pi\,\overline{\mathbf{H}}^* \cdot \mathbb{\mu}^i \cdot \overline{\mathbf{H}} = U$ leads to the imaginary component of complex permeability.

Homogenization strategy can be applied to build the relationship between the macroscopic field excitation, $\overline{\mathbf{H}}$, and the (average) field in the inclusion, $\mathbf{H}_2$:

$$\mathbf{H}_2 = \frac{1}{\xi_2\,(\mu_2 - \mu_1)}\,(\mathbb{\mu}^r - \mu_1 \mathbb{I}) \cdot \overline{\mathbf{H}} \tag{4.9}$$

where $\mathbb{\mu}^r$ is the effective magnetic permeability (real component).

For SMC with high filling factor of inclusions, Maxwell-Garnett (MG) estimate provides a reliable effective permeability of SMC. $\mathbb{\mu}^r$ is determined by the formula (2.20). Furthermore, effective complex permeability can be determined accordingly.

Because the tensors $\mathbb{K}$, $\mathbb{N}$ and $\mathbb{\mu}^r$ are diagonal, $\mathbb{\mu}^i$ is also diagonal and writes,

$$\mathbb{\mu}^i = \frac{\pi L_2^2 f \sigma_2 \mu_2^2}{\xi_2 (\mu_2 - \mu_1)^2} (\mathbb{\mu}^r - \mu_1 \mathbb{I}) \cdot \mathbb{K} \cdot (\mathbb{\mu}^r - \mu_1 \mathbb{I}) \tag{4.10}$$

And the complex permeability is determined,

$$\tilde{\mathbb{\mu}} = \mathbb{\mu}^r - j\mathbb{\mu}^i \tag{4.11}$$

For the case of 2D SMC with a perpendicular field, the real effective permeability is an exact determination. The effective permeability (real component) of 2D SMC (in-plane) from MG estimate is examined by comparing with FEM calculations. In this case, the effective permeability is isotropic. The results are plotted in Fig. 4.4.

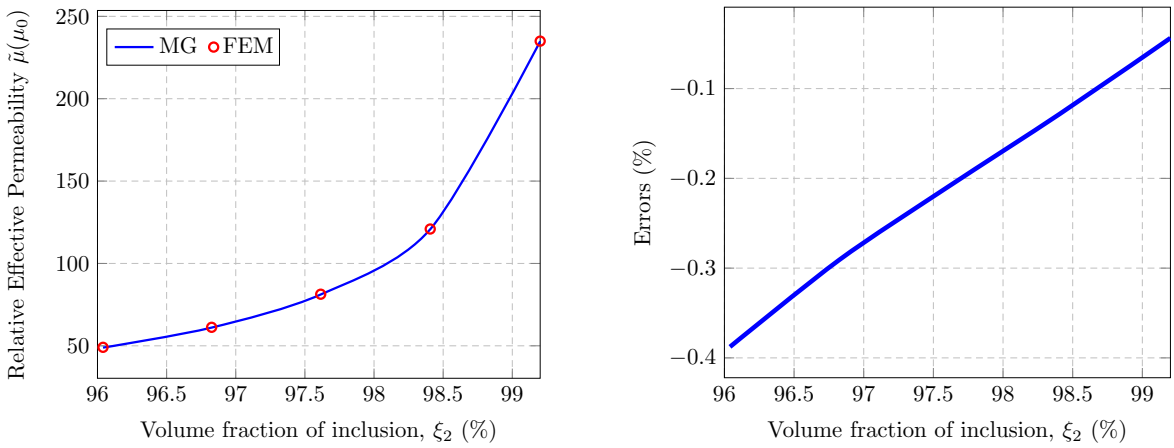

Fig. 4.4 Effective permeability (real component) from MG estimate by comparing to FEM results, and the corresponding discrepancy. (2D SMC, cross-section magnetic permeability). Lattice size $L_1 = 50\,\mu$m, $\mu_2 = 4000\mu_0$, $\mu_1 = \mu_0$, magnetostatics.

The plots show that as the filling factor increases, the discrepancy between MG estimate and the FEM result decreases. This trend is well correlated with the phenomena of field distribution: higher filling factor of the inclusion gives better uniformity of magnetic field in the inclusion.

By comparison, it is worth noting that SMC with circular or spherical inclusions have better uniformity of magnetic field in the inclusion when the volume fraction is lower. The

lower the volume fraction of the inclusion, the better of approximation of the effective permeability and EC loss density.

The EC loss density for an equivalent virtual material with complex permeability is,

$$U_{\mathrm{MG}} = \pi \overline{\mathbf{H}}^{*} \cdot \mathbb{\mu}^{i} \cdot \overline{\mathbf{H}} \tag{4.12}$$

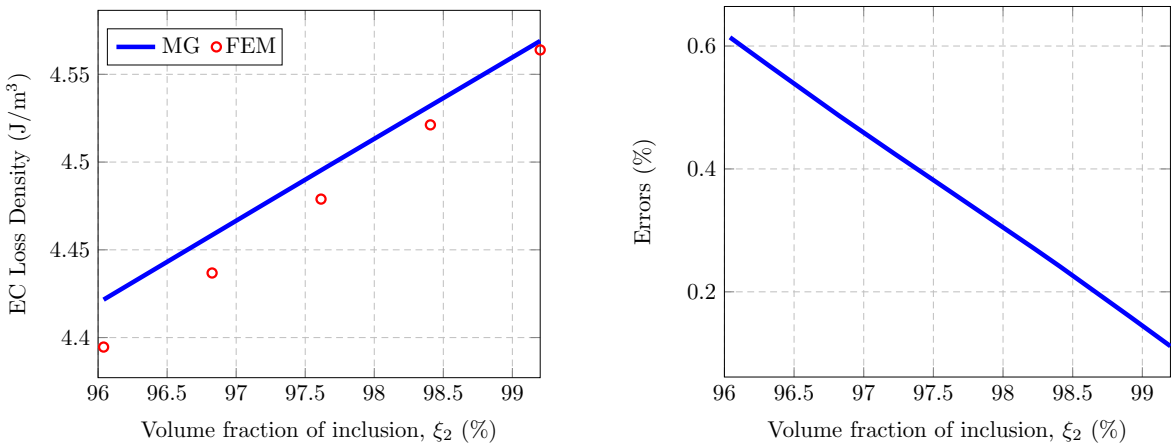

Fig. 4.5 EC loss density from complex permeability (MG) by comparing to FEM results, and the corresponding discrepancy. Lattice size $L_1 = 50\,\mu$m, $\mu_2 = 4000\mu_0$, $\mu_1 = \mu_0$, $\sigma_2 = 1.12 \times 10^7$ S/m. The applied field is along y-axis, and the average flux density $B_0 = 1$ T, frequency $f = 100$ Hz.

The EC loss density obtained by (4.12) is compared with FEM results, as in Fig. 4.5. High concentration periodic SMC with square-shaped inclusions can be homogenized into an equivalent virtual material with a complex permeability. The EC loss density determined by the complex permeability attains high accuracy. The discrepancies are below 0.6% comparing to numerical reference results from FEM calculations.

The size of the device made of SMC is usually much greater than the size of inclusions. The spatial periodicity of inclusion can be assumed from the perspective of the whole structure. Therefore, devices made of SMC can be designed and analyzed with this complex permeability. A magnetic circuit made of high concentration SMC is taken as an application example.

4.2 Magnetic Circuit Application

A schematic magnetic circuit is drawn in Fig. 4.6. It is made of periodic SMC with square-shaped inclusions. Pure Iron is selected as the magnetic inclusion and Epoxy as the insulating

matrix. The Copper coils are wound to provide magnetic field input to the magnetic circuit. The developed complex permeability is designed as a constitutive property of material. It does not rely on the geometric structure of the devices. For simplicity, the example is thereby performed only for the two-dimensional configuration.

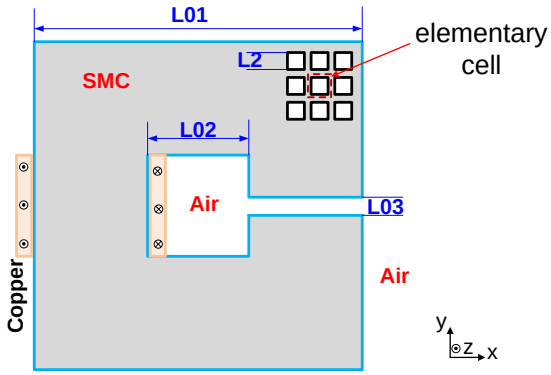

Fig. 4.6 Sketch of a schematic magnetic circuit made of SMC with square inclusions. The domain confined by red dashed lines forms an elementary cell of periodic pattern.

FEM calculations are conducted with the commercial software COMSOL Multiphysics®. The software runs on a workstation equipped with 4-core Intel®Xeon®CPU @ 3.7GHz and 128GB memory. The size of the magnetic circuit and the number of inclusion are chosen according to the capacity of the workstation.

In the calculations, the dimensions of the magnetic circuit are $L_{01} = 3\,\text{mm}$, $L_{02} = 1\,\text{mm}$. The width of the air gap is $L_{03} = 0.1\,\text{mm}$. The length of the inclusion square is $L_2 = 49\,\mu\text{m}$ and the filling factor of the inclusions is $\xi_2 = 96.04\%$.

Because of symmetry, only half the magnetic circuit is calculated, as shown in Fig. 4.7. The size of the air box is $L_{00} = 8\,\text{mm}$. The boundary condition on the symmetry line (green

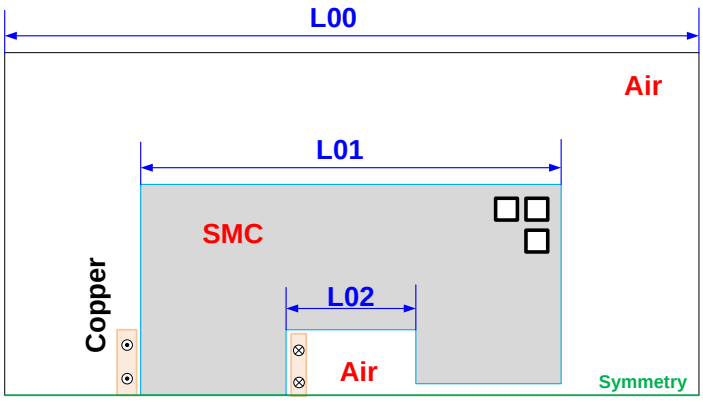

Fig. 4.7 Geometry of the heterogeneous magnetic circuit calculated.

line Fig. 4.7) is Perfect Magnetic Conductor ($\mathbf{n} \times \mathbf{H} = 0$ and $\mathbf{n} \cdot \mathbf{J} = 0$). Based on this configuration, there are 1580 inclusions in the heterogeneous magnetic circuit. A 2-D mesh made of triangular elements has been used. The mesh is constituted of approximately 3×10^5 elements. The computation time is about 200s.

The effective permeability of SMC can be obtained by MG estimate. Given inclusion size, filling factor, material properties, and frequency, the complex permeability can be determined. The heterogeneous magnetic circuit can be homogenized by an equivalent virtual material (EVM). The material has the properties of complex permeability and zero conductivity. Field and EC losses distribution for the heterogeneous magnetic circuit can be approximated through the homogeneous one with the same structure geometry, as in Fig. 4.8 and subjected to the same boundary conditions (in this case, the same surface density on the Copper coils).

A cut line (red line in Fig. 4.8) is plotted in the middle of the air gap so as to examine the field distribution in both cases.

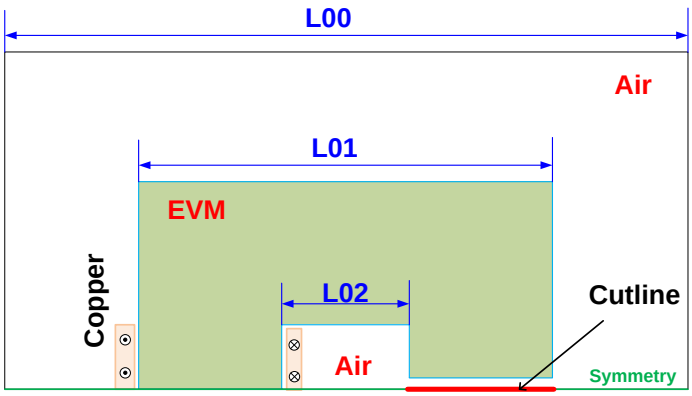

Fig. 4.8 Geometry of equivalent virtual material (EVM) calculated. The red line in the gap is the cutline to examine the magnetic field distribution.

As for the magnetic circuit made of EVM, based on the configuration of the heterogeneous magnetic circuit, by (4.11), the permeability (in-plane) of the EVM is a function of frequency,

$$\tilde{\mu}(f) = 48.9\mu_0 - j4.2 \times 10^{-5}\mu_0 f \tag{4.13}$$

and the electric conductivity of the EVM is set to zero. It takes only 6s to complete the calculation.

4.2.1 Magnetic Behavior

The magnetic field distributions in the homogeneous magnetic circuit are plotted in Fig. 4.9. Fig. 4.9a draws the streamline of the magnetic field. In Fig. 4.9b, magnetic field norm distribution is plotted. The unit of $\|\mathbf{H}\|$ is A/m.

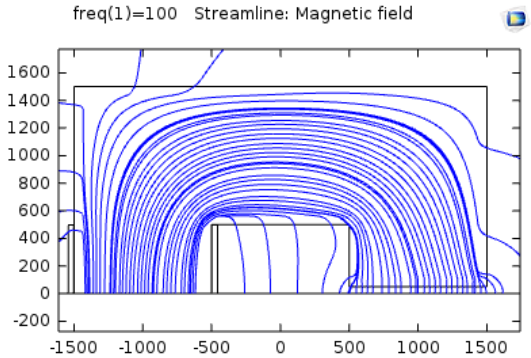

(a) Streamline

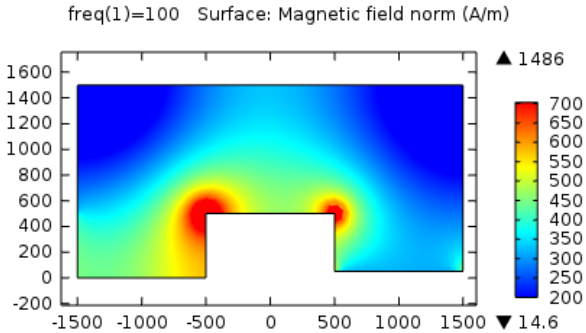

(b) Field norm (A/m)

Fig. 4.9 Magnetic field distributions on the homogeneous magnetic circuit. Relative Permeability: $48.9 - j4.2 \times 10^{-3}$, electric conductivity: 0. Frequency: 100 Hz.

It can be observed that the most intense magnetic field is around the inner corners of the magnetic circuit.

The magnetic behavior of the homogeneous magnetic circuit is also examined on the cut line in the middle of the air gap, as the red line shown in Fig. 4.8. Because of symmetry, H_x on the cutline is zero. H_y distribution is compared on the cut lines from the two magnetic circuits. The comparison is carried out from the perspective of the real part and imaginary part of the magnetic field, in Fig. 4.10. The real part and the imaginary part of H_y distributions on the cutline of EVM magnetic circuit are consistent with those of the SMC magnetic circuit. The steady discrepancy of EVM is of the order of 1.0% for the real part and 1.7% for the imaginary part.

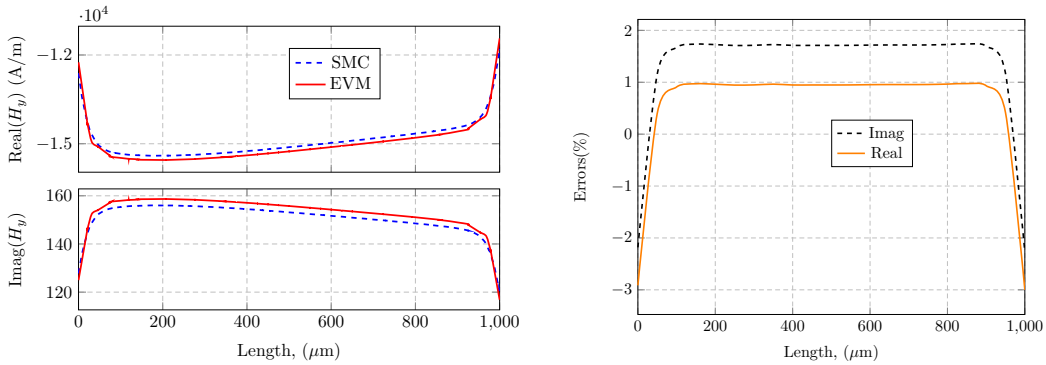

(a) H_y distribution (b) Errors

Fig. 4.10 H_y distribution comparison for magnetic circuit made of SMC (blue dashed line) and the homogeneous one (red line) and the corresponding errors. Parameters: same as the Fig. 4.9.

4.2.2 EC Loss Density

In the heterogeneous magnetic circuit, there are 1580 square-shaped inclusions. Therefore there are the same amount of elementary cells with each containing one inclusion and its surrounding matrix. The average EC loss density is calculated in each cell. Denote $U_{m,n}$ the EC loss density in the cell indexed (m,n). According to the EC loss density definition,

$$U_{m,n} = \frac{\left\langle \sigma \mathbf{E}^2 \right\rangle_{m,n}}{2f} \tag{4.14}$$

where $\langle \cdot \rangle_{m,n}$ means the surface average operator over the cell indexed (m,n). The EC loss distribution on heterogeneous magnetic circuit is plotted in Fig. 4.11. The EC loss density is in unit (mJ/m^3). The EC losses dissipate greatly around the inner corners, especially the

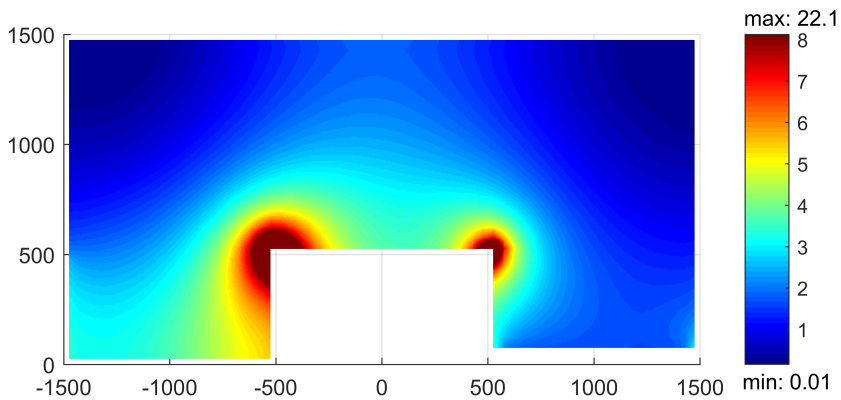

Fig. 4.11 EC loss density (mJ/m^3) distribution on the heterogeneous magnetic circuit.

one near the input electrical sources. By comparing this figure (Fig. 4.11) with Fig. 4.9, as expected, the EC loss density in the heterogeneous magnetic circuit can be reflected by the magnetic field norm distribution in the homogeneous one.

The EC loss density in the homogeneous magnetic circuit is obtained with the magnetic field. In the corresponding cell (m, n), two types of EC loss density are calculated in the homogeneous magnetic circuit:

$$V_{m,n} = \pi \, \tilde{\mu}^i \, \langle \|\mathbf{H}\| \rangle^2_{m,n} \tag{4.15}$$

and

$$W_{m,n} = \pi \, \tilde{\mu}^i \, \left\langle \|\mathbf{H}\|^2 \right\rangle_{m,n} \tag{4.16}$$

$V_{m,n}$ and $W_{m,n}$ are generated from the arithmetic mean and quadratic mean of the magnetic field norm, respectively.

Define the errors,

$$\eta^V_{m,n} = \frac{V_{m,n} - U_{m,n}}{U_{m,n}} \times 100\% \tag{4.17}$$

and

$$\eta^W_{m,n} = \frac{W_{m,n} - U_{m,n}}{U_{m,n}} \times 100\% \tag{4.18}$$

The distribution of the errors over the magnetic circuit cells is plotted in histogram, as shown in Fig. 4.12. The histograms are normalized. It can be observed that the errors

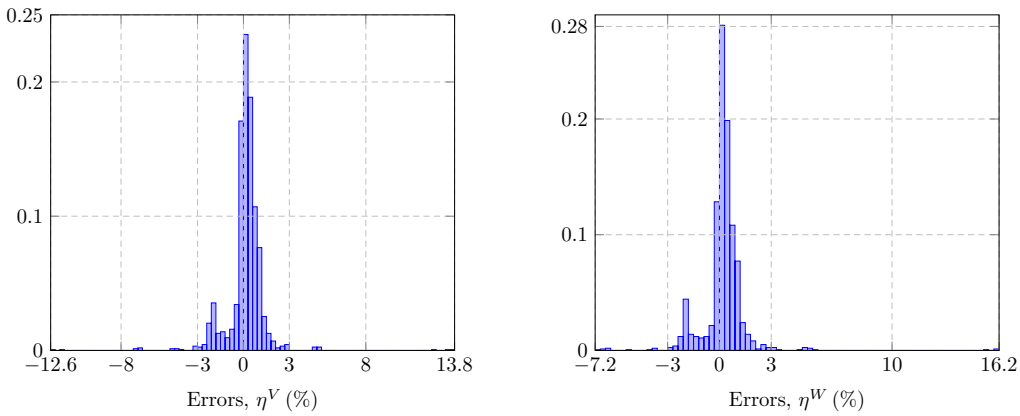

(a) Distribution of η^V (b) Distribution of η^W

Fig. 4.12 Distribution of the errors on the EC losses over the magnetic circuit cells, obtained by comparison between homogenization results and full field FEM calculation.

mainly (more than 98% of cells) lie in the range of (-3%, 3%). The errors $\eta^V_{m,n}$ and $\eta^W_{m,n}$ are

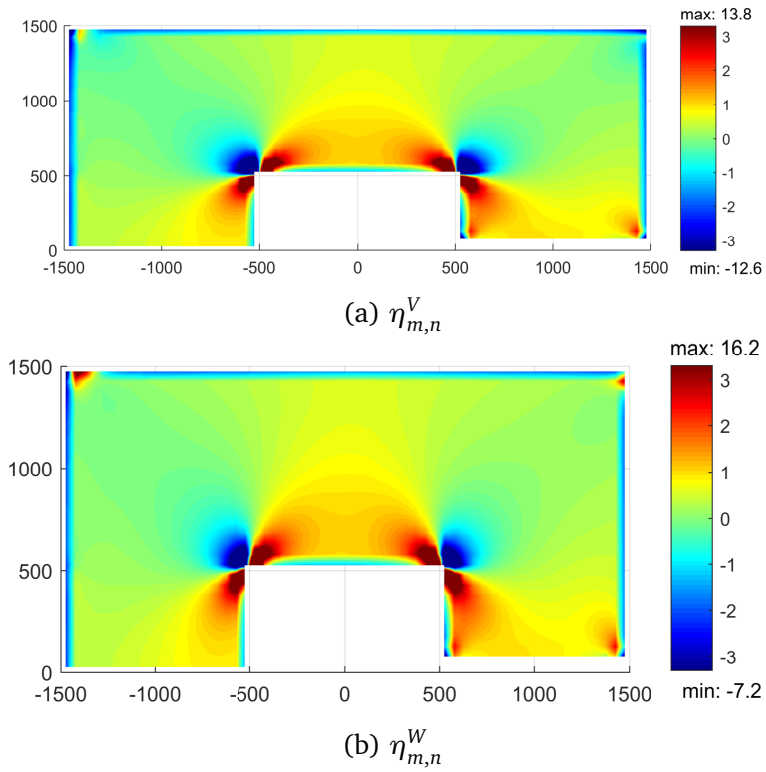

(a) $\eta^V_{m,n}$

(b) $\eta^W_{m,n}$

Fig. 4.13 EC loss error distribution of homogeneous magnetic circuit by comparing with the heterogeneous one. The color bar indicates the error values (%). The labels of the map are the dimensions of the magnetic circuit (in unit: μm)

plotted in Fig. 4.13. The most severe discrepancies (both positive and negative ones) occur at the inner corners. By comparing the data, $\eta^V_{m,n} \leq \eta^W_{m,n}$ holds for a given cell. On average, the error on the whole magnetic circuit is less than 0.5% for the two calculation methods.

The homogeneous magnetic circuit can capture the EC distribution of the heterogeneous one with the complex permeability model.

4.3 Conclusion

A complex permeability is designed for high concentration periodic SMC with square-shaped inclusions. The effective permeability (real part) is determined by MG estimate with high accuracy. The EC loss density is predicted through the complex permeability. This complex permeability is applied to homogenize a heterogeneous magnetic circuit made of periodic SMC.

Full-field FEM calculations have been conducted on the heterogeneous magnetic circuit and its corresponding homogeneous one. Magnetic field distribution has been compared

and examined especially on a cutline in the air gap. A good consistence is observed. EC loss density distributions can be easily plotted on the homogenized magnetic circuit. By comparing to the heterogeneous magnetic circuit, the EC loss density error distributions are also plotted. It can be observed that the overall error on the EC losses is very small (less than 0.5%) and the local errors don't exceed 3% except for very localized areas at the inner corners of the magnetic circuit. It is then concluded that the homogenization method can provide EC losses distribution with very satisfying accuracy. Of course local fluctuations are smoothed by the approach.

Chapter 5

Effect of Stress on Eddy Current Losses in Soft Magnetic Composites

Contents

5.1 Basic Constitutive Equations **91**

5.1.1 EC Loss Density in a Cube-shaped Inclusion 91

5.1.2 Stress-dependent Magnetic Permeability 91

5.1.3 EC Losses In a Cube Subjected To Stress 92

5.2 Loss Density in SMC **92**

5.2.1 Homogenization Technique 94

Mechanical Homogenization 95

Magnetic Homogenization 96

5.3 Model Prediction and Results **98**

5.3.1 Material Parameters 98

5.3.2 Stress Effect 99

Multiaxial Stress 103

5.4 Conclusion **105**

This chapter presents a homogenization model that enables to estimate both the magnetic permeability and Eddy Current (EC) Losses of Soft Magnetic Composites (SMC) subjected to a stress state. The model is applied to periodic SMC microstructures with cubic inclusions. It is shown that stress can be used to adjust the compromise between magnetic performance and EC losses.

In a first part, the stress-dependent magnetic susceptibility model is recalled in the case of homogeneous material. In a second part, a homogenization strategy is employed to find the average fields (stress, magnetic field) within the inclusions based on a homogenization technique. EC loss density as a function of macroscopic stress and field is deduced. Finally, the influence of stress on EC losses in SMC is studied.

5.1 Basic Constitutive Equations

5.1.1 EC Loss Density in a Cube-shaped Inclusion

A cube-shaped homogeneous isotropic magnetic material is placed in Cartesian coordinates xyz with its surfaces perpendicular to the axes. Consider a harmonic magnetic field of such low frequency f that the skin effect is negligible. If the magnetic field $\mathbf{H}$ in the cube is uniform along one axis, for instance, $\mathbf{x}$ ($\mathbf{H} = H\mathbf{x}$), the EC losses of the cube can be determined from the cross-section perpendicular to the field. Electromagnetic problem based on rectangle core with perpendicular field loading has been solved [86, 92]. For a square core, the EC loss density has been accurately approximated at low frequency (Appendix A), which further leads to the simple eddy current loss density formula of a cube:

$$U = \frac{9}{128}\pi^2 f L^2 \sigma (\mu \mathbf{H})^2 \tag{5.1}$$

where L is the size of the cube. σ and μ are the electric conductivity and magnetic permeability of the core, respectively.

5.1.2 Stress-dependent Magnetic Permeability

The stress state is described by a symmetric second order tensor $\mathbb{T}$:

$$\mathbb{T} = \begin{bmatrix} T_{11} & T_{12} & T_{13} \\ T_{12} & T_{22} & T_{23} \\ T_{13} & T_{23} & T_{33} \end{bmatrix} \tag{5.2}$$

The magnetic susceptibility as a function of stress can be expressed as [65]

$$\chi(\mathbb{T}) = \frac{3\,\chi_o}{A_1 + A_2 + A_3} \begin{bmatrix} A_1 & 0 & 0 \\ 0 & A_2 & 0 \\ 0 & 0 & A_3 \end{bmatrix} \tag{5.3}$$

where $A_m = \exp(\alpha\, T_{mm})$ with $m = \{1,2,3\}$. χ_o is the magnetic susceptibility of the material under no applied stress. α is a material parameter linked to the saturation magnetization M_s and saturation magnetostriction constant λ_s [65]:

$$\alpha = \frac{9\,\chi_o\,\lambda_s}{2\,\mu_0\,M_s^2}. \tag{5.4}$$

The magnetic constitutive law can then be written

$$\mathbf{B} = \mu(\mathbb{T}) \cdot \mathbf{H} \tag{5.5}$$

where $\mu(\mathbb{T}) = \mu_0(\mathbb{I} + \chi(\mathbb{T}))$ and $\mathbb{I}$ is the second order identity tensor.

5.1.3 EC Losses In a Cube Subjected To Stress

In this chapter, the effect of magnetostriction and elastoresistance is not considered. Given the constitutive equation (5.3), and the expression of the EC losses (5.1), the EC loss density in a cube subjected to a uniform magnetic field and stress is

$$U = \frac{9}{128}\,\pi^2\,f\,L^2\,\sigma\,\left(\mu(\mathbb{T}) \cdot \mathbf{H}\right)^2. \tag{5.6}$$

The effect of stress is incorporated into EC loss density through the permeability tensor $\mu(\mathbb{T})$.

5.2 Loss Density in SMC

SMC consist of electrically insulated ferromagnetic inclusions. In quasi-magneto-statics, global eddy current flowing between inclusions can be neglected. For a periodic pattern of cubic inclusions, as shown in Fig. 5.1, the magnetic field in the inclusion can be approximated as uniform if the filling factor is high.

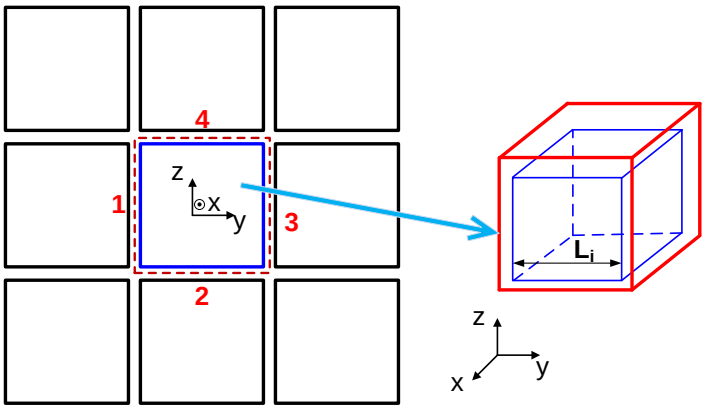

Fig. 5.1 Sketch of cubic lattice of cubic inclusions. The domain confined by its surrounding matrix (in red cube) forms an elementary cell of periodic pattern.

When the magnetic field is applied, for instance, along z direction, the magnetic field distribution is shown in Fig. 5.2. Because of symmetry, only half of the elementary cell is modeled and calculated in order to save computation time and memory.

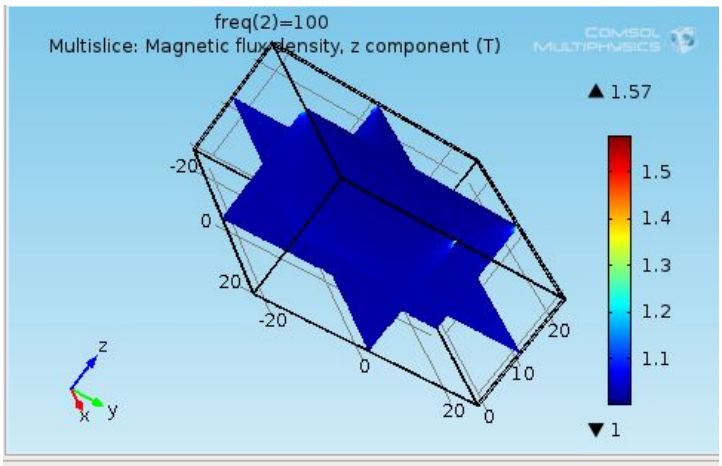

Fig. 5.2 Magnetic flux density distribution in the inclusion. Lattice size: $50\,\mu$m, volume fraction $\xi = 96\%$, $\mu_i = 4000\mu_0$, $\sigma_i = 1.12 \times 10^7\,$S/m, average flux density $B_0 = 1\,$T, frequency $f = 100\,$Hz.

The standard deviation introduced as a function of the field and the domain studied is examined:

$$\varsigma(\mathbf{B},\Omega) = \left\langle \|\mathbf{B} - \langle \mathbf{B} \rangle_\Omega\|^2 \right\rangle_\Omega^{\frac{1}{2}} \tag{5.7}$$

For different filling factors, the average flux density in the inclusion, $\langle \mathbf{B} \rangle_i$, and the standard deviation of flux density in the inclusion, $\varsigma(\mathbf{B}, i)$, are post-processed in the calculations. The ratio, $\varsigma(\mathbf{B}, i)/\| \langle \mathbf{B} \rangle_i \|$, as a function of the filling factor is plotted in Fig. 5.3.

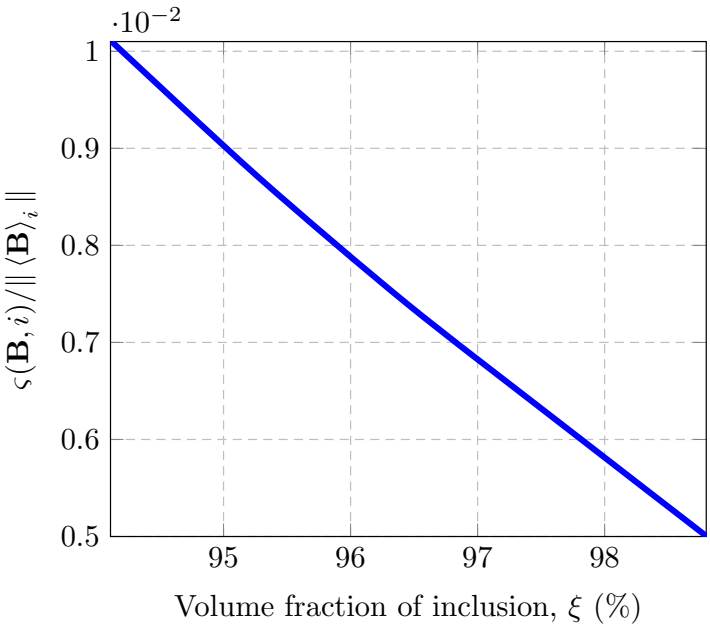

Fig. 5.3 Ratio of standard deviation of flux density to the average flux density norm in the inclusion as a function of the filling factor. Lattice size: $50\,\mu$m, $\mu_i = 4000\mu_0$, $\sigma_i = 1.12 \times 10^7$ S/m, average flux density $B_0 = 1$ T, frequency $f = 100$ Hz.

It can be concluded from Fig. 5.3 that, as expected, the higher the concentration of the inclusion, the better the uniformity of the field.

The average field $\langle\mathbf{H}\rangle_i$ in the inclusions can be used in (5.6) as an estimate for $\mathbf{H}$. Since the matrix is dielectric, EC occurs only in the inclusion, the macroscopic EC (flowing in the matrix) being negligible. From the perspective of the whole composite material, the EC loss density U is then:

$$U = \frac{9}{128}\,\xi\,\pi^2\,f\,L_i^2\,\sigma_i\,(\mathbb{\mu}_i \cdot \langle\mathbf{H}\rangle_i)^2 \tag{5.8}$$

where $\langle\cdot\rangle_i$ is the averaging operator over the inclusions. L_i is the size of the inclusion as depicted in Fig. 5.1. ξ is the volume fraction of inclusions (filling factor) and σ_i the electric conductivity. In order to make use of (5.8) to calculate the EC losses in SMC, the average magnetic field and stress inside inclusions are required. They differ from the macroscopic loading due to the heterogeneity of the material. In order to obtain these quantities, a homogenization technique can be applied.

5.2.1 Homogenization Technique

The purpose of the homogenization strategy is to find the localization operators establishing the relationship between the average local quantities (stress, magnetic field) and the

macroscopic loading. Mechanical homogenization is first applied and then magnetic homogenization is used. The flow chart of the modeling strategy is shown in Fig. 5.4, and the homogenization process is explained hereafter. In this study, the effect of magnetostriction is neglected, so that there is no loop required in the strategy.

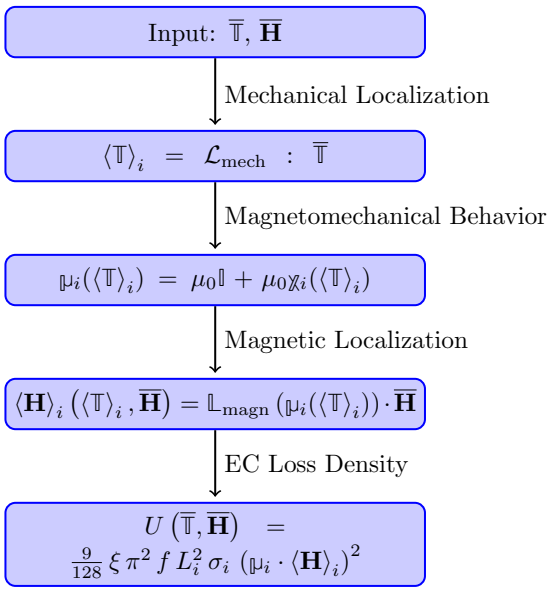

Fig. 5.4 Flow chart for the modeling scheme

Mechanical Homogenization

The relationship between the macroscopic stress $\overline{\mathbb{T}}$ and the average stress in the inclusion $\langle \mathbb{T} \rangle_i$ is built through a 4-th order localization tensor $\mathscr{L}_{\text{mech}}$.

$$\langle \mathbb{T} \rangle_i = \mathscr{L}_{\text{mech}} : \overline{\mathbb{T}} \tag{5.9}$$

Mori-Tanaka(MT) homogenization strategy [93] is used here to determine the mechanical localization tensor (see Appendix D for the detailed equations). Other homogenization strategies could be chosen depending on the material microstructure [89].

Here, as a validation illustration, we apply a 1D stress $\overline{T}_{11}$ along the x-direction. The average stress $\langle T_{11} \rangle_i$ in the inclusion is calculated by MT using (5.9). The results are compared to FEM calculations, as shown in Fig. 5.5.

Figure. 5.5 shows that the average stress in the inclusions is greater than that of the macroscopic stress (as expected because the inclusions are stiffer than the matrix). As the volume fraction of the inclusion increases, the average stress in the inclusions gradually

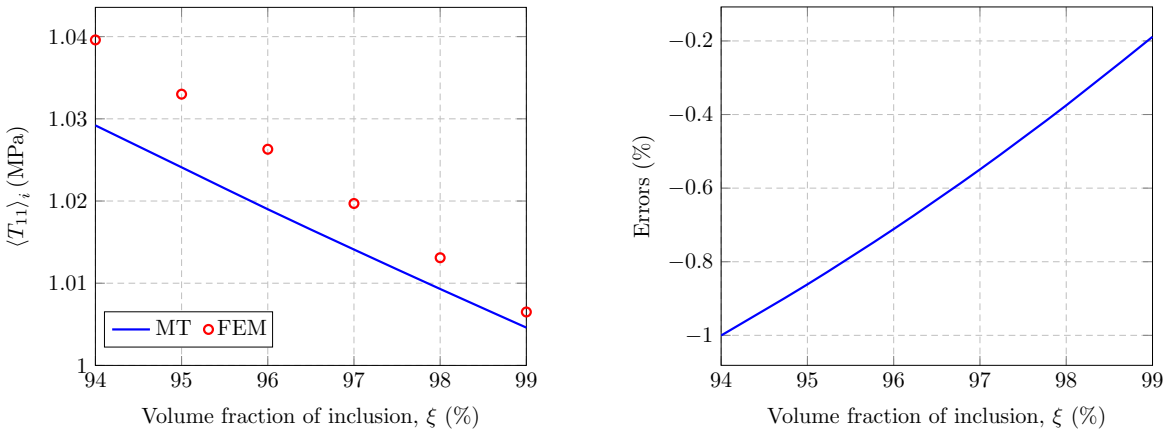

Fig. 5.5 Average stress in the inclusion from MT estimate (5.9) by comparison to FEM results, and corresponding discrepancy. Lattice size: 50 μm. $\overline{T}_{11} = 1$ MPa The mechanical parameters are listed in Tab. 5.1.

approaches the macroscopic stress. MT estimate provides acceptable approximation (errors less than 1%), and as the volume fraction increase, the errors decrease.

The average stress in the inclusion is substituted into (5.3) to obtain the susceptibility tensor $\chi_i(\langle \mathbb{T} \rangle_i)$ of the inclusion, which further leads to the permeability tensor

$$\mu_i(\langle \mathbb{T} \rangle_i) = \mu_0 \mathbb{I} + \mu_0 \chi_i(\langle \mathbb{T} \rangle_i) \tag{5.10}$$

Since the material is assumed to exhibit linear magnetic behavior, the permeability tensor is only a function of the applied stress.

Magnetic Homogenization

Similar to the mechanical case, the magnetic localization operation reads:

$$\langle \mathbf{H} \rangle_i = \mathbb{L}_{\text{magn}} \cdot \overline{\mathbf{H}} \tag{5.11}$$

where $\mathbb{L}_{\text{magn}}$ is a second order magnetic localization operator. Given the effective permeability $\tilde{\mu}$ of the SMC, the magnetic localization tensor $\mathbb{L}_{\text{magn}}$ [94] has the form

$$\mathbb{L}_{\text{magn}} = \frac{1}{\xi} (\tilde{\mu} - \mu_m \mathbb{I}) \cdot (\mu_i - \mu_m \mathbb{I})^{-1} \tag{5.12}$$

where μ_m is the permeability of the matrix. The effective property relies on a static homogenization approach built from basic Inclusion Problem [34, 89]. The choice of MG

estimate (Hashin and Shtrikman lower bound) provides a good estimate of the effective property for this type of microstructure. The effective permeability has the form,

$$\tilde{\mu}(\langle\mathbb{T}\rangle_i) = \mu_m\mathbb{I} + \xi\mu_m(\mu_i - \mu_m\mathbb{I})\cdot[\mu_m\mathbb{I} + (1-\xi)\mathbb{N}\cdot(\mu_i(\langle\mathbb{T}\rangle_i) - \mu_m\mathbb{I})]^{-1} \tag{5.13}$$

where $\mathbb{N}$ is the depolarization tensor and $\mathbb{N} = \frac{1}{3}\mathbb{I}$ for the configuration of cubic lattice of cubic inclusions.

The effective permeability (real component) from MG estimate is examined by comparing to FE calculations (reference values). Without stress, the effective permeability is isotropic. The results are plotted in Fig. 5.6. The error is less than 1% for high concentration

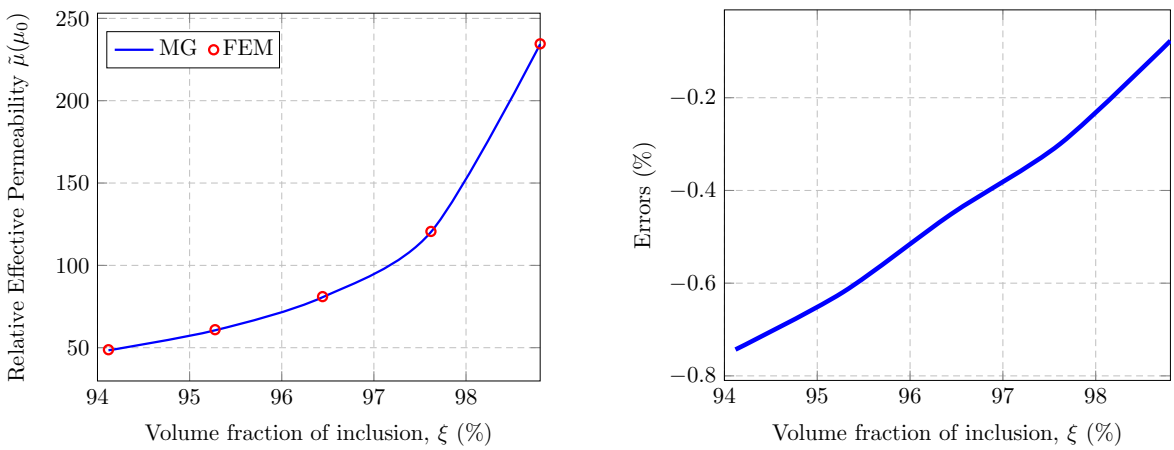

Fig. 5.6 Effective permeability (real component) from MG estimate by comparing to FEM results, and the corresponding discrepancy. Lattice size: 50 μm, $\mu_i = 4000\mu_0$.

composite. The higher the concentration, the less the error of the MG estimate. Combining (5.11)-(5.13), the average field in the inclusion has the form,

$$\langle\mathbf{H}\rangle_i\left(\overline{\mathbb{T}},\overline{\mathbf{H}}\right) = \mu_m\left[\mu_m\mathbb{I} + \frac{1}{3}(1-\xi)(\mu_i(\langle\mathbb{T}\rangle_i) - \mu_m\mathbb{I})\right]^{-1}\cdot\overline{\mathbf{H}} \tag{5.14}$$

The average field in the inclusion depends on both the macroscopic magnetic field and the macroscopic stress. This average field (5.14) and the permeability tensor (5.10) is substituted into (5.8) to obtain the EC loss density in SMC.

In the following section, specific materials (see material parameters in Tab. 5.1) are chosen to illustrate the relationship between EC loss density and the applied stress and field.

5.3 Model Prediction and Results

The proposed model is fully multiaxial. However, for the sake of simplicity, the analysis will be mostly performed for 2D-stress configuration.

5.3.1 Material Parameters

Iron is selected as the ferromagnetic inclusion material and epoxy as the insulating matrix. The material parameters are listed in Tab. 5.1. Inclusions are cubic and the length of the

Table 5.1 Material parameters used in the calculations for SMC [51, 58]

	Iron	Epoxy
Conductivity (S/m)	1.12×10^{7}	1.7×10^{-13}
Relative Permeability	2500	1
Saturation Magnetization (A/m)	1.71×10^{6}	-
Saturation Magnetostriction constant	6.1×10^{-6}	-
Young Modulus (Pa)	110×10^{9}	3.5×10^{9}
Poisson Ratio	0.23	0.32
$\alpha\,(\mathrm{Pa}^{-1})$	1.86×10^{-8}	-

elementary cell is fixed at 50 μm for all the FEM calculations. In the following calculations, the magnetic field stands along the x-direction. The working frequency is $f = 100$ Hz. The magnetic behavior is regarded as linear and no saturation is considered. Denote μ_i^o the original magnetic permeability of the isotropic inclusion under no applied mechanical stress. When the stress is applied, the permeability becomes a diagonal second order tensor $\mathbb{\mu}_i$. According to (5.3), $\mathbb{\mu}_i$ is a diagonal matrix, which writes,

$$\mathbb{\mu}_i = \begin{bmatrix} \mu_{i,11} & 0 & 0 \\ 0 & \mu_{i,22} & 0 \\ 0 & 0 & \mu_{i,33} \end{bmatrix} \tag{5.15}$$

Now that the magnetic field is applied in the x-direction, the average magnetic field in the inclusion in other direction should be null, namely,

$$\left\langle H_y \right\rangle_i = 0 \quad \text{and} \quad \langle H_z \rangle_i = 0 \tag{5.16}$$

Substituting (5.15) and (5.16) into (5.8) yields,

$$U = \frac{9}{128}\,\xi\,\pi^2\,f\,L_i^2\,\sigma_i\,\left(\mu_{i,11}\,\langle H_x\rangle_i\right)^2 \tag{5.17}$$

For the permeability tensor $\mathbb{\mu}_i$, only the component parallel to applied field is critical to the EC losses of SMC and the other two components do not contribute to the EC losses. In the following, denote $\mu_{i,\|}$ the parallel component of the permeability tensor $\mathbb{\mu}_i$.

5.3.2 Stress Effect

One classic multiaxial stress is the hydrostatic stress state ($\mathbb{T}_{\mathrm{HdS}}$),

$$\mathbb{T}_{\mathrm{HdS}} = T_{11}\begin{bmatrix} 1 & 0 & 0 \\ 0 & 1 & 0 \\ 0 & 0 & 1 \end{bmatrix} \tag{5.18}$$

Calculations show that the macroscopic hydrostatic applied on the structure does not influence the magnetic permeability on the inclusion, and therefore does not affect the EC loss density. The non-effect of applied hydrostatic stress on the magnetic behavior has been discussed in [95, 96].

A general 2D stress reads

$$\mathbb{T}_a = \begin{bmatrix} T_{11} & T_{12} & 0 \\ T_{12} & T_{22} & 0 \\ 0 & 0 & 0 \end{bmatrix} \tag{5.19}$$

When the stress $\mathbb{T}_a$ is applied macroscopically on the SMC, the parallel (to the magnetic field) component of the magnetic permeability of the inclusion as a function of (T_{11}, T_{22}) is shown in Fig. 5.7. The trace of tensor $\mathbb{T}_a$ (a square matrix) is the sum of the elements on the main diagonal,

$$\mathrm{trace}(\mathbb{T}_a) = T_{11} + T_{22}. \tag{5.20}$$

Therefore, the label of the horizontal axis in Fig. 5.7b, $\mathrm{trace}(\mathbb{T}_a)$, represents either T_{11} when $T_{22} = 0$ or T_{22} when $T_{11} = 0$.

The permeability of the inclusion is increased by the parallel tensile stress or perpendicular compressive stress. It attains to saturation at large stress values. The permeability of the inclusion is decreased by the parallel compressive stress or the perpendicular tensile stress. It vanishes at large stress values.

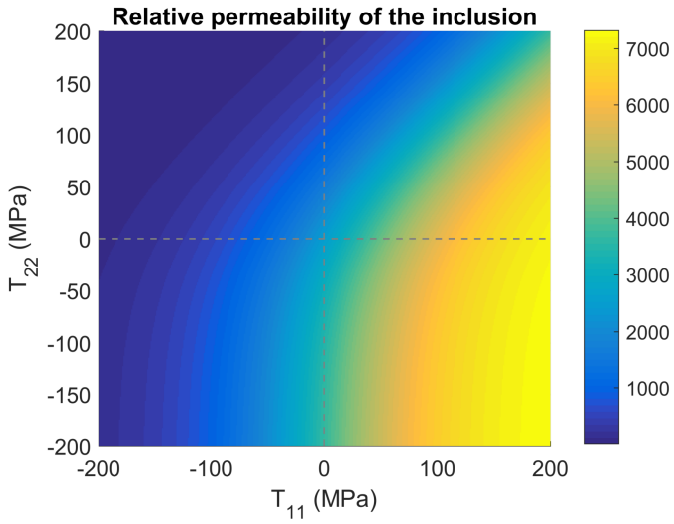

(a)

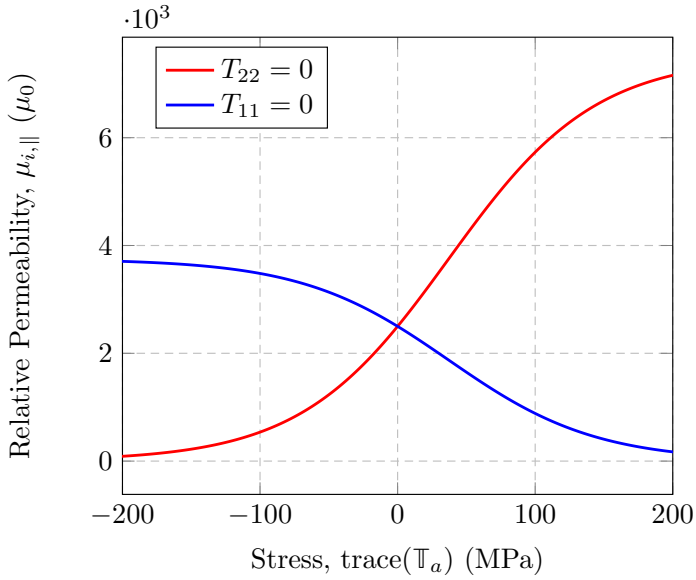

(b)

Fig. 5.7 Parallel component of the permeability of the inclusion as a function of macroscopic stress $\mathbb{T}_a$. Lattice length $= 50\,\mu$m, volume fraction of inclusion $\xi = 99\%$. Material parameters as in Tab. 5.1.

The parallel (to the magnetic field) component of the effective permeability of the composite as a function of (T_{11}, T_{22}) is shown in Fig. 5.8.

The effective permeability varies because the permeability of the inclusion is influenced by the stress. Fig. 5.8 shows that tensile stress along the magnetic field improves the magnetic performance of the composite. For instance, when the parallel tensile stress reaches 200MPa ($T_{22} = 0$), the effective permeability value increases by 7%. Greater stress

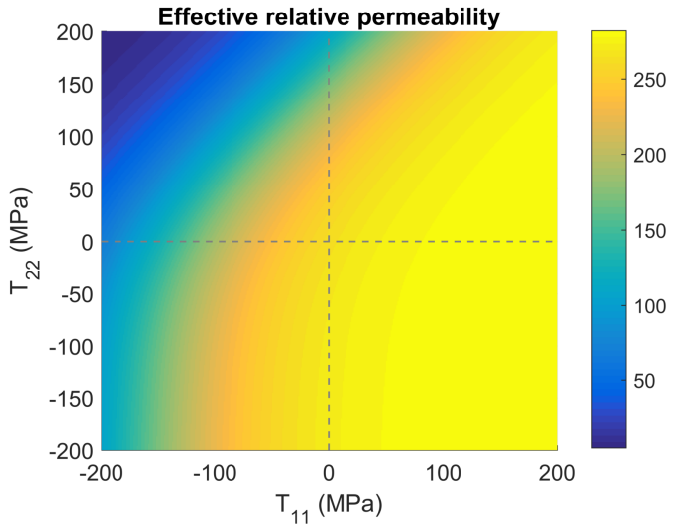

Fig. 5.8 Parallel component of the effective relative permeability as a function of macroscopic stress $\mathbb{T}_a$. Lattice length $= 50\,\mu$m, volume fraction of inclusion $\xi = 99\%$. Material parameters as in Tab. 5.1.

is not necessary because the effective permeability saturates. The compressive stress along the magnetic field decreases the effective permeability. The stress perpendicular to the magnetic field has the opposite effect comparing with the one along the field. To sum up, mechanical stress can be applied to improve the magnetic property of SMC. Since the magnetic behavior of the inclusion material is assumed to be linear magnetic behavior, $\mu_{i,\|}$ goes up when the mechanical stress is applied. However, in practice, the improvement of the magnetic permeability with stress has some limitations, when the nonlinearity is taken into consideration [51, 95], as presented in Fig. 5.9. The secant susceptibility increases first when mechanical stress is applied, but then decreases as the stress is reaching high amplitudes.

The EC loss density is examined under different mechanical stress. In the following EC loss density plots, the EC loss density values are normalized by setting $U = 1$ when there is no stress applied ($T_{11} = T_{22} = 0$). The normalized EC loss density of SMC varying as a function of (T_{11}, T_{22}) is plotted in Fig. 5.10.

In Fig. 5.10, the difference between the maximum value and the minimum one is 1.35%. It means that stress does not affect the EC loss density if the average flux density is kept constant.

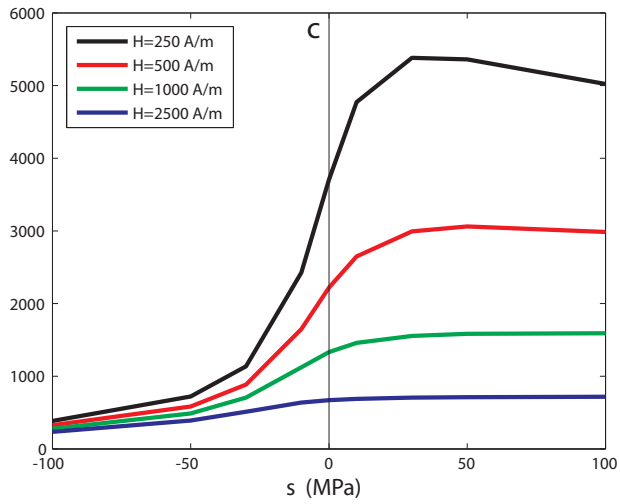

Fig. 5.9 Experimental secant susceptibility under mechanical loadings [95].

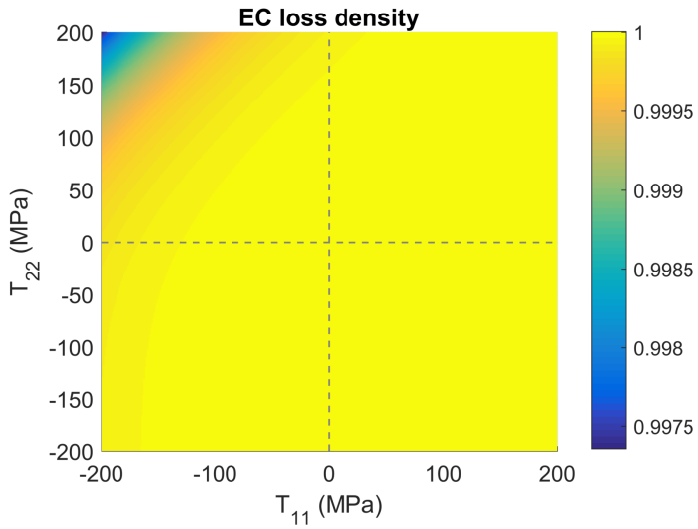

Fig. 5.10 Normalized EC loss density as a function of macroscopic stress $\mathbb{T}_a$. (Fixed flux density B_0). Parameters: the same as Fig. 5.7

Substituting (5.14) into (5.8) in view of the constitutive magnetic law (5.5), the EC loss density has the form,

$$U = \frac{9}{128}\,\xi\,\pi^2\,f\,L_i^2\,\sigma_i\,B_0^2\left(\frac{3\,\mu_{i,\|}}{2(1-\xi)\mu_m + (1+2\xi)\mu_{i,\|}}\right)^2 \tag{5.21}$$

With large parallel compressive stress (e.g. $T_{11} \approx -200\,\text{MPa}$, $T_{22} = 0$) or large perpendicular tensile stress (e.g. $T_{11} = 0$, $T_{22} \approx 200\,\text{MPa}$) as shown in Fig. 5.7, the magnetic

permeability vanishes $\mu_{i,\|} \to \mu_0$, so that

$$\lim_{\mu_{i,\|}\to\mu_0} U = \frac{9}{128}\,\xi\,\pi^2 f\,L_i^2\,\sigma_i B_0^2 \tag{5.22}$$

On the other hand, with large parallel tensile stress ($T_{11} \approx 200$ MPa, $T_{22} = 0$) or large perpendicular compressive stress ($T_{11} = 0$, $T_{22} \approx -200$ MPa) as shown in Fig. 5.7, the magnetic permeability attains saturation, denoted as μ_s. Judging by the choices of materials ($\mu_i^o = 2500\mu_0$, $\mu_m = \mu_0$) and high concentration of inclusion $\xi = 99\%$, the relationship $(1+2\xi)\mu_{i,\|} \gg (1-\xi)\mu_m$ holds, so that (5.21) turns:

$$\lim_{\mu_{i,\|}\gg\mu_m} U = \frac{9}{128}\,\xi\,\pi^2 f\,L_i^2\,\sigma_i B_0^2\left(\frac{3}{1+2\,\xi}\right)^2 \tag{5.23}$$

Comparing (5.22) with (5.23), in view of the volume fraction of the inclusion $\xi = 99\%$, there is little difference for the EC loss density values no matter how much stress is applied.

It can be concluded that, given a constant average flux density, mechanical stress can be applied to change the effective permeability of SMC without altering the EC losses.

The effect of multiaxial stress is analyzed in the following section. This discussion focuses on stress in a 2D state. The magnetic field is kept constant and along the x-direction.

Multiaxial Stress

Define β as the proportional coefficient between T_{22} and T_{11} in $\mathbb{T}_a$: $T_{22} = \beta\,T_{11}$. Equibiaxial stress is a special example of stress $\mathbb{T}_a$ when $\beta = 1$. When $\beta = -1$, it is the case of pure shear stress state.

The magnetic permeability varying as a function of the mechanical stress is plotted in Fig. 5.11 for different proportional coefficients β. The pure shear stress greatly decreases the magnetic permeability when $T_{11} < 0$ and increases it when T_{11} is positive. As for the case where $\beta \geq 0$, when the stress is compressive ($T_{22} < 0$, $T_{11} < 0$), the perpendicular compressive stress (T_{22}) prevents slightly the deteriorating effect on the magnetic behavior of the parallel stress (T_{11}). As β gets bigger ($\beta > 1$), the perpendicular one modifies significantly the permeability for a given tensile stress. For instance, when $\beta = 2$, the improving effect of the parallel tensile stress ($T_{11} > 0$) disappears.

From (5.3), the parallel component of permeability of inclusion can be approximated as:

$$\mu_{i,\|} = \frac{3\,\chi_o\mu_0\exp(\alpha\,\langle T\rangle_{i,11})}{1+\exp(\alpha\,\beta\,\langle T\rangle_{i,11})+\exp(\alpha\,\langle T\rangle_{i,11})} + \mu_0 \tag{5.24}$$

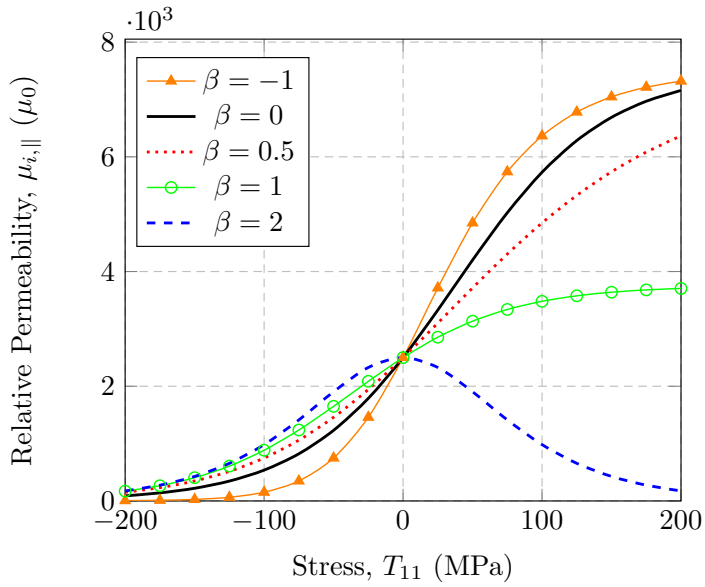

Fig. 5.11 Parallel component of the permeability of the inclusion as a function of $\mathbb{T}_a$ for certain proportional coefficients. Parameters: the same as Fig.5.7

This function has to be discussed in view of β. When $\beta \leq 1$, $\mu_{i,\|}$ is a monotonically increasing function of $\langle T \rangle_{i,11}$. On the other hand, when $\beta > 1$, at high stress values, magnetic permeability approaches μ_0,

$$\lim_{\substack{\beta>1 \\ T_{11}\to\pm\infty}} \mu_{i,\|} = \mu_0 \tag{5.25}$$

The corresponding effective permeability and EC loss density results are plotted in Fig. 5.12.

The same trend can be observed in Fig. 5.12 when there is stress applied on the composite. By comparing Fig. 5.12 to Fig. 5.11, it can be seen that the composite is less sensitive to the mechanical stress than the ferromagnetic materials.

It is worth noting that symmetry over the axis $T_{11} = 0$ can be observed from Figs 5.11–5.12 when $\beta = 2$. The average stress on the inclusion would have the same proportional relationship: $\langle T \rangle_{i,22} = 2 \langle T \rangle_{i,11}$, which gives rise to the magnetic permeability function,

$$\mu_{i,\|} = \frac{3\,\chi_o \mu_0}{1 + \exp(\alpha \langle T \rangle_{i,11}) + \exp(-\alpha \langle T \rangle_{i,11})} + \mu_0 \tag{5.26}$$

The magnetic permeability is an even function of $\langle T \rangle_{i,11}$, and so an even function of the macroscopic stress.

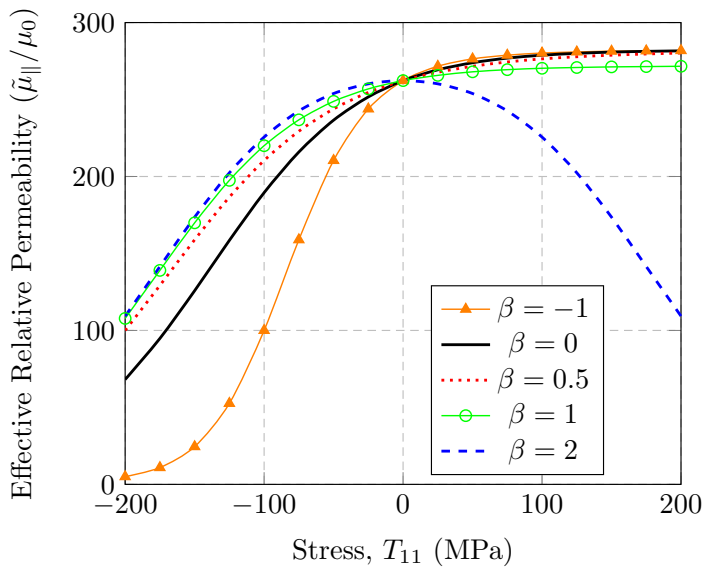

Fig. 5.12 Effective permeability (parallel component) as a function of $\mathbb{T}_a$ for certain proportional coefficients. Parameters: the same as Fig. 5.11

5.4 Conclusion

Macroscopic stress and magnetic field are integrated into EC loss density formula by localizing stress and magnetic field with homogenization strategy. It is found that the mechanical stress can be applied to improve the magnetic performance of SMC. The effective permeability reaches saturation as the stress increases. As for the EC loss density, when flux density is given, the mechanical stress affects the permeability of the inclusion but does not change the EC losses of SMC. Therefore an optimal stress value can be determined for the best magnetic performance without causing more EC loss dissipation.

An interesting conclusion is that the magnetic behavior of SMC seems to be less sensitive to mechanical stress than that of usual homogeneous ferromagnetic materials. This expectation would have to be confirmed by experimental measurements.

The linear magnetic material is assumed in this chapter to explore the effect of stress on the EC losses. The magneto-elastic model is simplistic. The magnetic nonlinearity and hysteresis losses are not considered. As for nonlinear magnetic material, the model would be more complicated. Still, the effect of magnetic field on the stress can be neglected. Since the magnetic permeability depends on the applied field, an iterative procedure has to be employed to retrieve the average field in the inclusion, the permeability tensor and the effective permeability tensor of the composite. Besides, the harmonic magnetic field has to be sampled over time in order to determine the final average field and permeability of the inclusion. And the EC loss density has to be integrated over a period of time.

Conclusion and Perspectives

Conclusion

In this thesis, a model based on a complex permeability is proposed to study Soft Magnetic Composites (SMC). In the model, the real and imaginary parts of the complex permeability are respectively employed to denote the magnetic behavior and the eddy current (EC) losses of the composites. The model originates from periodic SMC with circular or spherical inclusions under arbitrary magnetic field excitation. The distorted field in the inclusion is averaged. This complex permeability is independent of the structure as long as the periodicity is maintained. Thus, it can be used as a constitutive property in designing tools for machines using SMC.

The EC loss density in SMC can be approximated through the field averaging operations in the inclusions. The usual averaging manipulations are the first and second order moments of the magnetic field. For periodic SMC with circular or spherical inclusions, it is proved that the two approaches bound the EC loss density in SMC. The average field approach underestimates the EC loss density in SMC, thus providing a lower bound; whereas it is overestimated by the approach of the second order moment, thus providing an upper bound. Both the averaging approaches depend strongly on the determination of the effective permeability of the composite. The bound estimates are usually close, providing accurate values for EC losses as long as the effective permeability is estimated with good accuracy. EC loss can be approximated without the exact solution of the EC distribution thereby it relies only on a homogenization model for the effective permeability, which simplifies the approach compared to a full FEM computation.

As an application example, a magnetic circuit made of SMC is homogenized with complex permeability. It is made of high concentration periodic SMC. FEM computations were carried out on the heterogeneous magnetic circuit and the corresponding homogenized one. Magnetic field and EC losses distribution have been examined and compared between the two magnetic circuits. Good accordance has been obtained between the reference EC

loss density (generated from heterogeneous magnetic circuit) and the values calculated with complex permeability from the homogeneous one.

Moreover, the multi-physical behavior of SMC is explored. The effect of mechanical stress on the magnetic performance and on the EC loss density is studied on high concentration SMC. Property contrast (permeability, conductivity) is high for the constituents of SMC. Considering linear permeability and neglecting the effects of magnetostriction and elastoresistance, a formula is derived for the EC loss density as a function of the macroscopic magnetic field and the mechanical stress. The stress influences the EC loss density because the magnetic behavior of the ferromagnetic inclusion is sensitive to the stress. It is shown that stress has little effect on EC losses in SMC (while affecting the magnetic permeability).

The proposed models provide straightforward approaches to determine the EC losses of SMC at low working frequency. The complex permeability contains the magnetic behavior and links directly to the EC losses. The EC bounds approaches offer a simple way to approximate the EC losses in composites. The effect of the mechanical stress is directly integrated into the EC loss density formula. The models are suitable for different permeability contrasts and are discussed for a full range of volume fractions. They are developed for SMC with dielectric matrix. When the global eddy current in the matrix cannot be neglected, the models have to be revisited. The formulas of EC loss density are derived on SMC with periodic microstructure. But for SMC with randomly distributed microstructures, EC loss estimates could be obtained. In these models, the nonlinearity of the ferromagnetic materials is not considered, the hysteresis and excess losses are not taken into account.

Perspectives

The present work focuses on modeling the classical losses in Soft Magnetic Composites (SMC). The contributions open up new horizons for future improvements.

The present work builds a complex permeability by considering linear ferromagnetic materials. The coming contributions would begin to develop a generic complex permeability model which contains the magnetic non-linearity and furthermore the hysteresis and excess losses. Besides, it would be interesting to integrate the magnetomechanical coupling behavior of SMC into the complex magnetic model. Experiments are needed to verify the models.

The magnetomechanical model is the premier multi-physical attempt for the SMC. A follow up work could consider the effect of magnetostriction, elastoresistance, and magnetoresistance. The effect of temperature on electromagnetic properties could further

be taken into account. A generic formula could be developed to deal with the coupled behavior of SMC using homogenization techniques [51, 64, 94].

The EC loss bounds in the present work are analytically derived for SMC with circular or spherical inclusions. The future work will be devoted to EC loss bounds for SMC with randomly distributed inclusions through the bounds on the effective permeability of the composite [88].

Future works could also include the application of the complex permeability model to design motors and transformers with SMC. Prototype devices could be developed and fabricated. Electrical performance need to be examined and compared to that of traditional machines. Promoting the application of SMC in replacement of laminated steel in electrical devices in order to save energy will be a challenging and meaningful task.

References

[1] J. G. Zhu, J. J. Zhong, Z. W. Lin, and J. D. Sievert, "Measurement of magnetic properties under 3-d magnetic excitations," *IEEE Transactions on Magnetics*, vol. 39, pp. 3429–3431, Sept 2003.

[2] Z. Lin and J. Zhu, "Three-dimensional magnetic properties of soft magnetic composite materials," *Journal of Magnetism and Magnetic Materials*, vol. 312, pp. 158–163, May 2007.

[3] H. Shokrollahi and K. Janghorban, "Soft magnetic composite materials (SMCs)," *Journal of Materials Processing Technology*, vol. 189, no. 1-3, pp. 1–12, 2007.

[4] G. Cvetkovski and L. Petkovska, "Performance improvement of pm synchronous motor by using soft magnetic composite material," *IEEE Transactions on Magnetics*, vol. 44, pp. 3812–3815, Nov 2008.

[5] A. Chebak, P. Viarouge, and J. Cros, "Analytical computation of the full load magnetic losses in the soft magnetic composite stator of high-speed slotless permanent magnet machines," *IEEE Transactions on Magnetics*, vol. 45, pp. 952–955, March 2009.

[6] Y. Guo, J. Zhu, and D. Dorrell, "Design and analysis of a claw pole permanent magnet motor with molded soft magnetic composite core," *IEEE Transactions on Magnetics*, vol. 45, pp. 4582–4585, Oct. 2009.

[7] G. N. Sabri and T. Benouaz, "The soft magnetic materials for power applications," *AIP Conference Proceedings*, vol. 1569, no. 1, pp. 419–422, 2013.

[8] F. Bernot, A. Bernot, and J.-C. Vannier, *Innovative Design, Analysis and Development Practices in Aerospace and Automotive Engineering: I-DAD 2014, February 22-24, 2014*, ch. A Synchronous Wound Excitation Transverse Flux Machine with Solid Rotor, pp. 25–39. New Delhi: Springer India, 2014.

[9] T. Sato, S. Aya, H. Igarashi, M. Suzuki, Y. Iwasaki, and K. Kawano, "Loss computation of soft magnetic composite inductors based on interpolated scalar magnetic property," *IEEE Transactions on Magnetics*, vol. 51, pp. 1–4, March 2015.

[10] A. Jack, "Experience with using soft magnetic composites for electrical machines," in *IEE Half-Day Colloquium on New Magnetic Materials - Bonded Iron, Lamination Steels, Sintered Iron and Permanent Magnets (Digest NMo. 1998/259)*, (London, UK), pp. 3/1–3/4, IET, May 1998.

[11] Y. Guo, J. G. Zhu, P. A. Watterson, and W. Wu, "Development of a PM transverse flux motor with soft magnetic composite core," *IEEE Transactions on Energy Conversion*, vol. 21, pp. 426–434, June 2006.

[12] A. Schoppa and P. Delarbre, "Soft magnetic powder composites and potential applications in modern electric machines and devices," *IEEE Transactions on Magnetics*, vol. 50, pp. 1–4, April 2014.

[13] C. Liu, J. Zhu, Y. Wang, G. Lei, and Y. Guo, "Design considerations of PM transverse flux machines with soft magnetic composite cores," *IEEE Transactions on Applied Superconductivity*, vol. 26, pp. 1–5, June 2016.

[14] O. Maloberti, R. Figueredo, C. Marchand, Y. Choua, D. Condamin, L. Kobylanski, and E. Bommé, "3-D-2-D dynamic magnetic modeling of an axial flux permanent magnet motor with soft magnetic composites for hybrid electric vehicles," *IEEE Transactions on Magnetics*, vol. 50, pp. 1–11, June 2014.

[15] M. Morimoto and M. Inamori, "Induction motor made of SMC," in *2014 International Power Electronics Conference (IPEC-Hiroshima 2014 - ECCE ASIA)*, pp. 3509–3512, May 2014.

[16] W. Xu, C. Wu, and M. Yan, "Preparation of Fe–Si–Ni soft magnetic composites with excellent high-frequency properties," *Journal of Magnetism and Magnetic Materials*, vol. 381, pp. 116 – 119, 2015.

[17] Lord Rayleigh, "On the influence of obstacles arranged in rectangular order upon the properties of a medium," *Philosophical Magazine Series 5*, vol. 34, no. 211, pp. 481–502, 1892.

[18] J. C. Maxwell-Garnett, "Colours in metal glasses and in metallic films," *Philosophical Transactions of the Royal Society of London A: Mathematical, Physical and Engineering Sciences*, vol. 203, no. 359-371, pp. 385–420, 1904.

[19] O. Wiener, *Die theorie des mischkörpers für das feld der stationären strömung. 1. abhandlung: Die mittelwertsätze für kraft, polarisation und energie*, vol. 1 of *Abhandlungen der Königlich-Sächsischen Gesellschaft der Wissenschaften*. B. G. Teubner, 1912.

[20] Z. Hashin and S. Shtrikman, "A variational approach to the theory of the effective magnetic permeability of multiphase materials," *Journal of Applied Physics*, vol. 33, no. 10, pp. 3125–3131, 1962.

[21] R. C. McPhedran and D. R. McKenzie, "The conductivity of lattices of spheres. I. the simple cubic lattice," *Proceedings of the Royal Society of London. Series A, Mathematical and Physical Sciences*, vol. 359, no. 1696, pp. 45–63, 1978.

[22] J. Lam, "Magnetic permeability of a simple cubic lattice of conducting magnetic spheres," *Journal of Applied Physics*, vol. 60, no. 12, pp. 4230–4235, 1986.

[23] A. Sihvola, *Electromagnetic Mixing Formulas and Applications*. Electromagnetics and Radar Series, Institution of Electrical Engineers, 1999.

[24] B. Y. Balagurov and V. A. Kashin, "The conductivity of a 2D system with a doubly periodic arrangement of circular inclusions," *Technical Physics*, vol. 46, no. 1, pp. 101–106, 2001.

[25] Y. A. Godin, "Effective complex permittivity tensor of a periodic array of cylinders," *Journal of Mathematical Physics*, vol. 54, no. 5, p. 053505, 2013.

[26] A. Bossavit, "On the homogenization of Maxwell equations," *COMPEL - The international journal for computation and mathematics in electrical and electronic engineering*, vol. 14, no. 4, pp. 23–26, 1995.

[27] M. El Feddi, Z. Ren, A. Razek, and A. Bossavit, "Homogenization technique for Maxwell equations in periodic structures," *IEEE Transactions on Magnetics*, vol. 33, pp. 1382–1385, March 1997.

[28] M. Belkadi, B. Ramdane, D. Trichet, and J. Fouladgar, "Non Linear Homogenization for Calculation of Electromagnetic Properties of Soft Magnetic Composite Materials," *IEEE Transactions on Magnetics*, vol. 45, pp. 4317–4320, oct 2009.

[29] G. Meunier, V. Charmoille, C. Guerin, P. Labie, and Y. Marechal, "Homogenization for periodical electromagnetic structure: Which formulation?," *IEEE Transactions on Magnetics*, vol. 46, pp. 3409–3412, August 2010.

[30] I. Niyonzima, R. Sabariego, P. Dular, and C. Geuzaine, "Finite element computational homogenization of nonlinear multiscale materials in magnetostatics," *IEEE Transactions on Magnetics*, vol. 48, pp. 587–590, Feb. 2012.

[31] O. Bottauscio and A. Manzin, "Comparison of multiscale models for eddy current computation in granular magnetic materials," *Journal of Computational Physics*, vol. 253, pp. 1–17, 2013.

[32] C. Conca and S. Natesan, "Numerical methods for elliptic partial differential equations with rapidly oscillating coefficients," *Computer Methods in Applied Mechanics and Engineering*, vol. 192, pp. 47–76, Jan. 2003.

[33] P. Queffelec, D. Bariou, and P. Gelin, "A predictive model for the permeability tensor of magnetized heterogeneous materials," *IEEE Transactions on Magnetics*, vol. 41, pp. 17–23, Jan 2005.

[34] L. Daniel and R. Corcolle, "A note on the effective magnetic permeability of polycrystals," *IEEE Transactions on Magnetics*, vol. 43, pp. 3153–3158, July 2007.

[35] C. Holloway, M. Sarto, and M. Johansson, "Analyzing carbon-fiber composite materials with equivalent-layer models," *IEEE Transactions on Electromagnetic Compatibility*, vol. 47, pp. 833–844, Nov. 2005.

[36] F. Qin and C. Brosseau, "A review and analysis of microwave absorption in polymer composites filled with carbonaceous particles," *Journal of Applied Physics*, vol. 111, no. 6, pp. 1–24, 2012.

[37] V. Préault, R. Corcolle, L. Daniel, and L. Pichon, "Effective permittivity of shielding composite materials for microwave frequencies," *IEEE Transactions on Electromagnetic Compatibility*, vol. 55, pp. 1178–1186, Dec. 2013.

[38] T. G. Mackay and A. Lakhtakia, *Modern Analytical Electromagnetic Homogenization*. 2053-2571, Morgan & Claypool Publishers, 2015.

[39] J. Garland and D. Tanner, *Electrical Transport and Optical Properties of Inhomogeneous Media*. AIP conference proceedings, New York: American Institute of Physics, 1978.

[40] O. Levy and D. Stroud, "Maxwell Garnett theory for mixtures of anisotropic inclusions: Application to conducting polymers," *Physical Review B*, vol. 56, pp. 8035–8046, oct 1997.

[41] P. Mallet, C. A. Guérin, and A. Sentenac, "Maxwell-Garnett mixing rule in the presence of multiple scattering: Derivation and accuracy," *Physical Review B*, vol. 72, p. 014205, jul 2005.

[42] C. Brosseau, "Modelling and simulation of dielectric heterostructures: a physical survey from an historical perspective," *Journal of Physics D: Applied Physics*, vol. 39, no. 7, p. 1277, 2006.

[43] S. Giordano and W. Rocchia, "Predicting the dielectric nonlinearity of anisotropic composite materials via tensorial analysis," *Journal of Physics: Condensed Matter*, vol. 18, pp. 10585–10599, nov 2006.

[44] A. Sihvola, "Homogenization principles and effect of mixing on dielectric behavior," *Photonics and Nanostructures - Fundamentals and Applications*, vol. 11, no. 4, pp. 364–373, 2013.

[45] D. A. G. Bruggeman, "Berechnung verschiedener physikalischer konstanten von heterogenen substanzen. I. dielektrizitätskonstanten und leitfähigkeiten der mischkörper aus isotropen substanzen," *Annalen der Physik*, vol. 416, no. 7, pp. 636–664, 1935.

[46] G. Wasselynck, D. Trichet, B. Ramdane, and J. Fouldagar, "Interaction between electromagnetic field and cfrp materials: A new multiscale homogenization approach," *IEEE Transactions on Magnetics*, vol. 46, pp. 3277–3280, aug 2010.

[47] G. Papanicolau, A. Bensoussan, and J. Lions, *Asymptotic Analysis for Periodic Structures*. Studies in Mathematics and its Applications, Elsevier Science, 1978.

[48] M. Chiampi and D. Chiarabaglio, "Investigation on the asymptotic expansion technique applied to electromagnetic problems," *IEEE Transactions on Magnetics*, vol. 28, pp. 1917–1923, Jul 1992.

[49] D. Trichet, E. Chauveau, and J. Fouladgar, "Asymptotic calculation of equivalent electromagnetic and thermal properties for composite materials," *IEEE Transactions on Magnetics*, vol. 36, pp. 1193–1196, July 2000.

[50] A. Goldman, *Handbook of Modern Ferromagnetic Materials*, vol. 505 of *The Springer International Series in Engineering and Computer Science*. Boston, MA: Springer US, 1999.

[51] R. M. Bozorth, *Ferromagnetism*. Hoboken, New Jersey: John Wiley & Sons, Inc., 2003.

[52] B. Cullity and C. Graham, *Introduction to Magnetic Materials*. John Wiley & Sons, 2 ed., 2011.

[53] J. P. Joule, "On the effects of magnetism upon the dimensions of iron and steel bars," *Philosophical Magazine Series 3*, vol. 30, no. 199, pp. 76–87, 1847.

[54] E. Villari, "Ueber die aenderungen des magnetischen moments, welche der zug und das hindurchleiten eines galvanischen stroms in einem stabe von stahl oder eisen hervorbringen," *Annalen der Physik*, vol. 202, no. 9, pp. 87–122, 1865.

[55] É. Du Tremolet de Lacheisserie, *Magnetostriction: theory and applications of magnetoelasticity*. CRC Press, 1993.

[56] D. C. Jiles, "Theory of the magnetomechanical effect," *Journal of Physics D: Applied Physics*, vol. 28, no. 8, p. 1537, 1995.

[57] W. D. Armstrong, "A general magneto-elastic model of terfenol-d particle actuated composite materials," *Journal of Intelligent Material Systems and Structures*, vol. 13, no. 2-3, pp. 137–141, 2002.

[58] L. Daniel, O. Hubert, N. Buiron, and R. Billardon, "Reversible magneto-elastic behavior: A multiscale approach," *Journal of the Mechanics and Physics of Solids*, vol. 56, no. 3, pp. 1018 – 1042, 2008.

[59] L. Daniel, M. Rekik, and O. Hubert, "A multiscale model for magneto-elastic behaviour including hysteresis effects," *Archive of Applied Mechanics*, vol. 84, no. 9, pp. 1307–1323, 2014.

[60] G. Bertotti, "Physical interpretation of eddy current losses in ferromagnetic materials. I. theoretical considerations," *Journal of Applied Physics*, vol. 57, no. 6, pp. 2110–2117, 1985.

[61] G. Bertotti, "General properties of power losses in soft ferromagnetic materials," *IEEE Transactions on Magnetics*, vol. 24, pp. 621–630, Jan 1988.

[62] J. Reinert, A. Brockmeyer, and R. W. A. A. D. Doncker, "Calculation of losses in ferro- and ferrimagnetic materials based on the modified steinmetz equation," *IEEE Transactions on Industry Applications*, vol. 37, pp. 1055–1061, Jul 2001.

[63] A. DeSimone and R. D. James, "A constrained theory of magnetoelasticity," *Journal of the Mechanics and Physics of Solids*, vol. 50, no. 2, pp. 283 – 320, 2002.

[64] T. Miyazaki and H. Jin, *The Physics of Ferromagnetism*, vol. 158 of *Springer Series in Materials Science*. Springer Berlin Heidelberg, 2012.

[65] L. Daniel, "An analytical model for the effect of multiaxial stress on the magnetic susceptibility of ferromagnetic materials," *IEEE Transactions on Magnetics*, vol. 49, pp. 2037–2040, May 2013.

[66] C. Brosseau and A. Beroual, "Computational electromagnetics and the rational design of new dielectric heterostructures," *Progress in Materials Science*, vol. 48, no. 5, pp. 373 – 456, 2003.

[67] B. Sareni, L. Krähenbühl, A. Beroual, and C. Brosseau, "Complex effective permittivity of a lossy composite material," *Journal of Applied Physics*, vol. 80, no. 8, pp. 4560–4565, 1996.

[68] K. Abeywickrama, T. Daszczynski, Y. Serdyuk, and S. Gubanski, "Determination of complex permeability of silicon steel for use in high-frequency modeling of power transformers," *IEEE Transactions on Magnetics*, vol. 44, pp. 438–444, April 2008.

[69] H. Hamzehbahmani, P. Anderson, J. Hall, and D. Fox, "Eddy current loss estimation of edge burr-affected magnetic laminations based on equivalent electrical network part I: Fundamental concepts and FEM modeling," *IEEE Transactions on Power Delivery*, vol. 29, pp. 642–650, April 2014.

[70] O. Moreau, L. Popiel, and J. L. Pages, "Proximity losses computation with a 2D complex permeability modelling," *IEEE Transactions on Magnetics*, vol. 34, pp. 3616–3619, Sep 1998.

[71] X. Nan and C. R. Sullivan, "A two-dimensional equivalent complex permeability model for round-wire windings," in *Power Electronics Specialists Conference, 2005. PESC '05. IEEE 36th*, (Recife, Brazil), pp. 613–618, June 2005.

[72] M. De Wulf, L. Anestiev, L. Dupré, L. Froyen, and J. Melkebeek, "Magnetic properties and loss separation in iron powder soft magnetic composite materials," *Journal of Applied Physics*, vol. 91, pp. 7845–7847, May 2002.

[73] O. de la Barrière, C. Appino, F. Fiorillo, C. Ragusa, M. Lecrivain, L. Rocchino, H. B. Ahmed, M. Gabsi, F. Mazaleyrat, and M. LoBue, "Characterization and prediction of magnetic losses in soft magnetic composites under distorted induction waveform," *IEEE Transactions on Magnetics*, vol. 49, pp. 1318–1326, April 2013.

[74] B. Ślusarek, B. Jankowski, K. Sokalski, and J. Szczygłowski, "Characteristics of power loss in soft magnetic composites a key for designing the best values of technological parameters," *Journal of Alloys and Compounds*, vol. 581, pp. 699–704, Dec. 2013.

[75] M. Sadiku, *Numerical Techniques in Electromagnetics, Second Edition*. Taylor & Francis, 2000.

[76] J. C. Maxwell, *A Treatise on Electricity and Magnetism*, vol. 1. Oxford:Clarendon, 2nd ed., 1881.

[77] J. D. Jackson, *Classical Electrodynamics*. John Wiley & Sons Ltd., 1962. p. 67.

[78] J. A. Stratton, *Electromagnetic Theory*. Hoboken, New Jersey: John Wiley & Sons, Inc., 2007.

[79] M. H. Nayfeh and M. K. Brussel, *Electricity and Magnetism*. John Wiley & Sons Inc, 1985.

[80] D. Jiles, *Introduction to magnetism and magnetic materials*. Chapman and Hall, 2nd ed., 1998.

[81] R. Szewczyk, "Validation of the anhysteretic magnetization model for soft magnetic materials with perpendicular anisotropy," *Materials*, vol. 7, no. 7, pp. 5109–5116, 2014.

[82] J. Kwiczala and B. Kasperczyk, "Standardization of anhysteretic magnetization curves," *Journal of Applied Physics*, vol. 97, no. 10, p. 10E504, 2016.

[83] J. Daintith, *A Dictionary of Physics*. Oxford Paperback Reference, OUP Oxford, 6 ed., 2009.

[84] L. Daniel, O. Hubert, and M. Rekik, "A simplified 3-D constitutive law for magnetomechanical behavior," *IEEE Transactions on Magnetics*, vol. 51, pp. 1–4, March 2015.

[85] G. Bertotti, F. Fiorillo, and G. Soardo, "The prediction of power losses in soft magnetic materials," *Le Journal de Physique Colloques*, vol. 49, no. C8, pp. C8–1915 – C8–1919, 1988.

[86] O. de la Barrière, M. LoBue, and F. Mazaleyrat, "Semianalytical and analytical formulas for the classical loss in granular materials with rectangular and elliptical grain shapes," *IEEE Transactions on Magnetics*, vol. 50, pp. 1–8, Oct 2014.

[87] L. O. Hultman and A. G. Jack, "Soft magnetic composites-materials and applications," in *Electric Machines and Drives Conference, 2003. IEMDC'03. IEEE International*, vol. 1, pp. 516–522 vol.1, June 2003.

[88] R. Corcolle, L. Daniel, and F. Bouillault, "Intraphase fluctuations in heterogeneous magnetic materials," *Journal of Applied Physics*, vol. 105, no. 12, p. 123913, 2009.

[89] M. Bornert, P. Gilormini, and T. Bretheau, *Homogénéisation en mécanique des matériaux*. Hermès Science Publications, 2001.

[90] K. T. Tang, *Mathematical Methods for Engineers and Scientists 3*. Springer, 2007. pp.196-202.

[91] O. de la Barrière, C. Appino, F. Fiorillo, C. Ragusa, H. B. Ahmed, M. Gabsi, F. Mazaleyrat, and M. LoBue, "Loss separation in soft magnetic composites," *Journal of Applied Physics*, vol. 109, no. 7, 2011.

[92] S. K. Mukerji, M. George, M. B. Ramamurthy, and K. Asaduzzaman, "Eddy currents in solid rectangular cores," *Progress In Electromagnetics Research B*, vol. 7, pp. 117–131, 2008.

[93] T. Mori and K. Tanaka, "Average stress in matrix and average elastic energy of materials with misfitting inclusions," *Acta Metallurgica*, vol. 21, no. 5, pp. 571 – 574, 1973.

[94] R. Corcolle, L. Daniel, and F. Bouillault, "Generic formalism for homogenization of coupled behavior: Application to magnetoelectroelastic behavior," *Physical Review B*, vol. 78, p. 214110, Dec 2008.

[95] L. Daniel and O. Hubert, "Equivalent stress criteria for the effect of stress on magnetic behavior," *IEEE Transactions on Magnetics*, vol. 46, pp. 3089–3092, Aug 2010.

[96] O. Hubert and L. Daniel, "Energetical and multiscale approaches for the definition of an equivalent stress for magneto-elastic couplings," *Journal of Magnetism and Magnetic Materials*, vol. 323, pp. 1766–1781, July 2011.

[97] J. D. Eshelby, "The determination of the elastic field of an ellipsoidal inclusion, and related problems," *Proceedings of the Royal Society of London A: Mathematical, Physical and Engineering Sciences*, vol. 241, no. 1226, 1957.

[98] T. Mura, *Micromechanics of Defects in Solids*, vol. 3 of *Mechanics of Elastic and Inelastic Solids*. Springer Netherlands, 2 ed., 1987.

Appendix A

EC Loss Density For Basic Shapes

Consider an isotropic, homogeneous and linear material of permeability μ, electric conductivity σ and permittivity ϵ. The material is submitted to a harmonic magnetic field $\mathbf{H}$ of frequency f (angle frequency: $\omega = 2\pi f$). Combining Maxwell's equations with constitutive laws of material, the problem becomes a Poisson equation,

$$\nabla \times \nabla \times \mathbf{H} = -j\omega\mu(j\omega\epsilon + \sigma)\mathbf{H} \tag{A.1}$$

Since the domain is cut from 3D structure with infinite dimension along the z-axis, the magnetic field and the induced electric field are z-invariant,

$$\frac{\partial \mathbf{H}}{\partial z} = 0, \qquad \frac{\partial \mathbf{E}}{\partial z} = 0 \tag{A.2}$$

Apply a magnetic field $\mathbf{H} = [0, 0, H]^t$, where the superscript t indicates a matrix transpose. Consider a low frequency such that that $\omega\epsilon \ll \sigma$. Denoting $k^2 = -j\omega\mu\sigma$, the Poisson equation (A.1) becomes,

$$\nabla^2 H + k^2 H = 0 \tag{A.3}$$

subject to the Dirichlet boundary condition $H|_{\partial\Omega} = H_z$ with $\partial\Omega$ denoting the boundary of the domain. According to the boundary condition and z-invariance, and consider null current flow in the fiber,

$$E_z = 0, \qquad J_z = 0 \tag{A.4}$$

To solve (A.3) in a domain of a basic shape, shown in Fig. A.1, the magnetic field and electric field can be obtained. The eddy current density formulas can be determined.

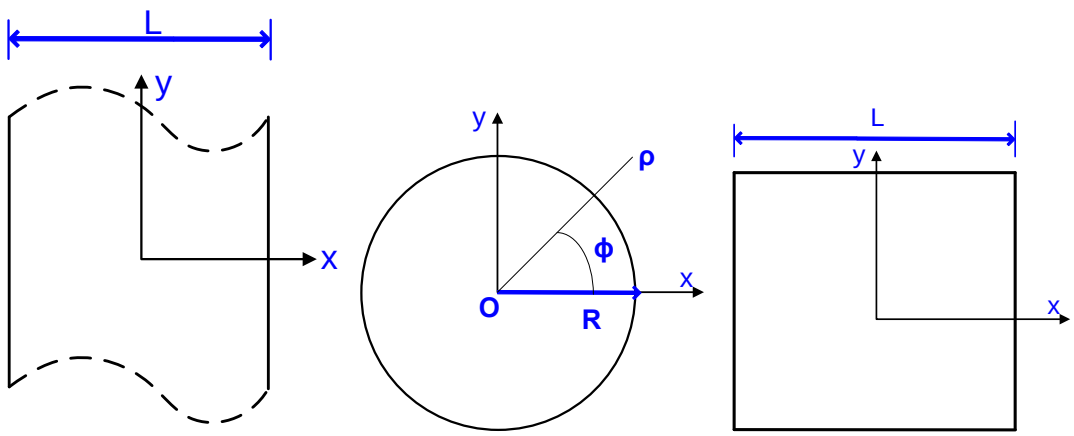

(a) Plate (b) Circle (c) Square

Fig. A.1 Sketch of homogeneous structure

A.1 Homogeneous Plate

Since the domain is assumed to be infinite in the y direction, magnetic and electric field will be y-invariable.

In Cartesian coordinates, the Laplace operator is given by:

$$\nabla^2 H = \frac{\partial^2 H}{\partial x^2} + \frac{\partial^2 H}{\partial y^2} + \frac{\partial^2 H}{\partial z^2} \tag{A.5}$$

Applying the y- and z-invariable ($\partial_y = 0$ and $\partial_z = 0$), the partial differential equation (PDE) (A.3) turns,

$$\frac{\mathrm{d}^2 H}{\mathrm{d}x^2} + k^2 H = 0 \tag{A.6}$$

By applying the boundary condition $H(-L/2) = H(L/2) = H_z$, the solution to (A.6) is,

$$H(x) = \frac{\cos(kx)}{\cos(kL/2)} H_z \tag{A.7}$$

The solution to the Maxwell-Ampère equation $\mathbf{J} = \nabla \times \mathbf{H}$ in the circle domain Ω is,

$$J(x) = \frac{\sin(kx)}{\cos(kL/2)} k H_z \tag{A.8}$$

At low frequency, the skin effect can be considered negligible, so that $|kL/2| \to 0$, which leads to $\cos(kL/2) \approx 1$ and $\sin(kx) \approx kx$. Thus, from (A.8) and considering the direction,

$$\mathbf{J} \approx k^2 H_z \, x \, \vec{u}_y = -j \, \omega \, \mu \, \sigma \, H_z \, x \, \vec{u}_y \tag{A.9}$$

where $\vec{u}_y$ is a unit vector in the y direction.

Substituting the eddy current density (A.9) into the EC loss density definition (1.16) in view of Ohm's law ($\mathbf{J} = \sigma \, \mathbf{E}$) yields:

$$U = \frac{\omega^2 \, \sigma \, \mu^2 \, H_z^2 \int_{-L/2}^{L/2} x^2 \, \mathrm{d}x}{2 f L} = \frac{\pi^2}{6} f \, \sigma \, \mu^2 \, H_z^2 \, L^2. \tag{A.10}$$

If magnetic constitutive law is applied, $B = \mu H_z$, the EC loss density is a function of magnetic flux density,

$$U = \frac{\pi^2}{6} f \, \sigma \, B^2 \, L^2. \tag{A.11}$$

A.2 Homogeneous Circle

In cylindrical coordinates,

$$\nabla^2 H = \frac{1}{\rho} \frac{\partial}{\partial \rho} \left(\rho \frac{\partial H}{\partial \rho} \right) + \frac{1}{\rho^2} \frac{\partial^2 H}{\partial \phi^2} + \frac{\partial^2 H}{\partial z^2} \tag{A.12}$$

Applying the cylindrical symmetry ($\partial_\phi = 0$ and $\partial_z = 0$), PDE (A.3) becomes:

$$\rho^2 \frac{\partial^2 H}{\partial \rho^2} + \rho \frac{\partial H}{\partial \rho} + (k \, \rho)^2 \, H = 0 \tag{A.13}$$

The solution to (A.13) is a Bessel function. The problem is viewed in polar coordinates $O\rho\phi$. The magnetic field in the circle domain Ω is,

$$H(\rho, \phi) = H_z \frac{\mathscr{J}_0(k\rho)}{\mathscr{J}_0(kR)} \tag{A.14}$$

where $\mathscr{J}_n(\cdot)$ is the first kind Bessel function of order n.

By $\mathbf{J} = \nabla \times \mathbf{H}$, the current density in the circle domain Ω is,

$$\mathbf{J}(\rho, \phi) = k \, H_z \frac{\mathscr{J}_1(k\rho)}{\mathscr{J}_0(kR)} \vec{u}_\phi. \tag{A.15}$$

Bessel functions have asymptotic forms, for instance, when $|k\rho| \ll 1$, $\mathscr{J}_0(k\rho) \approx 1$ and $\mathscr{J}_1(k\rho) \approx \frac{k\rho}{2}$. Thus the current density (A.15) simplifies as,

$$\mathbf{J}(\rho, \phi) = -\frac{1}{2} j\, \omega\, \sigma\, \mu\, H_z\, \rho\, \vec{u}_\phi. \tag{A.16}$$

Substituting the eddy current density (A.9) into the EC loss density definition (1.16) with respect to Ohm's law ($\mathbf{J} = \sigma\, \mathbf{E}$) gives,

$$U = \frac{\pi^2}{4} R^2 f\, \sigma\, \mu^2 H_z^2 \tag{A.17}$$

If magnetic constitutive law is applied, $B = \mu H_z$, the EC loss density is a function of magnetic flux density,

$$U = \frac{\pi^2}{4} f\, \sigma\, B^2 R^2. \tag{A.18}$$

A.3 Homogeneous Square

The PDE (A.3) for a square domain in a Cartesian coordinate system is,

$$\frac{\partial^2 H}{\partial x^2} + \frac{\partial^2 H}{\partial y^2} + k^2 H = 0 \tag{A.19}$$

Using the Fourier series expansion for (A.19), the solution has the form,

$$H(x, y) = H_z \sum_{p=1}^{\infty} \frac{4}{n\pi} \sin\left(\frac{n\pi}{2}\right) \left[\cos\left(\frac{n\pi}{L} x\right) \frac{\cosh(\zeta_n y)}{\cosh\left(\frac{\zeta_n L}{2}\right)} + \cos\left(\frac{n\pi}{L} y\right) \frac{\cosh(\zeta_n x)}{\cosh\left(\frac{\zeta_n L}{2}\right)} \right] \tag{A.20}$$

for $x, y \in [-L/2, L/2]$ where

$$\begin{aligned} \zeta_n &= \sqrt{\left(\frac{n\pi}{L}\right)^2 - k^2} \\ n &= 2p - 1, \quad p \in \mathbb{N}^+ \end{aligned} \tag{A.21}$$

The distribution of eddy current density in the homogeneous core can be found by substituting (A.20) into Maxwell-Ampère equation (1.1b), so that the EC loss density can

therefore be developed as:

$$U = \frac{16}{\pi^2} H_z^2 \omega \mu L \sum_{p=1}^{\infty} \frac{\Im(\zeta_n)\sinh(\Re(\zeta_n)L) - \Re(\zeta_n)\sin(\Im(\zeta_n)L)}{n^2|\zeta_n|^2[\cosh(\Re(\zeta_n)L) + \cos(\Im(\zeta_n)L)]} \tag{A.22}$$

where $\Re(\cdot), \Im(\cdot)$ denote respectively the real and imaginary part of a complex number.

A detailed deduction for a rectangle-shaped inclusion can be found in [92] to model the EC losses in laminated materials.

Equation (A.22) is a general EC loss density working for full frequency range. This equation is complicated to simplify and the relationship between the EC loss density and the field, frequency and the size is not clearly observed. At low frequency range for a homogeneous square, a formula as simple as (A.11) and (A.18) is expected. Numerical approach is applied to find the corresponding coefficient.

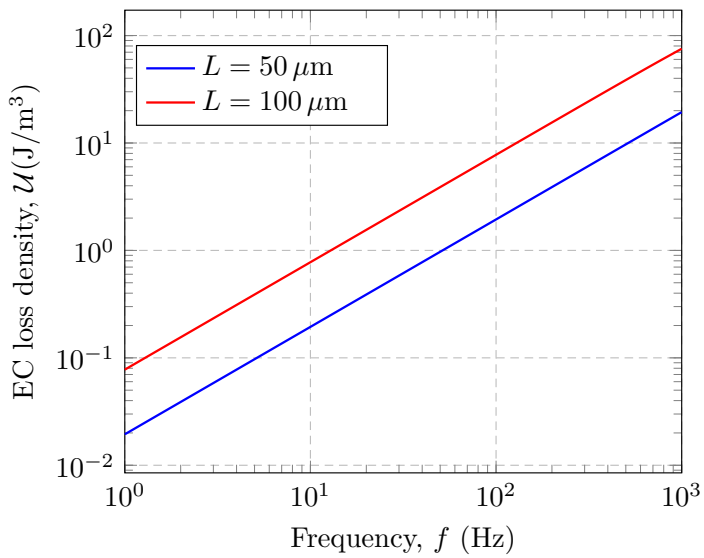

Fig. A.2 EC loss density in a homogeneous square as a function of frequency. $\sigma = 1.12 \times 10^7$ S/m, permeability $\mu = 4000\mu_0$; Average flux density: 1 T.

Since the proportional relationship holds [85, 86]:

$$U \propto f\,\sigma\,B^2\,L^2 \tag{A.23}$$

For instance, perfect linearity of $U - f$ can be observed from Fig. A.2. When the working frequency is low such that the skin effect can be ignored, (A.22) can be approximated by linear fitting,

$$U_{\text{fit}} = \frac{9\pi^2}{128} f \sigma B^2 L^2 \tag{A.24}$$

Define the discrepancies

$$\eta_{\text{fit}} = \frac{U_{\text{fit}} - U}{U} \times 100\% \tag{A.25}$$

to examine the accuracy of (A.24) comparing with the reference values from (A.22). The results are plotted in Fig. A.3.

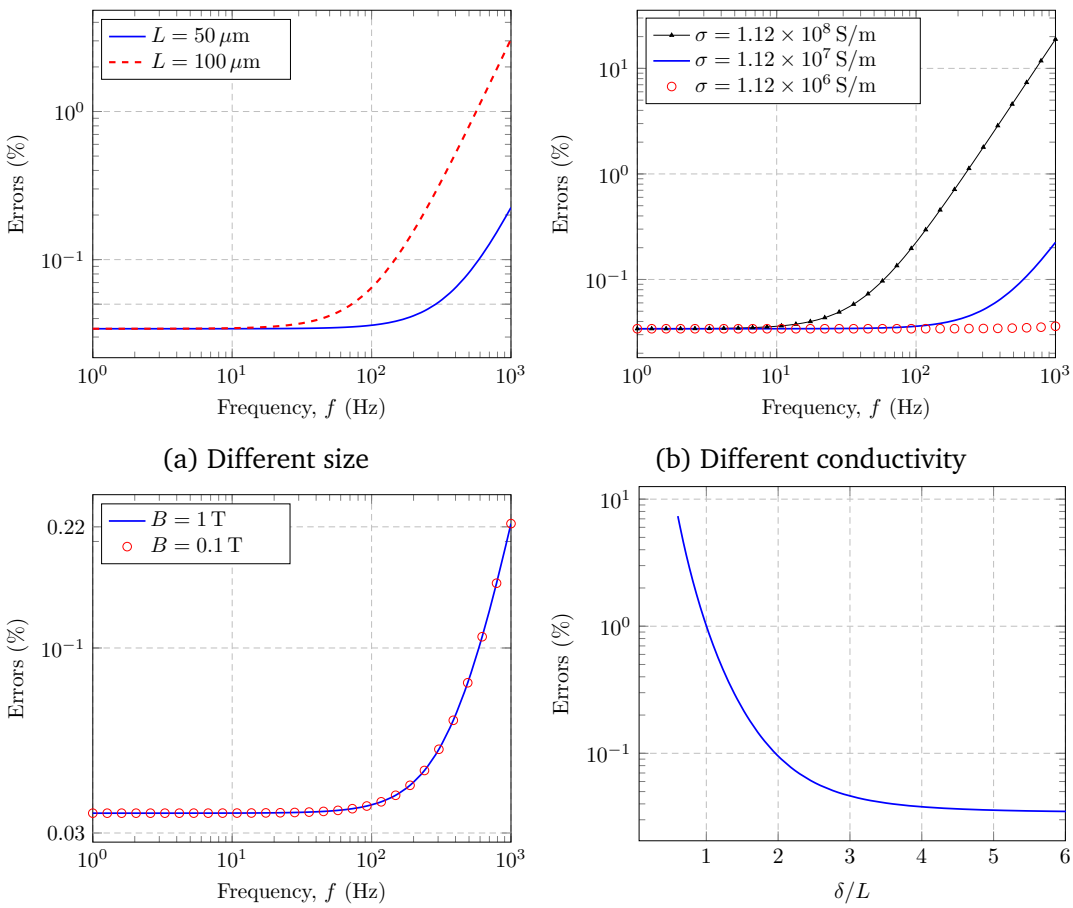

(a) Different size

(b) Different conductivity

(c) Different flux density

(d) η_{fit} as a function of δ/L

Fig. A.3 Discrepancies between EC loss density by the linear fitting equation (A.24) and the reference values from (A.22).

It can be seen from Figs. A.3a–A.3c that at low frequency, the errors are below 0.05%. The discrepancies are independent of the flux density. At higher frequency (greater than 100 Hz), the errors increase with the size or the electric conductivity. The formula of skin

depth δ is given by:

$$\delta = \sqrt{\frac{1}{\pi \mu \sigma f}} \tag{A.26}$$

Skin depth δ does not depend on the flux density so long that the permeability does not change. Calculations reveal that for a certain ratio between the skin depth and the size, the discrepancy η_{fit} remains unvaried. The η_{fit} as a function of δ/L is plotted in Fig. A.3d. The η_{fit} decreases with δ/L . The η_{fit} curve becomes shallow when the ratio is high enough (for instance, greater than 5).

A.4 Validity Range of Frequency

In the previous sections, the simple formulas are obtained under the condition of low frequency. At higher frequency, because of skin effect, the current is restricted to a very thin layer near the conductor surfaces, as indicated in Fig. A.4. The EC density distribution is examined on a cut-line along a radius. For each frequency, the EC density values are normalized by setting the maximum value to unit. The blue line in Fig. A.4 shows that, at

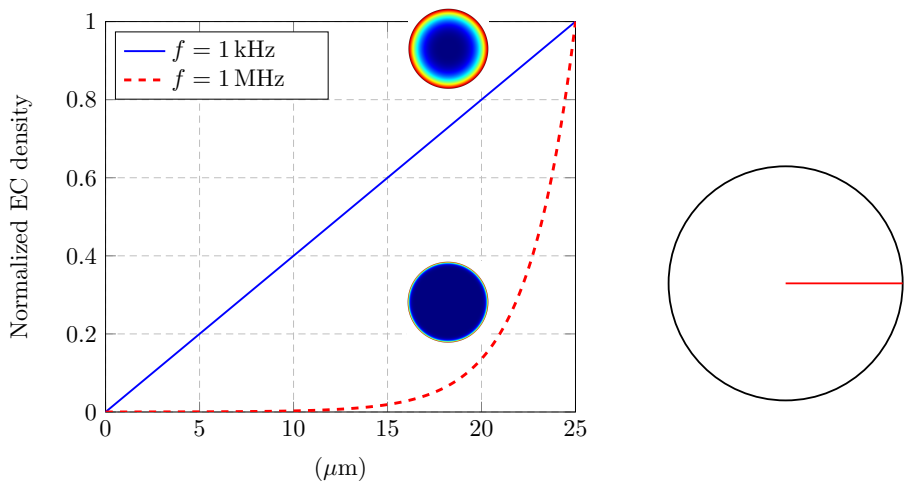

(a) Normalized EC density distribution (b) Cut-line

Fig. A.4 Distribution of normalized eddy current density of a circle along a radius (red cut line in (b)). Radius: $R = 25\,\mu\text{m}$

frequency $f = 1\,\text{kHz}$, EC density is linear along the radius. Equation (A.16) describes this relationship. While the frequency rises to $f = 1\,\text{MHz}$, shown by the red curve in Fig. A.4, EC density mainly occurs along the border. Equation (A.16) is not suitable to describe this phenomenon. When the low-frequency assumption is not valid anymore, the current

distribution has to be described from Fourier series or Bessel functions, for instance, as in (A.14).

Denote U_{ref} the EC loss density reference values from the full formulas (using (A.22) for the square domain; for the circle, substituting the full expression of EC density (A.15) into the EC loss density definition (1.16)). U_{ana} represents the EC loss density values from the simplified formulas, for instances, of (A.18) and (A.24) for the square and circle domain, respectively. U_{ref} and U_{ana} are normalized by the maximum of U_{ref}.

The normalized EC loss density values as a function of the ratio between skin depth and size (for a circle domain, L is the diameter, $L = 2R$) are plotted in Fig. A.5a and Fig. A.5b for the square and the circle domain, respectively. It can be seen from Figs. A.5a and A.5b

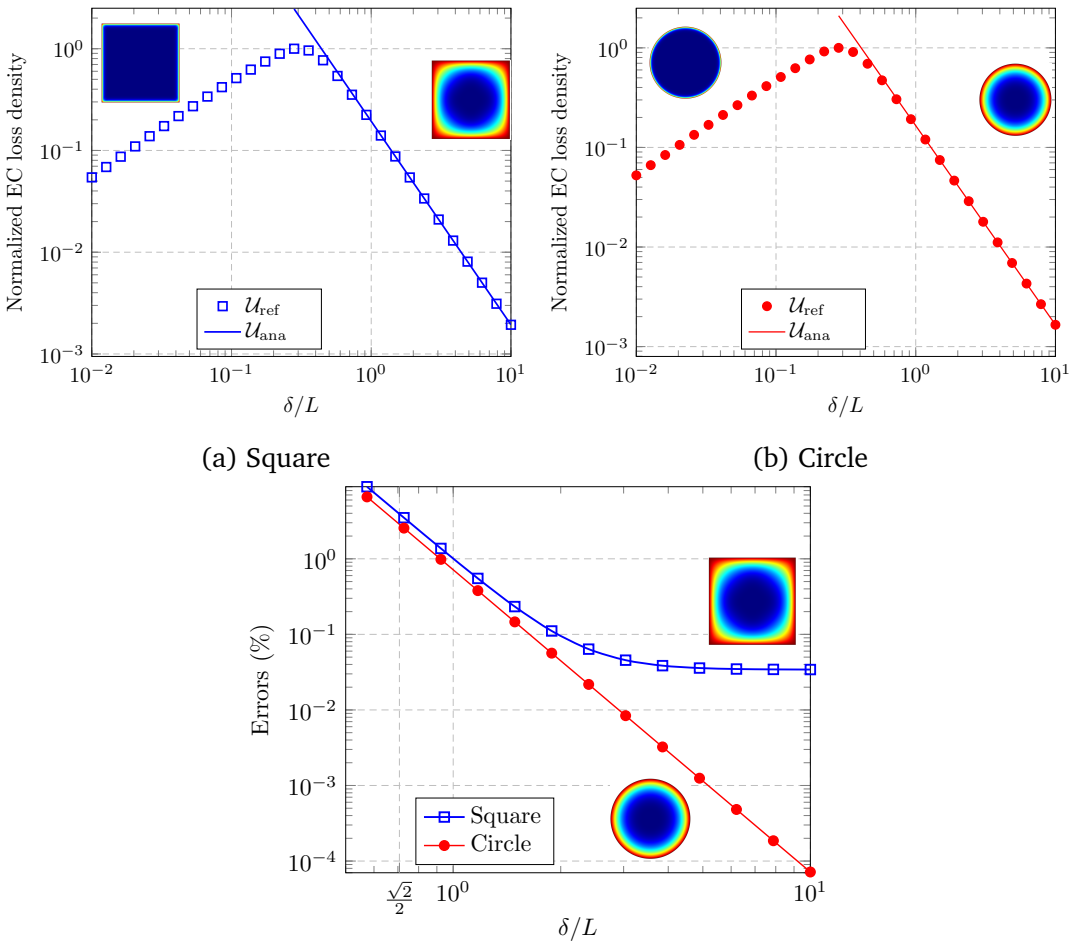

(a) Square (b) Circle

(c) Errors

Fig. A.5 Normalized eddy current density (and the corresponding errors) as a function of the ratio between skin depth and size.

that EC loss density reaches its maximum at $\delta/L \approx 0.28$. The discrepancies between the

analytical results and their corresponding references values are drawn in Fig. A.5c. The errors decrease with the ratio. When $\delta/L \geq \frac{\sqrt{2}}{2}$, the errors are below 5%. A skin depth threshold is introduced:

$$\delta_{\mathrm{TH}} = \frac{\sqrt{2}}{2} L \tag{A.27}$$

Substituting (A.27) into (A.26), the frequency threshold has the form:

$$f_{\mathrm{TH}} = \frac{1}{\pi\,\mu\,\sigma\,\delta_{\mathrm{TH}}^2} = \frac{2}{\pi\,\mu\,\sigma\,L^2} \tag{A.28}$$

The frequency range: $f \leq f_{\mathrm{TH}}$ provides a criterion for what is assumed 'low frequency' in this manuscript.

Appendix B

Energy Density

This appendix is the proof of (2.29), recalled hereafter, giving the energy loss density for a homogeneous and linear magnetic material under sinusoidal excitation.

$$S = \pi \mathbf{H}_0^* \cdot \mu^i \cdot \mathbf{H}_0 \tag{B.1}$$

Consider a homogeneous and linear material of permeability μ excited by a harmonic magnetic field $\mathbf{H}(t) = \mathbf{H}_0 e^{j\omega t}$ ($\mathbf{H}_0$ is the magnetic field magnitude and ω the angle frequency). Locally, the magnetic behavior of the material is given by $\mathbf{B}(t) = \mu \cdot \mathbf{H}(t)$. There is no hysteresis loss in magnetic linear materials. For quasi-static magnetic fields, the phase shift between $\mathbf{B}(t)$ and $\mathbf{H}(t)$ is negligible. If we introduce an imaginary part in the permeability tensor, $\mathbf{B}(t)$ and $\mathbf{H}(t)$ now exhibit a phase shift, as shown in Fig. B.1.

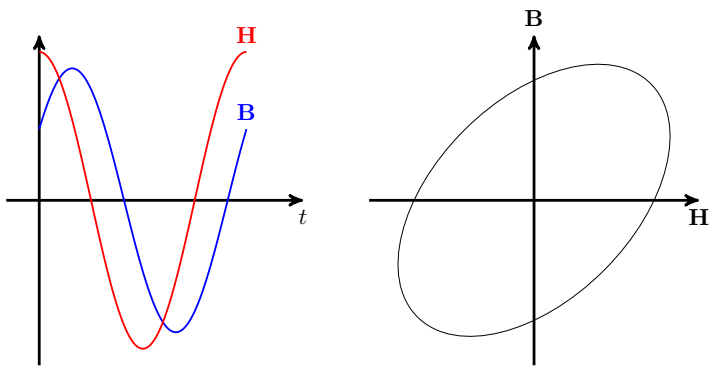

Fig. B.1 Phase shift between **B** and **H**, forming an ellipse in a period time. The area of this ellipse is the energy density during one time-period.

In a period of time, $\mathbf{B}(t)$ and $\mathbf{H}(t)$ form an ellipse. The area of this ellipse is the energy density during one period. We can make use of this energy density to represent the EC loss density. Let consider a complex magnetic permeability $\tilde{\mu} = \mu^r - j\mu^i$, where μ^r is the usual

material magnetic permeability. The area of the **B**-**H** ellipsoid is directly connected to the imaginary part of permeability so that $\mathbb{\mu}^i$ can be dedicated to the description of the EC loss density.

To obtain the area of the ellipse, a classical integration is performed over a period of time T:

$$\begin{aligned} S &= \frac{1}{2}\Re\left(\int_0^T \mathbf{H}^*(t)\cdot\frac{\mathrm{d}\mathbf{B}(t)}{\mathrm{d}t}\,\mathrm{d}t\right) \\ &= \frac{1}{2}\Re\left(\int_0^T \left(\mathbf{H}_0^* e^{-j\omega t}\right)\cdot\tilde{\mu}\cdot\left(j\omega\mathbf{H}_0 e^{j\omega t}\right)\mathrm{d}t\right) \\ &= \frac{1}{2}\Re\left(2\pi\mathbf{H}_0^*\cdot(j\mathbb{\mu}^r+\mathbb{\mu}^i)\cdot\mathbf{H}_0\right) \\ &= \pi\mathbf{H}_0^*\cdot\mathbb{\mu}^i\cdot\mathbf{H}_0 \end{aligned} \tag{B.2}$$

Equation (2.29) is finally retrieved. This result can also be found in [71].

Appendix C

Spherical Symmetry

This appendix aims at proving that the EC loss density due to a magnetic field can be decomposed as the addition of EC loss densities generated separately from the normal decompositions of the magnetic field.

The microstructure is a cubic lattice of spherical inclusions, shown in Fig. C.1. Because of spatial periodicity, the whole structure can be represented by an elementary cubic cell. It contains a sphere and its surrounding matrix.

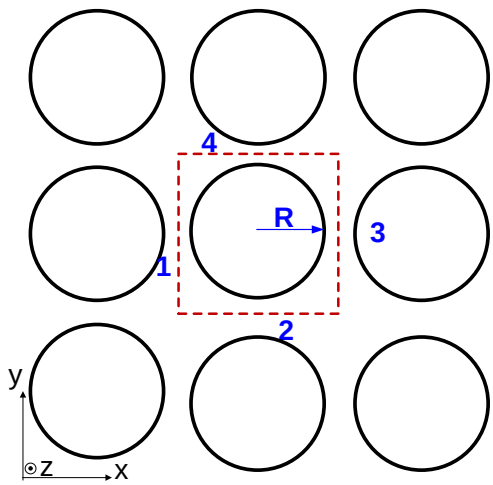

Fig. C.1 Sketch of the cubic lattice of spherical inclusions.

Magnetic field $\overline{\mathbf{H}}_{\mathrm{I}}$ is imposed along x-direction on the cell: $\overline{\mathbf{H}}_{\mathrm{I}} = [\overline{H_1}, 0, 0]^t$ with the superscript t the transpose operator. At a point $P(\mathbf{x})$ with $\mathbf{x} = (x, y, z)$, denote $\mathbf{H}_{\mathrm{I}}$, $\mathbf{E}_{\mathrm{I}}$ receptively the magnetic field and the electric field at that point.

The matrix is dielectric, so the eddy current in the matrix is negligible. According to the definition, the eddy current loss density of the cell writes:

$$U_{\mathrm{I}} = \frac{\left\langle \sigma \mathbf{E}^2 \right\rangle}{2f} = \xi_2 \sigma_2 \frac{\left\langle \mathbf{E}_{\mathrm{I}}^2 \right\rangle_{\mathrm{sphere}}}{2f} \tag{C.1}$$

where f is the working frequency. ξ_2 is the volume fraction of the sphere. σ_2 denotes the electric conductivity of the sphere. $\langle \cdot \rangle_{\mathrm{sphere}}$ indicates the volume average operator over the sphere:

$$\langle \cdot \rangle_{\mathrm{sphere}} = \frac{1}{V_{\mathrm{sphere}}} \int_{\mathrm{sphere}} \cdot \, \mathrm{d}V \tag{C.2}$$

Because of symmetry, the average magnetic field in the inclusion will be in the x-direction:

$$\langle \mathbf{H}_{\mathrm{I}} \rangle_{\mathrm{sphere}} = \beta \, \overline{\mathbf{H}}_{\mathrm{I}} \tag{C.3}$$

where β is a coefficient depending on the volume fraction and properties of materials. β is scalar since the constituent materials are isotropic.

Magnetic field $\overline{\mathbf{H}}_{\mathrm{II}}$ is imposed along y-direction: $\overline{\mathbf{H}}_{\mathrm{II}} = [0, \overline{H_2}, 0]^t$. Denote $\mathbf{H}_{\mathrm{II}}(\mathbf{x})$, $\mathbf{E}_{\mathrm{II}}(\mathbf{x})$ receptively the magnetic field and the electric field at the point P. Similarly, the average magnetic field in the sphere is:

$$\langle \mathbf{H}_{\mathrm{II}} \rangle_{\mathrm{sphere}} = \beta \, \overline{\mathbf{H}}_{\mathrm{II}} \tag{C.4}$$

and the EC loss density is,

$$U_{\mathrm{II}} = \xi_2 \sigma_2 \frac{\left\langle \mathbf{E}_{\mathrm{II}}^2 \right\rangle_{\mathrm{sphere}}}{2f} \tag{C.5}$$

It is clear that:

$$\overline{\mathbf{H}}_{\mathrm{I}} \perp \overline{\mathbf{H}}_{\mathrm{II}} \Longrightarrow \mathbf{H}_{\mathrm{I}} \perp \mathbf{H}_{\mathrm{II}} \textbf{ and } \mathbf{E}_{\mathrm{I}} \perp \mathbf{E}_{\mathrm{II}} \tag{C.6}$$

and

$$\overline{\mathbf{H}}_{\mathrm{I}} \perp \overline{\mathbf{H}}_{\mathrm{II}} \Longrightarrow \langle \mathbf{H}_{\mathrm{I}} \rangle_{\mathrm{sphere}} \perp \langle \mathbf{H}_{\mathrm{II}} \rangle_{\mathrm{sphere}} \tag{C.7}$$

The perpendicular relationship between $\mathbf{E}_{\mathrm{I}}$ and $\mathbf{E}_{\mathrm{II}}$ is indicated in Fig. C.2.

Now the magnetic field $\overline{\mathbf{H}}_{\mathrm{I}}$ and $\overline{\mathbf{H}}_{\mathrm{II}}$ are imposed simultaneously, noted $\overline{\mathbf{H}}_{\mathrm{III}}$. $\overline{\mathbf{H}}_{\mathrm{III}} = [\overline{H_1}, \overline{H_2}, 0]^t$.

The electric field at point P will be the addition of $\mathbf{E}_{\mathrm{I}}$ and $\mathbf{E}_{\mathrm{II}}$:

$$\mathbf{E}_{\mathrm{III}} = \mathbf{E}_{\mathrm{I}} + \mathbf{E}_{\mathrm{II}} \tag{C.8}$$

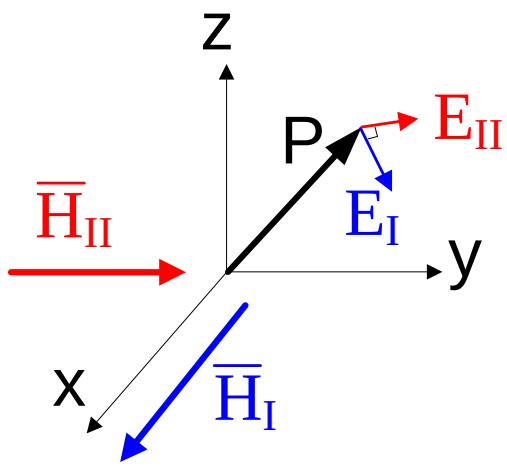

Fig. C.2 Induced electric field.

The EC loss density of the cell writes:

$$U_{\mathrm{III}} = \xi_2 \sigma_2 \frac{\left\langle \mathbf{E}_{\mathrm{III}}^2 \right\rangle_{\mathrm{sphere}}}{2f} \tag{C.9}$$

Because $\mathbf{E}_{\mathrm{I}} \perp \mathbf{E}_{\mathrm{II}}$, then

$$\mathbf{E}_{\mathrm{III}}^2 = \mathbf{E}_{\mathrm{I}}^2 + \mathbf{E}_{\mathrm{II}}^2 \tag{C.10}$$

so that

$$U_{\mathrm{III}} = U_{\mathrm{I}} + U_{\mathrm{II}} \tag{C.11}$$

The magnetic field at point P will be the addition of $\mathbf{H}_{\mathrm{I}}$ and $\mathbf{H}_{\mathrm{II}}$:

$$\mathbf{H}_{\mathrm{III}} = \mathbf{H}_{\mathrm{I}} + \mathbf{H}_{\mathrm{II}} \tag{C.12}$$

The average magnetic field in the sphere is:

$$\langle \mathbf{H}_{\mathrm{III}} \rangle_{\mathrm{sphere}} = \langle \mathbf{H}_{\mathrm{I}} + \mathbf{H}_{\mathrm{II}} \rangle_{\mathrm{sphere}} = \langle \mathbf{H}_{\mathrm{I}} \rangle_{\mathrm{sphere}} + \langle \mathbf{H}_{\mathrm{II}} \rangle_{\mathrm{sphere}} = \beta(\overline{\mathbf{H}}_{\mathrm{I}} + \overline{\mathbf{H}}_{\mathrm{II}}) \tag{C.13}$$

which leads to the relationship:

$$\left(\langle \mathbf{H}_{\mathrm{III}} \rangle_{\mathrm{sphere}}\right)^2 = \left(\langle \mathbf{H}_{\mathrm{I}} \rangle_{\mathrm{sphere}}\right)^2 + \left(\langle \mathbf{H}_{\mathrm{II}} \rangle_{\mathrm{sphere}}\right)^2 \tag{C.14}$$

Because $\mathbf{H}_{\mathrm{I}} \perp \mathbf{H}_{\mathrm{II}}$, then

$$\mathbf{H}_{\mathrm{III}}^2 = \mathbf{H}_{\mathrm{I}}^2 + \mathbf{H}_{\mathrm{II}}^2 \tag{C.15}$$

so that

$$\left\langle \mathbf{H}_{\mathrm{III}}^2 \right\rangle_{\mathrm{sphere}} = \left\langle \mathbf{H}_{\mathrm{I}}^2 \right\rangle_{\mathrm{sphere}} + \left\langle \mathbf{H}_{\mathrm{II}}^2 \right\rangle_{\mathrm{sphere}} \tag{C.16}$$

The discussion is based on the two components of applied magnetic field. If the third component is not zero, the EC loss density generated by this component can be added directly to the final value. It is the same for the first (average field, vector) and second order moment of the magnetic field.

Appendix D

Mechanical Localization Tensor

This appendix provides the formula of the mechanical localization tensor from Mori-Tanaka homogenization scheme.

According to Inclusion Based Problem (IBP) [89], each phase of a composite can be treated as an inclusion embedded in an infinite reference medium. The shape of the inclusion is determined by the spatial distribution of the phase in the composite. Consider a composite containing n constituents, the stiffness localization tensor $\mathscr{A}_i$ is defined as,

$$\mathscr{A}_i = \left(\mathscr{I} + \mathscr{N}_i : \mathscr{C}_{ref}^{-1} : (\mathscr{C}_i - \mathscr{C}_{ref})\right)^{-1} : \left(\sum_{j=1}^{n} \xi_j (\mathscr{I} + \mathscr{N}_j : \mathscr{C}_{ref}^{-1} : (\mathscr{C}_j - \mathscr{C}_{ref}))^{-1}\right)^{-1} \tag{D.1}$$

where $\mathscr{C}$ is the material stiffness tensor and $\mathscr{I}$ denotes the 4th order identity tensor. ξ represents the volume fraction of the constituent and the subscript i is the index of each constituent. $\mathscr{N}_j$ is the so-called Eshelby tensor of the phase j [97].

For the bi-phase composite, to achieve homogenization by Mori-Tanaka [93], the matrix material is chosen as the infinite material, that is, $\mathscr{C}_{ref} = \mathscr{C}_1$, so that,

$$\begin{aligned} \mathscr{A}_1 &= \left(\xi_1 \mathscr{I} + \xi_2 \left(\mathscr{I} + \mathscr{N}_2 : \mathscr{C}_1^{-1} : (\mathscr{C}_2 - \mathscr{C}_1)\right)^{-1}\right)^{-1} \\ \mathscr{A}_2 &= \left(\mathscr{I} + \xi_1 \mathscr{N}_2 : \mathscr{C}_1^{-1} : (\mathscr{C}_2 - \mathscr{C}_1)\right)^{-1} \end{aligned} \tag{D.2}$$

The effective stiffness tensor of the composite reads,

$$\begin{aligned} \tilde{\mathscr{C}} &= \xi_1 \mathscr{C}_1 : \mathscr{A}_1 + \xi_2 \mathscr{C}_2 : \mathscr{A}_2 \\ &= \mathscr{C}_1 + \xi_2 (\mathscr{C}_2 - \mathscr{C}_1) : \left[\mathscr{I} + \xi_1 \mathscr{N}_2 : \mathscr{C}_1^{-1} : (\mathscr{C}_2 - \mathscr{C}_1)\right]^{-1} \end{aligned} \tag{D.3}$$

The stress localization tensor $\mathscr{L}_{\text{mech}}$ has the form,

$$\mathscr{L}_{\text{mech}} = \mathscr{C}_2 : \mathscr{A}_2 : \tilde{\mathscr{C}}^{-1} \tag{D.4}$$

Only the $\mathscr{N}_2$ exists for bi-phase composite, therefore the subscript is removed in the following. The Eshelby tensor $\mathscr{N}$ depends on the shape of the inclusion and the stiffness tensor of the infinite medium $\mathscr{C}_{ref}$. In this case, the field in the inclusion can be considered uniform so the virtual inclusion in the IBP is sphere [89]. And the selection of the infinite reference medium is the matrix material. The elements of the Eshelby tensor $\mathscr{N}$ are [98]

$$\begin{cases} N_{1111} = N_{2222} = N_{3333} = \dfrac{7-5\nu_1}{15(1-\nu_1)} \\ N_{1122} = N_{2233} = N_{3311} = N_{1133} = N_{2211} = N_{3322} = \dfrac{5\nu_1 - 1}{15(1-\nu_1)} \\ N_{1212} = N_{1221} = N_{2112} = \cdots = \dfrac{4-5\nu_1}{15(1-\nu_1)} \end{cases} \tag{D.5}$$

where ν_1 is the Poisson ratio of the matrix.

Practically, because of symmetry, the 4th order tensor degenerates into 2nd order by Voigt notation. Denote material Young modulus Y, and Poisson ratio ν. The bulk modulus, κ, and shear modulus, G, can be determined by:

$$\begin{cases} \kappa = \dfrac{Y}{3(1-2\nu)} \\ G = \dfrac{Y}{2(1+\nu)} \end{cases} \tag{D.6}$$

The material stiffness tensor in matrix form is,

$$\mathbb{C} = \begin{bmatrix} \kappa + \frac{4}{3}G & \kappa - \frac{2}{3}G & \kappa - \frac{2}{3}G & 0 & 0 & 0 \\ \kappa - \frac{2}{3}G & \kappa + \frac{4}{3}G & \kappa - \frac{2}{3}G & 0 & 0 & 0 \\ \kappa - \frac{2}{3}G & \kappa - \frac{2}{3}G & \kappa + \frac{4}{3}G & 0 & 0 & 0 \\ 0 & 0 & 0 & 2G & 0 & 0 \\ 0 & 0 & 0 & 0 & 2G & 0 \\ 0 & 0 & 0 & 0 & 0 & 2G \end{bmatrix} \tag{D.7}$$

According to the material properties listed in Tab. 5.1, the material stiffness tensor is obtained as well as the Eshelby tensor. As a result, the mechanical localization tensor $\mathscr{L}_{\text{mech}}$ can be determined.

Publications

JOURNAL PAPERS

Submitted

X. T. Ren, R. Corcolle, L. Daniel, "Equivalent Complex Permeability for Soft Magnetic Composites: Application to Magnetic Circuit", submitted to *IEEE Transactions on Magnetics*.

Published

[1] X. T. Ren, R. Corcolle, L. Daniel, "A Homogenization Technique to Calculate Eddy Current Losses in Soft Magnetic Composites Using a Complex Magnetic Permeability", *IEEE Transactions on Magnetics*, Vol. 52, No. 12, 2016.

[2] X. T. Ren, R. Corcolle, L. Daniel, "Losses Approximation for Soft Magnetic Composites Based on a Homogenized Equivalent Conductivity", *Advanced Electromagnetics*, Vol. 5, No. 2, pp. 59-64, 2016.

[3] X. T. Ren, R. Corcolle, L. Daniel, "A 2D Finite Element Study on the Role of Material Properties on Eddy Current Losses in Soft Magnetic Composites", *The European Physical Journal - Applied Physics*, Vol. 73, No. 2, p. 20902, 2016.

In Preparation

[1] X. T. Ren, R. Corcolle, L. Daniel, "Bounds and Estimates on Eddy Current Losses in Soft Magnetic Composites", *Journal of Applied Physics*, in preparation.

[2] X. T. Ren, R. Corcolle, L. Daniel, "A Model for the Effect of Stress on Classical Losses in Soft Magnetic Composites", *Journal of Physics D: Applied Physics*, in preparation.

CONFERENCE PAPERS

Oral communications

X. T. Ren, R. Corcolle, L. Daniel, "A Model for the Effect of Stress on Eddy Current Losses in Soft Magnetic Composites", *17th International IGTE Symposium 2016*, September 2016, Graz, Austria.

X. T. Ren, R. Corcolle, L. Daniel, "A finite element study on the role of material properties in the eddy current losses in soft magnetic composites", *8ème Conférence Européenne sur les Méthodes Numériques en Electromagnétisme (NUMELEC 2015)*, June 2015, Saint-Nazaire, France.

Poster communications

X. T. Ren, R. Corcolle, L. Daniel, "Equivalent Complex Permeability for Soft Magnetic Composites Application to Transformer", *21th Conference on the Computation of Electromagnetic Fields (Compumag 2017)*, June 2017, Daejeon, Korea.

X. T. Ren, R. Corcolle, L. Daniel, "Bounds on Eddy Current Losses Estimate For Soft Magnetic Composites", *4th Advanced Electromagnetics Symposium (AES 2016)*, July 2016, Torremolinos, Spain.

X. T. Ren, R. Corcolle, L. Daniel, "Homogenization of soft magnetic composites with the incorporation of eddy current losses into complex permeability", *10th International Symposium on Electric and Magnetic Fields (EMF 2016)*, April 2016, Lyon, France.

X. T. Ren, R. Corcolle, L. Daniel, "Losses approximation for soft magnetic composites based on a homogenized equivalent conductivity", *20th Conference on the Computation of Electromagnetic Fields (Compumag 2015)*, June 2015, Montréal, Canada.

ÉCOLE DOCTORALE
Physique et ingénierie : électrons, photons, sciences du vivant (EOBE)

Titre : Modélisation semi-analytique des pertes par courants de Foucault dans les matériaux composites

Mots clefs : Homogénéisation, Matériaux hétérogènes, Modélisation, Pertes par courants induits, SMC

Résumé : Ce travail consiste à développer un modèle de perméabilité complexe pour composites magnétiques doux (SMC - Soft Magnetic Composites). La perméabilité magnétique et les pertes par courants de Foucault (EC - Eddy Current) sont intégrées respectivement comme les parties réelle et imaginaire d'une perméabilité complexe. La perméabilité magnétique effective macroscopique peut s'obtenir par des estimations classiques en homogénéisation. Une détermination correcte de la perméabilité effective, i.e. la partie réelle de la perméabilité complexe, est cruciale pour une estimation précise de pertes EC. Les formules de pertes EC sont dérivées pour des SMC à microstructure périodique dans les cas 2D et 3D. En outre, différentes approches s'appuyant sur différentes moyennes du champ magnétique permettent d'obtenir des limites inférieures et supérieures pour l'estimation des pertes EC dans les SMC.
La perméabilité complexe ainsi obtenue est ensuite appliquée à une structure de circuit magnétique. Le champ magnétique et la répartition des pertes EC peuvent être obtenus sur le circuit magnétique équivalent (homogénéisé). Les résultats sont comparés aux calculs en champ complet du circuit magnétique hétérogène. Un bon accord est observé.
Enfin, on étudie l'effet des contraintes mécaniques sur la perméabilité magnétique et les pertes EC des SMC, ce qui conduit à une formule couplée de la densité de pertes EC en fonction de la contrainte mécanique macroscopique et du champ magnétique.

Title: Classical Losses in Soft Magnetic Composites using Homogenization Techniques

Keywords: Homogenization, Heterogeneous Materials, Modeling, Eddy Current Losses, SMC

Abstract: This work consists in developing a complex permeability model for soft magnetic composites (SMC). The static magnetic permeability and eddy current (EC) losses are integrated respectively as the real and imaginary part of the complex permeability. Classical estimates are applied to determine the macroscopic effective magnetic permeability. A correct determination of the effective permeability, i.e. the real part of the complex permeability, is crucial for the estimate of EC losses. EC losses formulas are derived for SMC with periodic microstructure in 2D and 3D cases. Furthermore, different approaches of field averaging are employed to obtain lower and upper bounds on the EC losses in SMC.
The complex permeability model is then applied to analyze a magnetic circuit structure. The magnetic field and EC losses distribution can be obtained on the equivalent homogenized magnetic circuit. The results are compared to the full-field calculations on the heterogeneous magnetic circuit. A good consistency is observed.
Finally, the effect of mechanical stress on the magnetic permeability and loss property of SMC is studied, which leads to a coupled formula of EC loss density as a function of macroscopic stress and magnetic field.

Université Paris-Saclay
Espace Technologique / Immeuble Discovery
Route de l'Orme aux Merisiers RD 128 / 91190 Saint-Aubin, France